University of Twente

Faculty of
Science and Technology

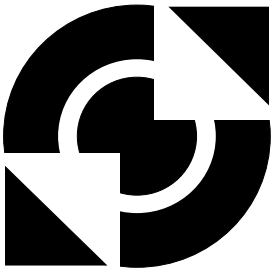

Autothermal Reactor Concept for Combination of Oxidative Coupling and Steam Reforming of Methane

T. Kolkman

Enschede, January 2008

University of Twente

Faculty of
Science and Technology

Autothermal Reactor Concept for Combination of Oxidative Coupling and Steam Reforming of Methane

T. Kolkman
Born on March 27, 1983 in Groenlo

Graduation Colloquium January 11, 2008, LA 1814, UT

Graduation Committee

Prof. Dr. Ir. J.A.M. Kuipers (Chairman)
Ir. T.P. Tiemersma (Mentor)
Ir. P.O. Graf
Dr. Ir. A.G.J. van der Ham
Dr. Ir. M. van Sint Annaland

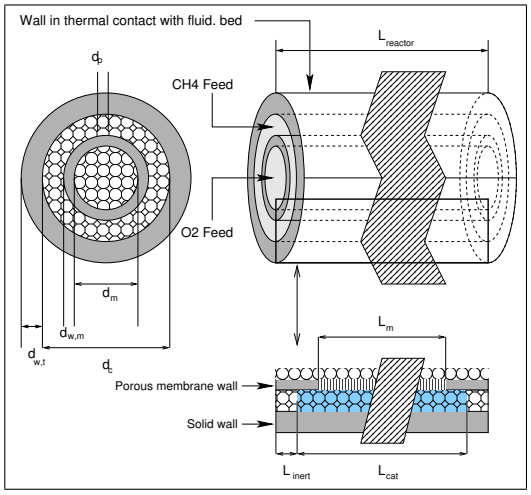

In the end, Mother Nature has the final say.

James Steward, in *Calculus* [Ste03]
(Page 25)

Preface (Voorwoord)

Dit verslag is het resultaat van een afstudeerperiode die behalve erg leerzaam ook erg leuk was.

Leerzaam vanwege de inhoud, waarover u meer kunt lezen in het hierna volgende, maar ook vanwege de manier van werken. Ik werd door Tymen, mijn mentor, volledig vrij gelaten in de manier van aanpak. De besprekingen waren altijd erg efficient en tegelijk ook erg nuttig. Daar waar er daar tijd voor was, was er altijd de mogelijkheid om zelf eens iets nader uit te zoeken en als daar geen tijd voor was, had Tymen altijd wel een snelle oplossing, ook als hij daar zelf misschien eigenlijk wel geen tijd voor had. En gelukkig bleven scherpe vragen en opmerkingen niet achterwege. Ik ben Tymen erg dankbaar voor deze manier van begeleiden en het zo gestelde vertrouwen. Ook over van alles buiten het werk was er altijd een zinnig gesprek te voeren. Tymen, bedankt!

Leuk waren (naast het werk zelf) iedere dag de koffiepauzes, waar afwisselend over inhoudelijke zaken of juist over de meest grote onzin werd gepraat. Dergelijke gesprekken gingen vaak door bij eigen borrels of bij de door de vakgroep goed bezochte borrels van studievereniging Alembic, een vereniging die ik ook door de door haar aan mij geboden mogelijkheden veel dank verschuldigd ben. Ook de vakgroepuitjes leverden een belangrijke bijdrage aan de sfeer.

De afstudeerperiode betekende voor mij ook een ommekeer van een aanvankelijke voorkeur het bedrijfsleven in te gaan naar de keuze voor een promotie. Ik wil eenieder die mij heeft geholpen bij deze beslissing hiervoor hartelijk danken.

De leden van de de afstudeercommissie ben ik zeer dankbaar voor de beschikbaar gestelde tijd, de getoonde belangstelling en de ongetwijfeld nieuwe inzichten die tijdens de presentatie naar voren zullen komen.

Tot slot wil ik, naast mijn flatgenoten, graag mijn ouders en mijn broer bedanken. Zij hadden voor mij ook tijdens het afstuderen altijd een luisterend oor en de nodige humor.

Tom
4 januari 2008

Summary

The conversion of relatively inexpensive methane into more valuable derived chemical products is expected to gain importance in the coming decades. The current project focusses on a combination of two processes for conversion of methane into more valuable products. *Steam reforming* (SRM) is a well-known industrial process that can be used to produce synthesis gas (CO + H_2), which is the precursor used in Fischer-Tropsch synthesis. The products obtained in this process can be relatively easily transported and can be used for example as fuel. *Oxidative coupling* (OCM) of methane is a process that up to now has only been researched in laboratories. Reactants for this catalytic process are oxygen and methane. It's function is to convert methane into ethane and, more preferably, ethene. These products, as well as derivatives possibly produced on-site, represent high economic value. The process faces considerable obstacles before commercial application can be realized, but with rising oil prices and improved reactor concepts this process might become feasible.

The challenge of this project is to come to a reactor concept for combining these two processes into one reactor. The goal is to come to an overall autothermal process. Steam reforming is a strongly endothermic process. The product distribution is mainly thermodynamically determined. The OCM reaction is strongly exothermic. The product distribution is reaction rate controlled.

Before coming to a reactor concept, a thorough understanding of the processes at hand is needed in order to determine boundary conditions. After considering thermal integration, among different alternatives generated a reactor concept was chosen. The principle is to perform oxidative coupling of methane inside a tube in which distributive feeding of oxygen takes place. Besides allowing for maintaining a low partial pressure of oxygen, increasing selecitivity, this results in a relatively uniform production of heat along the tube. In order to come to a smooth temperature profile, the relatively uniform production of heat needs to be matched with a relatively uniform cooling, driven by the SRM reaction. This (conceptually) was achieved by performing the steam reforming in a fluidized bed. An extension of the concept has been the addition of the concept of reverse flow to the OCM reaction tube. Not only was a favourable effect on the temperature profile in the OCM catalytic section expected. Additionally, the addition of inert sections in a reverse flow configuration allows for cold feeding and, more importantly, quenching directly at the outlet of the reactor.

A model was built to simulate the OCM membrane reactor, including the possibility of reverse flow operation. Uniform cooling by the fluidized bed has also been included. Central assumptions have been that radial temperature and concentration gradients, both for the catalyst particles as for the catalyst compartments as a whole, were ignored. A homogeneous model was employed. The model was largely based on the work of Smit [Smi06].

Simulation results reflect the expected increase in selectivity. Calculated results show a far higher selectivity than was ever experimentally obtained (45 vs. 35%); resulting figures are to be considered indicative for the feasibility the concept conceived. After initial calculations a base setup was chosen. The length of the catalyst section of the OCM tube was $1\mathrm{m}$ of which the middle $\frac{2}{3}$ meter was fed with oxygen. Oxygen was fed from an inner tube with an outer diameter of $1.3\mathrm{cm}$ to the concentric catalytic section with an inner diameter of $2.5\mathrm{cm}$. The outer wall of the entire catalyst section was in thermal contact with the fluidized bed at a temperature of $780^{\circ}\mathrm{C}$, whereas in the catalytic section for OCM a more or less constant temperature of about $810^{\circ}\mathrm{C}$ was reached in the reaction region. An indication of a desired length of inert sections is $1\mathrm{m}$. An overall molar feed ratio of CH_4:O_2=4 was chosen.

The effect of reverse flow operation within the OCM catalytic section was shown to be limited because of efficient cooling. Switching time will primarily depend on requirements for the inert sections.

On the part of overall thermal efficiency, it was found that reforming the outgoing stream minus the C_2 products per tube requires significantly more heat than released by the OCM tube. Possible countermeasures are adjustment of the molar feed ratio for OCM or the use of a prereformer. It was however found for the base case chosen that the fluidized bed can be operated in a feasible fashion.

The current results show that conceptually the reactor concept can be feasible, for this process and possibly other processes. However, radial mass transport is the Achilles heel of the concept. Additionally the wish for integrated autothermal operation puts strong limitations on freedom for design. The current membrane reactor concept differs from conventional membrane reactor concepts in that generally reactant is fed distributively from the outside of a tube containing catalyst, whereas in this case this was done from the inside, in order to enhance thermal contact with the fluidized bed. Additionally, initial calculations show that a homogeneous radial concentration profile of oxygen is far from what is to be expected. Reactions will occur relatively close to the point of injection, enlarging the overall resistance to heat transport and reducing product selectivity by undesired reactions and bypassing.

In future work (counteracting) diffusion limitation and it's effects should be the first thing considered, possibly backed up by experiments.

Contents

Preface iii

Summary iv

List of symbols ix

I. Theoretical Background 1

1. Background 2
1.1. Uses of methane . . . 2
1.2. Combination of exothermic and endothermic processes . . . 2
1.3. Transport of products . . . 3
1.4. The goal of this project . . . 3

2. Reactions 5
2.1. Catalytic oxidative coupling . . . 5
2.2. Steam reforming . . . 8

II. Reactor concept 13

3. Reactor design: practical 14
3.1. Approach . . . 14

4. Separation technologies 17
4.1. Cryogenic distillation and chromatographic methods . . . 17
4.2. Adsorption . . . 17
4.3. Conclusions . . . 18

5. Resulting process schemes 19

6. Selection of promising reactor concepts 21
6.1. Fixed bed family . . . 21
6.2. Tubular fluidized reactor . . . 22
6.3. Selected concept . . . 23

III. Demonstration of concept 25

7. Reactor model 26
7.1. Dynamic model . . . 26
7.2. The high frequency switching model (HFSM) . . . 28

8. Design Calculations on reverse flow membrane reactor 30
8.1. Yield vs. tube length . . . 30
8.2. Cooling . . . 31
8.3. Demonstration of the membrane reactor . . . 35
8.4. Effect of switching time on results . . . 38
8.5. Application of cooling of only the reaction section . . . 41

9. Full process considerations 43
9.1. Overall thermal efficiency . . . 43
9.2. On the geometry of the fluidized bed . . . 45
9.3. Benchmarking . . . 46

IV. Discussion and Conclusions 47

10. Discussion and recommendations 48
10.1. On the concept of reverse flow with membrane feed . . . 48
10.2. On the catalyst activity and other catalysts . . . 49
10.3. On increasing tube diameters and radial profiles . . . 50
10.4. Process safety . . . 51
10.5. On the model . . . 51
10.6. On the results . . . 51
10.7. Other processes . . . 52
10.8. Concepts in literature . . . 52
10.9. Materials to be used . . . 52
10.10. On the viability of the process . . . 52
10.11. Catalyst stability . . . 53
10.12. Suggested experimental procedure . . . 53

11. Conclusion 54

V. Background information 55

Bibliography 56

A. Model validation 60
A.1. Validation of kinetics . . . 60
A.2. Analytical solution . . . 62
A.3. An inconsistency in the model . . . 64

B. Dead end reactor 66

C. Adiabatic temperature change for OCM reactions 68

D. Calculation of u_{mf} 70

E. Porous tube oxygen flux 71

F. Physical properties 72

F.1. Thermal properties of CaO 72

G. Modelling for increased troughput 73

H. Some modifications to increase the speed of convergence of the model 75
H.1. Larger minimum timestep 75
H.2. Initial high tolerance 75
H.3. Initial high timestep for HFSM 75
H.4. Initial high tolerance for DM 75

I. Overall heat balance for CH_4: O_2= 3 77

J. Reactor design: conceptual approach 78
J.1. Both catalysts in the same space 78
J.2. Separation of catalysts in space: OCM followed by SRM 79
J.3. Conclusions 79

K. Materials of construction 80
K.1. Reactor wall 80
K.2. Gaskets 80
K.3. Catalyst carrier 80

L. Required radial diffusion of mass 81
L.1. Mass balance 81
L.2. Reaction kinetics 81
L.3. Solution of the differential equation 82
L.4. Some more considerations 83

M. Minimum required radial heat conduction 84
M.1. Energy balance and solution 84
M.2. Results 84

N. Changing the ratio CH_4:O_2 86

List of symbols

a	Specific surface	M	Molar mass
A	Surface	OCM	Oxidative coupling of methane
ad	Adiabatic	P	Pressure
Ar	Archimedes number	PO	Partial oxidation
ATR	Autothermal reforming	Q	Total heat production
Av	Specific surface	Q	Volumetric heat production
c	Concentration	q	Volumetric heat production
C_2	The collection of ethane and ethene	R	Gas constant
C_p	Heat capacity	r	Radius
D_A	Diffusion coefficient	r_i	Inner diameter
d_c	Inner diameter of outer tube OCM	s	Solid
Dil	Catalyst dilution factor	SRM	Steam reforming
DM	Dynamic model. For calculating single direction flow.	T	Temperature
d_m	Inner diameter of porous tube	u_{mf}	Minimum fluidization superficial velocity
$\dot{m}$	Mass flow rate	V	Volume
$\dot{V}$	Volumetric flow rate	x	Mole fraction
d_p	Diameter particle	w	Weight fraction
$d_{w,m}$	Wall thickness of porous tube		**Greek**
d_w, t	Thickness of outer tube OCM	$\alpha_{cb,fb}$	Overall heat transfer coefficient from OCM catalytic bed to SRM fluidized bed
e	Emissivity	$\alpha_{cb,w}$	Heat transfer coefficient from catalytic bed to wall
eff	Effective	$\alpha_{w,fb}$	Heat tranfer coefficient from outer wall OCM tube to SRM fluidized bed
fb	Fixed bed or fluidized bed. Context dependent.	δ	Specific distance
F_p	Fraction of catalytic bed OCM fed with oxygen	δ_m	Membrane thickness
g	Gas	ε	Porosity
g	Mass fraction	η	Viscosity
H	Enthalpy	γ	Conversion factor
$HAZOP$	Hazard and operability	λ	Heat conduction coefficient
$HFSM$	High frequency switching model	μ	Viscosity
J	Flux	Φ	Thiele modulus
k	Reaction rate constant	Φ_m	Mass flow
L_{cat}	Length of catalytic bed OCM tube	Φ_n	Mole flow
L_m	Length of porous tube that is permeable	ρ	Density

Part I.

Theoretical Background

1. Background of the project

The current chapter gives a background in the field of the use of methane, especially methane found far from populated areas. This includes different trends of using methane gas from remote areas, including advantages and disadvantages. Also shortly attention is given to the combination of exothermic and endothermic processes. Resulting in the goal of the current project.

The reader that is interested in the chemical conversion of low molecular mass feedstock is referred to reviews in literature, e.g. given by Baerns and Buyevskaya [BB98a]. Examples are oxidative dehydrogenation of ethane and oxidative coupling.

1.1. Uses of methane

Methane is mostly found as the major component of natural gas. Typical compositions of natural gas are found in Ullmann's Encyclopedia of Industrial Chemistry [HRM+06]. It typically contains about 80% CH_4 and about 1% CO_2. The geographical distribution of methane (CH_4) is, for example, given by Lunsford et al. [Lun00] and by Smit [Smi06].

Methane is often found far away from industrial complexes, and often offshore. For transportation to inhabited areas, two options prevail. The first is direct liquefaction of methane by cryogenic techniques, requiring the energy-intensive cryogenic cooling of the gas, after which the gas can be transported by ship. After transport the methane can be heated by burning part of the methane.

Smit [Smi06] points out that given the existing infrastructure for liquid fuels, liquefaction of natural gas is a good mid-term solution for the energy demand in the transport sector as well as large-scale power generation. This is the second option. For this option, methane needs to be converted.

For conversion of methane into other chemicals, a distinction is made between *direct* and *indirect* routes. The latter always involves the conversion of methane into synthesis gas, which is subsequently converted into desired products. The current project aims to combine an exothermic direct route, the exothermic oxidative coupling of methane, with an indirect endothermic route, steam reforming. Thus, the aim is to combine two processes for production of bulk chemicals.

1.2. Combination of exothermic and endothermic processes

The idea of combining exothermic and endothermic processes is not new. See for example Van Sint Annaland [Ann00], Kolios et al. [KFE02] and Sundmacher et al. [SKSM05]. It is clear that advantages are mostly found for application in remote areas where there is no possibility for useful integration of waste heat of separate processes, which in contrast can be and is done in large industrial complexes. For example, it is reported that in conventional steam reformers, only about 50% of the heat released by the burners is used for steam reforming. [KFE02] Waste heat can for example be used for steam reforming.

It must be noted that doubts about the feasibility of integrated processes have been expressed in literature. Stitt [Sti04] points out that although multifunctional reactors have been exten-

sively researched for over 50 years, only a few applications can be found. These have in common that they benefit from process or engineering **simplicity**. Of special interest is the *stability* and *ease of control* of the processes, since the integration might lead to chaotic behaviour. The so-called 80-20 rule should be kept in mind when considering full integration versus partial integration; an increase of complexity versus an increase of process integration must be carefully considered. Integration typically results in loss of degrees of freedom, often accompanied by other problems.

A special focus on industrially applicability, thus, is needed in this project.

1.3. Transport of products

A possible product from methane on remote locations is ethene. When cryogenic technology is used to recover this product from a gaseous stream with unreacted methane as major component, it will be in the liquid, low-volume state after recovery already. This is in terms of density the preferred state for transport, in which it will have a density in a similar order of magnitude as methane (opposed to the gaseous state). Of course, any transport of methane that would normally be converted into unavoidable waste products would be avoided by conversion on the location of methane recovery.

In order to ensure safer transport conditions, the ethene produced could also be converted into final products. This causes loss of flexibility for application of the ethene produced opposed to transporting it to the main land and selling it on the spot market. The final choice in this respect will be a matter of economic analysis and safety considerations. Tankers for the transport of ethene have been employed already [SSO01].

As for the products derived from the steam reforming, it is assumed that these will be transported in the liquid state, as was proposed by Smit [Smi06].

1.4. The goal of this project

Two processes to produce chemical feedstock in remote locations from methane are oxidative coupling and steam reforming, the latter followed by Fischer-Tropsch synthesis. Oxidative coupling is exothermic and steam reforming is endothermic. The main reactions are given in table 2.1. Combination of these into one process could conceptually result overall in a preferentially slightly exothermic process. Since production in remote locations is targeted, it is assumed that in the end hydrogen gas is always produced to be used in synthesis gas and not for use as fuel.

In short, the goal of the project is twofold:

1. To create understanding on combining OCM with SRM. For example it is of interest which type of reactor can be used. A theoretical overview should be created. Different (membrane) concepts will be compared.

2. To arrive at a demonstration model for combining OCM with SRM.

In order to arrive at a feasible reactor concept, the following conditions are needed:

- A thorough understanding of the process at hand. For this purpose, information on the elementary reactions was gathered and is presented in this report.

- Boundary conditions for design. Typically this includes many non-quantitative aspects. Therefore, information on design strategies for reactors has been gathered.

- Creativity. In the end, reactor design is a creative process. Based on the information found in literature, multiple reactor concepts have been elaborated, reflecting the needs found in literature. A selection, having typical characteristics, is presented in this report.

Once a feasible reactor concept has been selected, it's validity needs to be confirmed. First by numerical experiments, next by real-world experiments. Numerical demonstration of the key characteristics of the process at hand was achieved in this project. Technical realization of a demonstration reactor remains and will have to depend in part on the practical experience of qualified technicians.

2. Reactions: mechanisms, kinetics and thermodynamics

This chapter discusses reaction mechanisms, kinetics and thermodynamics. First catalytic oxidative coupling is discussed and next steam reforming is discussed. In this chapter no choice has yet been made on combining or separating the reactions in space.

Since some reactions can occur for both steam reforming and oxidative coupling, all reactions to be discussed in this chapter are given in table 2.1. For some trivial names are given, which were taken from the work of Smit. [Smi06]

The outcome of this chapter will be the selection of an appropriate kinetic scheme for oxidative coupling of methane (OCM) and a firm understanding of steam reforming (SRM). Typical reaction conditions and boundary conditions for performing the reactions will be given.

2.1. Catalytic oxidative coupling

Catalytic oxidative coupling of methane to higher hydrocarbons is regarded as a potential route to ethylene or liquid fuels. More than 600 publications have appeared on this topic. After the most promising areas of catalyst development had been explored, a yield that would make the process commercially feasible had not been found.[1] Research efforts were then focussed studying reactor configurations and modes of contact [LSM94]. However, knowledge of the characteristics of the reaction is crucial in order to come to an optimum reactor design.

2.1.1. Reaction schemes

The number of reaction steps involved in the oxidative coupling of methane is tremendous; it concerns a very complex reaction system. A compromise between desired accuracy and constraints resulting from computation time thus needs to be found [PM98] for any reactor model built on the basis of a given more or less complex reaction scheme. Some reactions in this field have gotten specific names.

After comparing multiple models from literature, it is stated by Mleczko and Baerns [MB95] that "a reaction scheme applicable for all catalysts was not found"; the scheme thus in general differs per catalyst. Common features, however, were found. Examples are a lower reaction order in oxygen for C_2 formation [LDMM97] than for combustion and a drop in selectivity for increasing methane conversion. Schemes for both homogeneous and heterogeneous reactions are given by Mleczko and Baerns. They also warn, like Tuinier [Tui07] does, for using reactors in which backmixing occurs, since consecutive reactions can be detrimental for yield. [MB95].

As a basis for the current work the scheme as developed by Stansch et al. [SMB97] for the very active La_2O_3 catalyst is used. By eliminating reactions from this scheme, simpler schemes relating to other catalysts can be obtained, as was shown by Tuinier [Tui07], in his case for the $Mn/Na_2WO_4/SiO_2$ catalyst.

[1] Lu et al. [LDMM97] indicate that for an OCM process to be feasible, single pass C_2 yields should be higher than 30 percent. Despite extensive catalyst screening, a catalyst able to accomplish this by itself has not been found, so that improvement of single pass yield should be found from reactor design improvements. Cordi et al. [CPRL97] even indicate a minimum required yield for single pass mode of 40%. Lafarga et al. state that yields should be between 25 and 30%, depending on selectivity, when undiluted methane and oxygen are used. Lu et al. [LDMM97] precise this to be based on a single-pass conversion of 35-37% with a selectivity of 85-88%.

Table 2.1.: Common reactions in the field as given by Stansch [SMB97] and Smit [Smi06]. Reaction enthalpies based on the data by Daubert and Danner [DD85] and evaluated at 810 °C, 1bar.

Oxidative coupling reactions [SMB97]			
Full combustion	$CH_4 + 2O_2 \rightarrow CO_2 + 2H_2O$	(2.1)	$\Delta H_r = -802$ kJ/mol CH_4
	$2CH_4 + 0.5O_2 \rightarrow C_2H_6 + H_2O$	(2.2)	$\Delta H_r = -87$ kJ/mol CH_4
	$CH_4 + O_2 \rightarrow CO + H_2O + H_2$	(2.3)	$\Delta H_r = -271$ kJ/mol CH_4
	$CO + 0.5O_2 \rightarrow CO_2$	(2.4)	$\Delta H_r = -282$ kJ/mol CO
	$C_2H_6 + 0.5O_2 \rightarrow C_2H_4 + H_2O$	(2.5)	$\Delta H_r = -105$ kJ/mol C_2H_6
	$C_2H_4 + 2O_2 \rightarrow 2CO + H_2O$	(2.6)	$\Delta H_r = -547$ kJ/mol C_2H_4
	$C_2H_6 \rightarrow C_2H_4 + H_2$	(2.7)	$\Delta H_r = 144$ kJ/mol C_2H_6
	$C_2H_4 + 2H_2O \rightarrow 2CO + 4H_2$	(2.8)	$\Delta H_r = 234$ kJ/mol C_2H_4
Water-gas-shift reaction	$CO + H_2O \rightarrow CO_2 + H_2$	(2.9)	$\Delta H_r = -34$ kJ/mol CO
	$CO_2 + H_2 \rightarrow CO + H_2O$	(2.10)	$\Delta H_r = 34$ kJ/mol CO_2
Main steam reforming reactions [Smi06]			
Steam reforming	$CH_4 + H_2O \rightleftharpoons CO + 3H_2$	(2.11)	
Water-gas shift	$CO + H_2O \rightleftharpoons CO_2 + H_2$	(2.12)	
Dry reforming	$CH_4 + CO_2 \rightleftharpoons 2CO + 2H_2$	(2.13)	

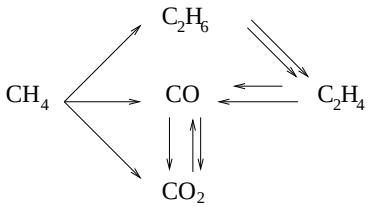

Reaction scheme of heterogeneous OCM reactions as presented by Stansch [SMB97].

Pak [PQL98] states that a considerable body of experimental evidence supports the view that $CH_3\cdot$ radicals formed over the catalyst couple in the gas phase to produce ethane. It is thus important that the catalyst efficiently forms these radicals without scavenging the radicals in side reactions over the surface.

By adopting the heterogeneous reaction scheme of Stansch et al. it is assumed that all of the reactions take place at or very close to the surface of the catalyst; when increasing the volume of the gas relative to the catalyst surface this assumption might not be valid. A reaction scheme for homogeneous (thus gas-phase) reactions as provided by Mleczko and Baerns [MB95] and their references, which can serve as a means to do a worst case calculation. Of special interest is the thermal dehydrogenation of ethane (relation 2.7), which often is reported as occurring in the gas-phase [AP06, Tui07, ZB91] at high temperatures. It must however also be mentioned that in conventional production of ethene by steam cracking residence time is kept low on purpose to prevent consecutive reactions towards higher hydrocarbons, which proceeds at a temperature of 800-850°C and is quenched at a temperature of 550-650°C.[ZW07] More on the equipment used for quenching, the so-called transfer-line heat exchangers, is given by Sundaram et al. [SSO01]

The approach in this work will be that for proof of principle only the heterogeneous reactions as described by Stansch et al. is taken into account and that experimental validation will have to show the validity of this assumption. It was shown by Tuinier [Tui07] for the $Mn/Na_2WO_4SiO_2$ catalyst that gas-phase reactions can have a significant contribution especially at higher O_2 partial pressures.

2.1.2. Influence of temperature

High temperatures ($> 580^\circ$C) are needed to initiate the OCM reactions [AP06, SMB94], the exact temperature depending on the catalyst.

The exact catalyst also determines the temperature of maximum product selectivity and yield, which is also dependent on partial pressures of reactants and mixing patterns. A common feature for all OCM catalysts is that the activation energy of the primary selective step, the formation of ethane from methane is greater than that of nonselective primary steps, causing product selectivity to be higher at higher temperatures for heterogeneous kinetics [MB95].

In the current work, the kinetics as measured by Stansch will be preferentially kept within the window in which they were measured (700-830°C), unless stated otherwise.

2.1.3. Influence of pressure

A high total pressure, increasing the partial pressure of oxygen, may be beneficial to the ability of the catalyst to produce radicals. [PQL98] At elevated pressures the extent of gas-phase reactions is substantial for the conditions for high CH_4 conversions [PM98]. Experimental influence of pressure on methane conversion is given by Hou and Hughes [HH01]; it is also indicated by them that increasing pressure increases both forward and backward reaction rates.

In the current work, the choice is made to adhere to the typical experimental conditions of atmospheric pressure, since the reactions of primary interest take place at the catalyst surface and increasing the extent of gas-phase reactions typically would be detrimental for product yield. Since the use of low pressure is also common in ethane cracking [SSO01] this is also thought to be a realistic choice for the full process.

2.1.4. Undesired catalysis

Besides the catalyst, the gas stream contacts other materials, in particular the materials of construction. In literature catalytic effects of these materials in the case of methane and oxygen in contact have been reported. These are:

Stainless steel This catalyses the fast oxidation of methane and hydrocarbon products in the presence of O_2 and high temperature. [LSM94, QZWT96]. Also, severe coke formation was observed when using stainless steel for OCM experiments [Tui07].

Alumina and silica In order to reduce the acidity and associated catalytic effects of the alumina and silica phases present in their porous membrane, Lafarga et al. [LSM94], using a packed bed membrane reactor, treat the membrane with Li_2CO_3 impregnation in order to make it more alkaline and therewith decreasing the intrinsic activity; the methane conversion over an empty membrane decreased. [CMS94b] Quartz (SiO_2) reactor walls seem to catalyze gas-phase OCM somewhat less than ceramic (Al_2O_3) reactor walls.[QZWT96]

2.2. Steam reforming

As a potential route to relief the strong exothermicity of the OCM reaction, a combination with the strongly endothermic steam reforming has been proposed.

There are basically three major processes used to produce hydrogen from hydrocarbon fuels [DC04]:

1. Steam reforming (SRM)
2. Partial oxidation (PO)
3. Autothermal reforming (ATR), which basically combines the thermal effects of SRM and PO.

The most extensively studied of these is *steam reforming*. In this process, methane reacts with steam in the presence of a catalyst. The products are hydrogen, carbon dioxide and carbon monoxide. This process is *highly endothermic*. The adiabatic temperature drop for the SRM reaction corresponds to about 1000K [KFE02]. These reactions also serve to produce synthesis gas. Ideal ratios for different components within this product gas are given by Smit [Smi06]. An overview of the composition and temperature of the product gas for different purposes such as H_2 production or methanol synthesis gas can be found in Ullmann's Encyclopedia of Industrial Chemistry [HRM$^+$06]. The choice is made in this project to use steam reforming not as a source of hydrogen, but as a source of synthesis gas.

2.2.1. Reaction schemes

The catalytic reaction mechanism of steam reforming as generally agreed upon is given by Trimm [Tri99]. Given a sufficient supply of heat, the dissociative adsorption of hydrocarbons seems to be the rate limiting step. For *higher hydrocarbons* this step is *much faster* than that for methane.

A graphical representation of the reaction steps is given by Trimm [Tri97].

Steam reforming is generally done over a nickel (or the more expensive Rhutenium [SCB$^+$01]) catalyst. However, nickel catalysts are also reported to be used in *oxidative reforming of methane* [CYE03]. A widely accepted reaction mechanism for this is methane combustion followed by both steam

and carbon dioxide reforming. A set of rate equations for a Ni/Al_2O_3 catalyst is given by Chen et al. [CYE03]

Whether combustion and reforming occur in parallel is dependent on the state of oxidation of the Ni catalyst. If it is fully reduced, the reactions do occur in parallel.[SCB$^+$01].

2.2.2. Kinetic parameters

Hoang and Chan [DC04] give kinetic data by Xu and Froment for a Ni catalyst based on the Langmuir-Hinshelwood model. Data for gas-phase reactions is not given by Hoang and Chan.

Chen et al. [CYE03] refer to the same kinetics as the most general and reliable expression for this process over a nickel catalyst. Many researchers have used these kinetics. Chen et al. also give the rate expressions and also do not give gas phase reactions. The possibility of occurence of gas phase reactions is considered by De Smet et al. [SCB$^+$01] for the case of partial catalytic oxidation. It is stated that when operating at high temperatures and pressures, homogeneous gas-phase reactions can become important. This should of course be checked for the current case, for which the models as referenced by De Smet et al. can be usefull.

Another convenient overview of combined kinetics for methane combustion and SRM, as well as a literature review of measurements of SRM kinetics, is given by C.S. Patil [Pat05]. This overview is recommended as a basis for the current project.

Normally, the composition of the gas at the outlet of the reactor reflects the chemical equilibrium, although within the reactor the gas is not in equilibrium at all places. The exception is the formation of coke, which has been shown to be controlled by kinetics above 700°C [HRM$^+$06].

In case the catalyst is too active, measures as described by Aguiar et al. [ALRCK01] can be taken.

Especially at high temperatures, not kinetics but diffusion limitation may be limiting to reaction [HRM$^+$06]. Diffusion limitation may be overcome by using a powdered catalyst in a fluidized bed. [CYE03] Kolios et al. [SKSM05] show that even when assuming infinitely fast reaction, still a rather large (10m) tubular reactor is needed to achieve an acceptable conversion because of heat transfer limitations, which should be fulfilled before kinetics can play a role at all.

2.2.3. Influence of temperature

Temperatures applied in industrial tubular steam reformers nowadays go up to 950°C, whereas until the early 1950's the temperature was limited to 800°C. [HRM$^+$06] A similar temperature region is often the choice in studies in literature. More on industrial conditions is given in section 2.2.5.

The spectrum of products formed in steam reforming is mainly controlled by thermodynamics [Tri97, GPB04], which may partially be due to the swift kinetics at high temperatures [ALRCK01].

An important finding related to the current project is that even at lower temperatures (400-550°C), higher hydrocarbons can be converted to methane, as is discussed by Christensen [Chr96]. In this case, also a nickel catalyst is used.

Glöckler et al. [GGM$^+$04] indicate that to ensure sufficient conversion, the temperature should rise to 800°C and upon cooling the reverse reaction should be avoided by using non-catalytic material. Of special interest is the strong sensitivity of the thermodynamic equilibrium on temperature around 800K or 530°C. Kolios et al. [KFE02] confirm the desired operating temperature of more than 800°C. Aguiar et al. [ALRCK01] confirm that the process is usually performed between 750 and 900°C, resulting in swift kinetics, although they take 850K as local

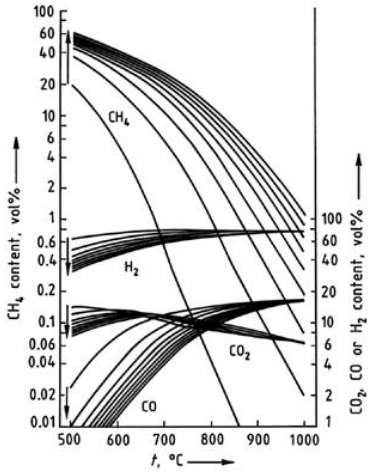

Figure 2.1.: Equilibrium composition for methane reforming at 500 to 1000°C and pressures (in the direction of the arrows) of 0.1, 0.5, 1, 1.5, 2, 2.5, 3, 3.5, 4 MPa. Molar steam: methane ratio 3.333. Adapted from Ullmann's Encyclopedia of industrial chemistry [HRM+06]

temperature for their simulations of a SRM catalyst particle. Thermodynamic limitations can be possibly overcome by the use of hydrogen-selective membranes in a fluidized bed [CYE03].

The current work takes a best case approach with regards to steam reforming. Reaction is considered to always proceed towards equilibrium for a chosen temperature. The temperature is defined by cooling requirements for the OCM reaction. Thus, amongst others it is assumed that no bypassing of heated yet unreacted steam reforming feed into the reactor exhaust occurs.

2.2.4. Influence of pressure

The process has been performed in tubular furnaces at various pressures in the past. Initially, it was performed at 0.4-1MPa. Nowadays, pressures up to 4MPa are employed.[HRM+06]

For a thermodynamic reactor, typically methane conversion decreases with increasing pressure.[GPB04] This is also shown by the results shown in figure 2.1

The adsorption of a species on the surface of a catalyst is dependent on the partial pressure of the species itself as well as of the partial pressures of the other components present when using the Langmuir-Hinselwood model.

For the current work the assumption is made that the steam reforming takes place at laboratory conditions, thus at relatively low pressure.

2.2.5. Typical industrial operating conditions

Opposed to the OCM process, steam reforming is a well known process in industry. The exact conditions strongly depend on the final goal of the steam reforming, such as the production of hydrogen or the production of synthesis gas. Typical operating conditions for the steam reforming are taken from literature, giving:

Table 2.2.: Feed gas composition of an industrial steam reformer [CYE03]. Feed composition approaches molar ratio H_2O:CH_4:H_2= 5.5:1:1 as given by Hou and Hughes [HH01]

Component	Feed rate (kmol/h)	Mole fraction
CH_4	3.953	0.20
CO_2	0.478	0.02
CO	0	0
H_2	0.961	0.05
H_2O	14.08	0.72

- Temperature: 700-800°C [Tri99]. Hou and Hughes [HH01] used a temperature of 525°C (798K) for their experiments. Patil [Pat05] indicates that a typical temperature range for a steam reformer is 850-950°C. A wide range of temperatures, thus, is available. In conventional steam reforming reactors the process gas is preheated up to 500°C [HRM+06] before being released into the high temperature steam reformer.

- Pressure: 0.1 MPa (experimental conditions for OCM [MB95]). Syngas production technologies pressures however are typically 20-60 bar [Smi06], presumably to limit the required size of the equipment. Indeed, it is confirmed by Mleczko and Baerns [MB95] that the total pressure will be a major factor in determining the reactor size and the duty of the compressors in the separation section. A more specific range of 15-30 bar is given by Patil [Pat05], and is given to originate from thermodynamic limitations and downstream compression requirements. However, at this point it is not clear if the OCM reaction will occur at that pressure.

- Steam fraction: by using only steam and methane as a feed, coke formation was found to be severe as given by Hou and Hughes [HH01]. A reasonable composition to prevent coking (for their catalyst) seems to be molar ratios H_2O:CH_4:H_2= 5.5:1:1. Since their experiments were performed for low (incomplete) conversion, an equilibrium composition cannot be taken from their work. It should be mentioned that their study focussed on the production of hydrogen (and carbon dioxide), whereas in this study, since it is intended for production of liquid fuels at remote locations, the goal is to produce a mixture of synthesis gas (of which the ideal ratio is given by Smit [Smi06]) and ethane and methane.

  Chen et al. [CYE03] give the feed composition for an industrial fixed-bed steam reformer. It is given in table 2.2. It is in the same range as that given by Hou and Hughes [HH01] and will be used for the remaining part of this work.

The processes following steam reforming typically are Fisher Tropsch synthesis, operating at about 200°C, or high temperature shift for hydrogen and ammonia plants, operating at 400°C. Therefore, heat exchange reformers are applied in industry upfront autothermal reforming, taking care of about 75% of the reforming. [Sti04]

2.2.6. Using the SRM stream as coolant

Steam reforming itself is mentioned in literature as a possible transport carrier of heat using the so-called Adam-Eve principle. [HRM+06] In this case a forward reaction is used to remove heat from places with an excess of thermal energy and a reverse reaction is used to release this heat where it is needed.

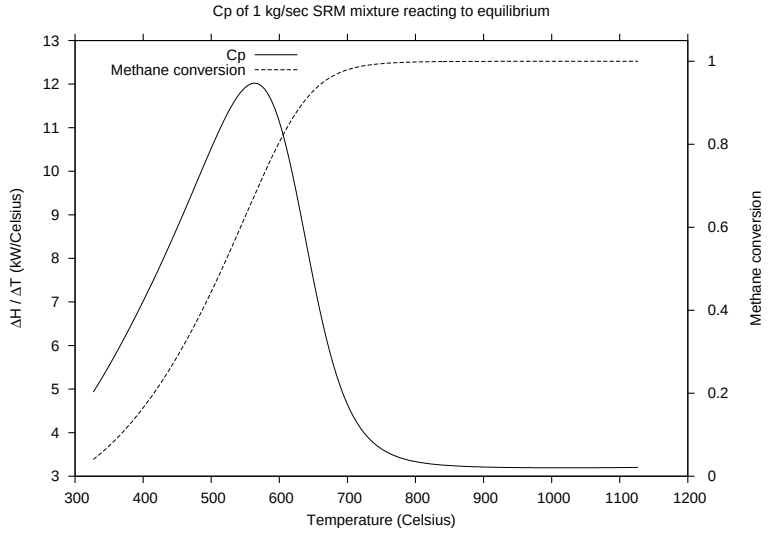

Figure 2.2.: Heat absorbing capacity of one kilogram of a typical SRM stream composition (given by table 2.2) as a function of temperature, assuming infinitely fast reaction rates and no heat transfer resistances, thus **for illustrational purposes only**

When considering the SRM a coolant for the exothermic OCM reaction, attention must be given to the point that the heat uptake capacity is strongly dependent of the temperature already reached by the SRM stream, reacting to equlibrium. This has already been mentioned by Kolios et al. [KFE02], who state that once the endothermic reaction reaches almost complete conversion, the heat sink in the respective part of the catalytic zone vanishes. This could cause a runaway of an associated exothermic reaction.

In order to study this effect in more detail, an Aspen simulation has been run.[2] When plotting the results into a graph, figure 2.2 is obtained. The reason that the heat capacity is plotted for one kg instead of e.g. one mole is that the total number of moles, and thus the volume flow, is not constant as conversion increases; it increases. However the mass flowing through is a constant.

From figure 2.2 it can be seen that indeed at a certain temperature range cooling capacity reaches it's maximum as far as thermodynamics is concerned. However, as was already indicated in section 2.2.2 other factors, amongst which additionally diffusion limitation and catalyst deactivation, may be determining the actual extent of conversion and hence this section can only be considered to be giving an indication.

[2]The simulation consisted of two equilibrium (Gibbs) reactors in series. The feed consisted of $1\mathrm{kg/s}$ of the typical SRM reaction mixture as given in table 2.2. The pressure was constant at 1 atmosphere. A setpoint T_{set} was chosen. The temperature of the first reactor in the sequence was set to $0.5^{\circ}\mathrm{C}$ below T_{set}; this reactor heats the mixture up and allows the reaction to proceed to equilibrium. The temperature of the second reactor in series is set at $0.5^{\circ}\mathrm{C}$ above T_{set}. Since by definition we have:

$$C_p \equiv \left(\frac{\partial H}{\partial T}\right)_p \tag{2.14}$$

now the heat duty of the second equilibrium reactor (approximatively) gives the heat capacity per $\mathrm{kg/s}$ of flow at the temperature T_{set}.

Part II.

Reactor concept

3. Reactor design: practical approach

3.1. Approach

Reactor design is a creative process, as it is stressed by Jacobs and Jansweijer [JJ00]. These authors argue in favour of a strategy that minimises the impact of retracting intermediate conclusions by moving information that is not likely to change to the front of the selection process. Their paper gives listings of properties to take into account when doing the selection. A distinction is made between hard properties (scale, heat and catalyst replacement), specific properties (e.g. temperature rise) and soft properties (e.g. pressure drop). This can be used as a checklist in the current project.

A subdivision into different families for Gas-Solid reactors is given by Van Swaaij, Van der Ham and Kronenberg [SHK02], who very actively reference to the work of Krishna and Sie[KS94]. Specific advantages and disadvantages of the different families are given, too.

It will be no surprise that this work first started with a (very limited) literature study to gather necessary data (while setting the framework for arranging the data) and modelling to fill the gaps was only done later. Learning (about different allowable concepts) was done along the way; hence going back to literature later on might be needed. However to avoid rework from the start on documentation was ensured.

A design strategy has not been enforced, however the aids given by the articles of Krishna and Sie [KS94] and of Van Swaaij et al. [SHK02] were used as an important guide. From the work of Krishna and Sie, the “musts” and “wants” as shown in table 3.2 were taken. Of special importance to the current project has been the wish for ease of operation. Figure 3.1 shows the different aspects taken into account along with references to literature and some of the conclusions that were made. A shortlist is given in table 3.1; these are aspects that are severely taken into account when choosing a reactor concept.

A central choice, before considering practical reactor configurations in section 6.3 has been whether the catalysts should be combined in one physical space, or should be physically separated from each other. The choice was made in section 5 to separate these in space.

Table 3.1.: Shortlist of highly desired characteristics of reactor design concept

- Safe operation
- Ease of operation
- Ease of construction
- No steep temperature gradients or other sources of mechanical strain
- No undesired catalysis
- Separation of mass streams
- Good thermal contact of SRM and OCM streams
- Catalyst diameter indication taken from Smit [Smi06]: 3mm
- SRM specific:
  - Good heat supply to SRM
  - Reaction is heat supply limited, runs to equilibrium
- OCM specific:
  - Product yield determined by kinetics, backmixing undesired
  - Catalyst typically difficult to fluidize
  - Highly exothermic
  - Preferably low oxygen partial pressure
  - Quick drop in temperature desirable for quenching

Table 3.2.: General “musts” and “wants” for reactor selection. Adapted from Krishna and Sie [KS94]

Musts	Wants
• Operability within reaction restaints of temperature, pressure and residence time • Safe operation (without runaways) • Environmentally acceptable • Feasible scale-up to economic size	• Maximum possible conversion • Maximum possible selectivity to desired products • Easy operation • Low capital and operation cost, e.g. from: – low pressure drop – effective utilization of reactor space – simple constructs • Feed and exit streams should be “cold”. [KFE00]; for this countercurrent heat exchange or regenerative heat exchange are to be considered.

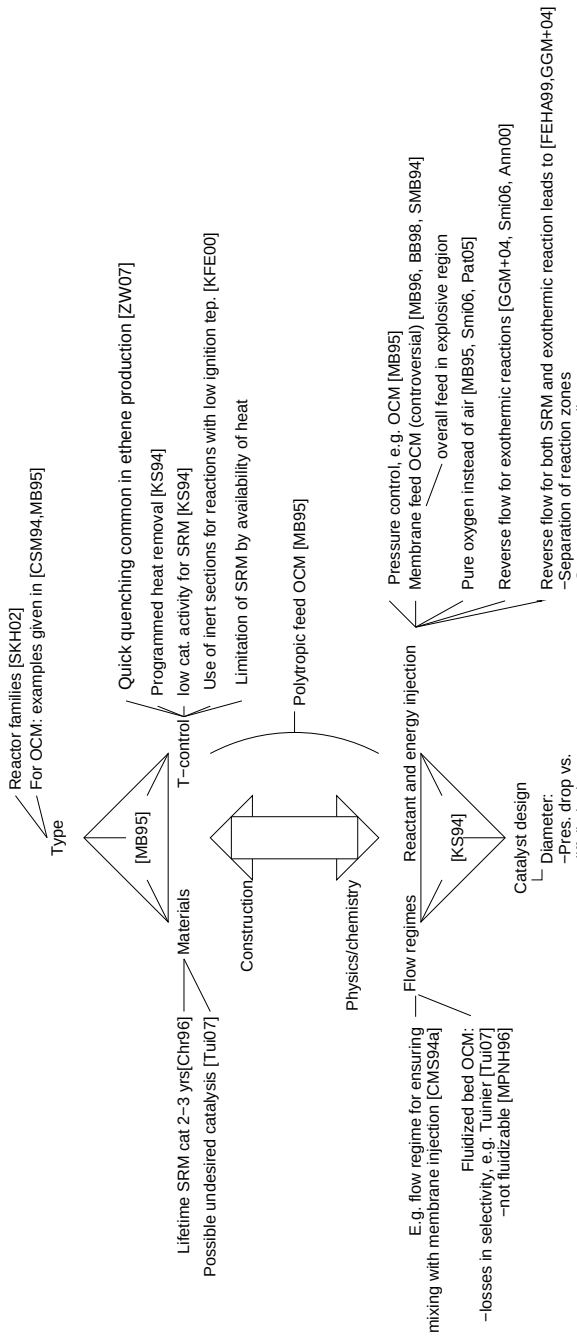

Figure 3.1.: Overview of different design strategies found in literature and parameters to take into account

4. Separation technologies

Although the current work is about the design of a reactor, of course when designing a reactor the impact of choices made on the remaining part of the chemical plant must be taken into account. A major part of the chemical plant normally consists of equipment for separation of chemical components. A short description of the separation technologies most commonly used in processes similar to those under consideration is given here, with special attention to the OCM reaction. Separation technologies related to preparation of natural gas for SRM are considered known technology and thus for example the removal of water (steam) or CO_2 from natural gas(-like) streams is not discussed here.

4.1. Cryogenic distillation and chromatographic methods

Cryogenic distillation has been generally considered for the separation of the reactor effluent in OCM studies. [MB95] Due to the low C_2 content of the product stream the separation of C_2 products is very expensive in this way. Baerns and Buyevskaya mention chromatographic methods as well as temperature- and pressure swing adsorption as alternatives. [BB98b] Related to this technology are the countercurrent moving bed reactor as discussed by Mleczko and Baerns [MB95] and the simulated moving bed reactor as discussed by Tonkovich [TCA93].

An example of a flowsheet for cryogenic separation in OCM can be found in Vereshchagin et al. [VGA+98]. They use part of the excess heat from the OCM reaction for pyrolitic dehydrogenation of ethane. A more advanced flowsheet, in this case for separation after ethane cracking, is given by Sundaram et al. [SSO01]

4.2. Adsorption

Adsorption has also been reported in literature as a means to separate C_2 hydrocarbons from the reactor stream, possibly improving reaction yield and selectivity significantly. Olefinic products can be selectively adsorbed [AP06]. However, afterward desorption with a carrier gas (nitrogen) at atmospheric pressure is reported to result in a gas stream with a 1% C_2 content. [TCA93] The advantages gained by added yield and selectivity, thus, are very likely offset by the added additional requirements for product recovery and by the increased complexity of operation. Materials of adsorption have been active charcoal [TCA93] and a molecular sieve trap [MV03]. The molecular sieve trap traps CO_2 and H_2O as well as C_2H_4 and, to a minor extent, C_2H_6. So, when considering the separation technology for removing CO_2 and H_2O prior to cryogenic distillation, care must be taken to ensure that the desired products are not removed along with these components.

An additional concern for adsorption is given by Stitt [Sti04]. At the operating temperature of oxidative coupling, typically capacity for physi-sorption is very low. In case of chemi-sorption of carbon dioxide, regeneration has to be performed at a temperature higher than that at operating conditions, which would destroy the catalyst. At this point it is considered that chemi-sorption is not an option, especially for C_2. An interesting concept is the “raining fluidized bed”, in which the adsorbent particles fall through a fluidized bed. However, combined with the difficulties of material handling reported [Sti04], this is not considered an option for C_2 recovery.

Baronskaya et al. [BWDB96] discuss adsorption on more or less ambient conditions. Unfortunately no results for recovery are given. The relatively high average volumetric content of ethene (about 40%) was obtained after saturating the adsorbent, surely causing slip-through of product. Also problems with high adsorption of methane are reported.

4.3. Conclusions

From the above discussion, it is clear that cryogenic distillation will be the key element in the recovery of C_2 product from the gaseous stream. Adding to this adsorption could possibly reduce requirements on the cryogenic equipment but brings a capital investment itself and it does increase complexity of process operation. The choice of taking adsorption into account affects the composition of the gaseous stream leaving the OCM process in two ways:

1. The recovery of ethene could be slightly better or worse. It has been assumed in this work that a recovery of less than 70% (primarily by cryogenic techniques) is simply unacceptable. Adding adsorption to recover the remainder then concerns possible removal of the remainder of 30% of the initial C_2 content, which will then be at about 10 vol%. This is thought to be not severely affecting the final recovery, and hence not worth the trouble of considering adsorption.

2. When using an adsorber, when desorbing the carrier gas may be a another gas than methane, such as nitrogen, having a larger difference in boiling point with ethene than methane. In this case, assuming that no methane absorbs on the absorber, it could be considered that no methane at all is lost in the separation step. It would be necessary to use another gas than methane as carrier gas, since it has been found (using Aspen simulations) that in order to "knock out" C_2 from a stream using cryogenic techniques, a significant amount of methane would condense along with it in the first flash drum.

To make calculations independent on whether "ideal" adsorption or just cryogenic distillation is used, it will be considered that in all cases 70% of C_2 product is recovered and that all other components are sent to the steam reformer; in case of the cryogenic separation this comes down to increasing the number or flash stages, ergo building a distillation column (or a series of them) instead of just one flash vessel. The single flash vessel simulation in Aspen has shown that recovery of 70% of the C_2 is possible; isolation of this product from the resulting flash stream is of secondary concern. Also it will be assumed that water and CO_2 are removed from this stream, since this is necessary in case of using cryogenic equipment.

5. Resulting process schemes

Given the choice that the two catalysts are not employed in the same space (supplemented by considerations in appendix J), possible resulting process schemes are given here.

Figure 5.1 shows a conventional process scheme. Low yield and very low ethylene content in the reaction tail gas present a challenge in the utilization of this ethylene [XXL$^+$02]. This scheme is not feasible because of the low yield in OCM, requiring a huge recycle of natural gas along with undesired side-products, necessitating the use of a purge.

An alternative in order to prevent this is shown in figure 5.2. This option avoids the recycle of methane by sending all unconverted methane to the steam reforming section. At this point it is assumed that the heat required by the steam reforming is of the same order of magnitude as the heat released by the oxidative coupling.

The variant shown in figure 5.2 has the following advantages:

- Any side products, such as CO, that possibly are not removed in the separation section are not recycled to the OCM reactor, but are sent to the steam reforming section where they are converted into useful product instead. Since the size of gas-treatment equipment is very much dependent on the magnitude of the gas stream, this might significantly reduce the required size of the reactor and separation equipment, as well as significantly reduce compression costs.

- Compression costs may be further reduced because in contrast to the case of the recycle shown in figure 5.1, the non-product outlet stream of the separation section does not need to be fully depressurized after the separation. In contrast to the oxidative coupling, SRM is reported to be performed at elevated pressures, which reduces the size of the steam reforming equipment. A point of attention in this respect is if the reactor concept chosen can also operate at elevated pressures for SRM.

Hence the variant shown in figure 5.2 is chosen as the basis of this work. Although choosing this variant is expected to reduce operational costs and equipment size,a real advance can only be obtained if a more effective method of separation is found. However, in literature no convincing account of this was found. Hoping this advance will be made at some time this work continues to focus on the reactor concept. Reducing the load on the separation equipment, however, is useful in any case.

For calculations on heat integration the assumptions for the separation as given in chapter 4 will be used.

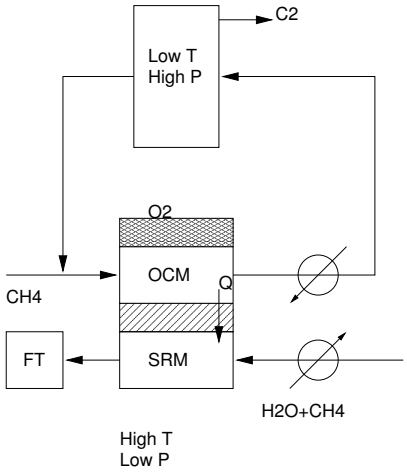

Figure 5.1.: A more conventional process scheme, leading to a very large recycle of methane for OCM

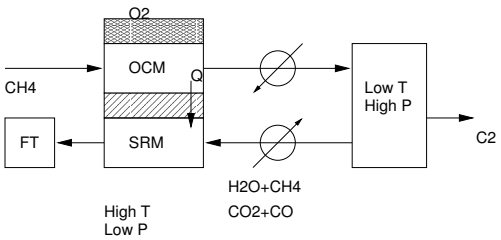

Figure 5.2.: A possible process layout with OCM and SRM in series

6. Selection of promising reactor concepts

Many different reactor concepts were already considered in literature to make OCM a viable option. [LSM94] When selecting a more complex reactor configuration over a more simple one, it must be kept in mind that the increased complexity must validate the increase in complexity. For example, Kao [KLL97] states for the results obtained by Lafarga et al. [LSM94] that the effect of using a porous membrane reactor instead of a fixed bed reactor on yield is only marginal. However, it is also reported that it allows a more controllable and safe operation. Different membrane reactors are compared by modeling by Kiatkittipong et al. [KTG$^+$05], using the Li/MgO catalyst and comparing with a fixed bed reactor, which typically has a C_2 yield of 20-25%. For a membrane reactor, the best experimental yield reported is 35%. [KTG$^+$05]

6.1. Fixed bed family

The fixed bed family shows some clear advantages, in the first place the relatively simple construction and operation. Concepts for multiple reactors of this type have been conceived. As an example, the "Dead End" reactor is described in appendix B because this is a good representation of different aspects to take into account. However, the fixed bed family also has a disadvantage in terms of thermal integration, as described by Kolios et al. [KFE00], which in the end has lead to it's elimination for use in both the steam reforming and oxidative coupling sections as an option for the reactor concept to be elaborated. Some examples of the work of Kolios et al. [KFE02] are shown in figure 6.2. The concept with distributed feed of oxygen will be discussed again for the selected concept. Also cocurrent is shown, indicating a large pressure drop at the onset of steam reforming. In the case of countercurrent the reaction fronts tend to separate, leading to very delicate, if at all achievable, operation.

In literature, one option described for fixed beds in oxidative coupling is to use the catalyst particles as oxygen carriers, so that feed flow can be switched between air (oxygen) and methane. However, typically the ability of the catalyst to store oxygen is very limited [Lun00, MB95]. Hence this option is not considered.

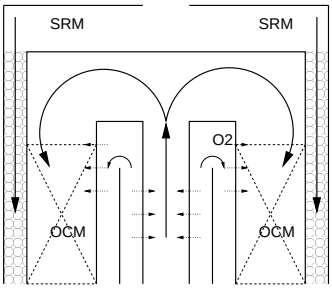

Figure 6.1.: Dead end reactor concept

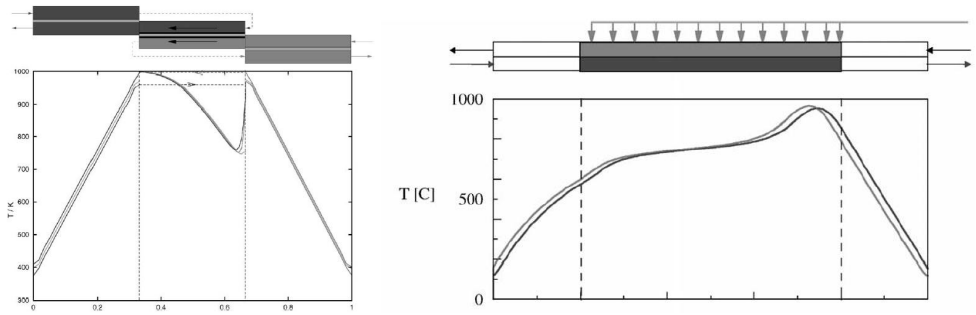

Figure 6.2.: Effect of cocurrent of methane combustion and steam reforming with cofeed of oxygen (left) or distributed feed of oxygen (right), as demonstrated by Kolios et al. [KFE02] Figure by Kolios et al.

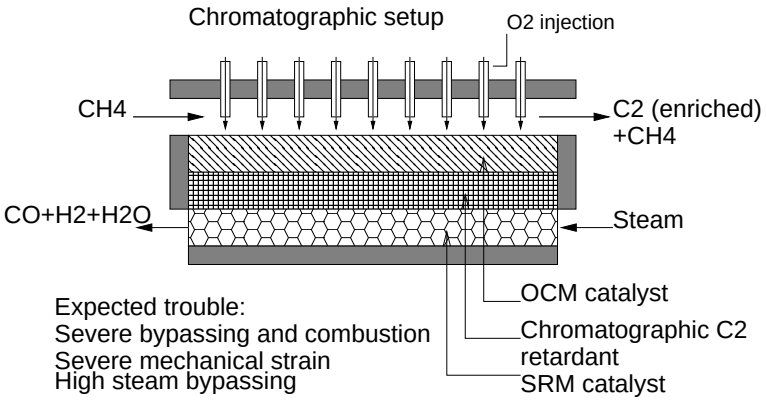

Figure 6.3.: Reactor concept with separation in situ, based on chromatographic principles

6.1.1. Chromatographic reactor

Based on the work of Tonkovich et al. [TCA93], figure 6.3 shows a reactor with a chromatographic separation section. The chromatographic section is supposed to work as a membrane: due to differences in ease of permeance, methane is selectively transported to the SRM section, favouring C_2 concentration in the OCM section. In the OCM section oxygen is distributed through the inlets shown at the very top of the setup.

Despite of the nice concept, the design is expected not to work in reality, partly due to the reasons already given in the figure.

6.2. Tubular fluidized reactor

The idea of the reactor setup as shown in figure 6.4 is as follows:

- The SRM reaction is considered to proceed until equilibrium. This is why backmixing is not an issue for this reaction and the choice has been made to fluidize the SRM catalyst

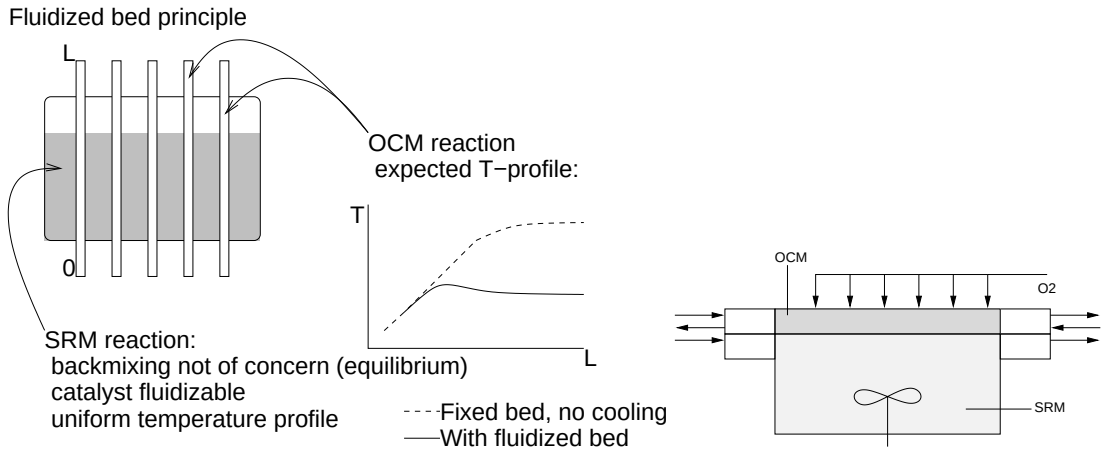

Figure 6.4.: Reactor concept with the SRM catalyst in the fluidized state and the OCM catalyst in a packed bed state, placed within tubes cooled by the fluidized bed. The concept shown assumes cofeed of oxygen and methane in one flow direction. Variants are the use of distributed feed of oxygen, possibly with the addition of reverse flow operation for the oxidative coupling, as shown on the right.

instead of that for OCM.

- At this point, it is assumed that the SRM catalyst can be readily fluidized.
- There is a uniform temperature within the fluidized bed. Hence, the temperature profile within the catalyst tubings is dampened at the hot spot, but the temperature is not significantly reduced in other parts of the tubes (as would be the case for example if cooling intensity were uniform), so that a flattened temperature profile evolves.
- The OCM catalyst in many cases cannot be fluidized; this is why it is preferred to place this catalyst in a fixed bed; moreover there is the risk of backmixing of products.

Fluidization has been reported as a concept for steam reforming [Sti04].

The intended configuration of the tubes is for example shown on page i. The tube in which the exothermic reaction occurs is on the outside in order to enhance transport of heat to the fluidized bed. A variant of the tubes, including distributive feed of oxygen, is shown in figure 6.5. This is intended for reverse flow operation.

6.3. Selected concept

The reactor of choice is the concept given in section 6.2. This avoids the possible very steep temperature gradients and separation of reaction zones as given in the work of Kolios et al. [KFE02] for fixed bed reactors. The chosen reactor concept is very simple and can be imagined to be a fluidized bed with some heating pipes that can be switched on and off. This is a familiar concept in process industry, although the tubes may also be used for cooling. No delicate operation in order to match the reaction fronts is needed, since the reaction front of the steam reforming is basically uniform. If straight tubes are used, the building of the conceptual reactor can be very

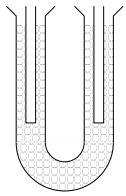

Figure 6.5.: Curved tube with distributed feed of oxygen for application in a fluidized bed. Intended for reverse flow operation.

similar to that build for Smit [Smi06], extended with a fluidized bed, both for which experience is available within the group. A tube for distributed feed as described by Smit can be used to obtain a low oxygen partial pressure for the oxidative coupling. In short, this concept of all considered corresponds best to the boundary conditions as highlighted in table 3.1.

Now that a choice for a reactor concept has been made, numerical (quantitative) evidence for the conceptual operability of this (lab-scale) reactor is needed. The next chapter is about how this information will be obtained. Of special interest is also the theoretical yield of the OCM reaction, which in any concept found in literature was too low for economical operation.

Part III.

Demonstration of concept

7. Reactor model

The final reactor concept is based on the principle shown in figure 7.1, which is basically the mathematical representation of the concept shown in figure 6.4 shown on page 23. Because it is desired to have the inlet and outlet temperature at about the temperature of the fluidized bed and to have a high temperature peak in between, it was expected that reverse flow will be needed in order to obtain a cyclic steady state for the location of the temperature peak. Hence a model capable of calculating reverse flow operation is implemented straight away in order to evaluate the possible benefits.

7.1. Dynamic model

Mathematically, the reactor shown in figure 7.1 is considered a reactor consisting of one or two concentric tubes filled with catalyst and/or catalytic particles. If present, the inner tube supplies oxygen to the outer tube according to the distributed feed principle as described by Smit [Smi06], although in the current case the flow is from the inside to the outside instead of the other way around, as was used by Smit. The surroundings of the outer tube can be either a perfectly isolated wall or a fluidized bed at a constant temperature and with a fixed heat transfer coefficient.

The model is based on an advanced in-house developed code, based on the principles as described by Joris Smit [Smi06]. This model can dynamically solve convection-diffusion equations with associated reactions and incorporates heat effects. It is a 1-D model with respect to space and currently does not take into account intraparticle diffusion limitations for the catalyst. Central assumptions are [Smi06]:

- "Radial temperature and concentration gradients in the compartments were ignored. [...] only the development of the axial temperature profiles was investigated. [...] Nevertheless, the differences in tube and shell temperature were accounted for via overall heat transfer coefficients.

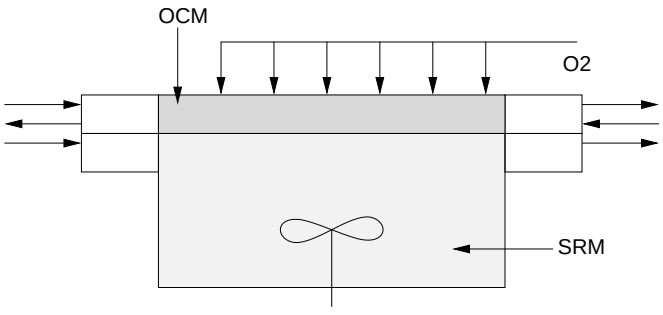

Figure 7.1.: Mathematical representation of the combination of the reverse flow reactor with a fluidized bed

- To reduce computational time a homogeneous model was adopted for the description of the thermal behaviour of the reactor."

Opposed to the model as used by Smit, the current model does take into account the accumulation terms for the mass transport. These were left in for practical reasons in order to be able to show the mass transport, but were overruled most of the time as described in appendix H because the component balances adjust typically at a much smaller timescale after a switch in flow direction than the temperature profiles do. (Typically 1s versus 300s in real time.)

Amongst others, the model includes after modification by the author:

1. Kinetics as described by Stansch et al. [SMB97]. The calculated kinetics have been validated by comparing with results as given by Stansch et al. and by comparing with the results of an individual experiment performed by Stansch et al. as given by Tye et al. [TMB02]. This was possible because basically the experimental setup as used by Stansch is also a tube surrounded by a fluidized bed. The results generally fall within the 20% error margin as indicated by Stansch. It was also found that changing the reaction rate of the thermal dehydrogenation of C_2H_6, for which it is unclear whether Stansch relates this to the gas volume or to the entire catalytic bed volume, does not significantly affect the results.

2. Heat effects of the reactions as described by Stansch. This has been validated by comparing the results of stoichiometric reactions with results as obtained with Aspen. Every reaction was considered separately for a stream diluted with nitrogen. (The latter was done in order to reduce the calculated temperature change.)

3. Addition of the physical properties of CaO, the catalyst carrier, as described in appendix F.

Further information on validation can be found from appendix A. Relations for amongst others the pressure drop and axial transport of heat by convection were not validated because these have been validated in other projects and were not modified.

Table 7.1.: Conservation equations of the High Switching Frequency Model (HFSM). “s” stands for shell tube (the outer tube), “t” stand for tube side (the inner tube).

Mass conservation equations, forward direction ($\rightarrow$)

$$\frac{\partial\left(\rho^s_{g,\rightarrow}v^s_{g,\rightarrow}\right)}{\partial z} = +\left\langle M^t_{\rightarrow}\right\rangle \frac{2\pi r_i}{\pi r^2_{i,s}-\pi r^2_{o,t}} J_{\rightarrow}$$

$$\frac{\partial\left(\rho^t_{g,\rightarrow}v^t_{g,\rightarrow}\right)}{\partial z} = -\left\langle M^t_{\rightarrow}\right\rangle \frac{2}{r_i} J_{\rightarrow}$$

$$\rho^t_{g,\rightarrow}v^t_{g,\rightarrow}\frac{\partial w^t_{j,g,\rightarrow}}{\partial z} = \frac{\partial}{\partial z}\left(\rho^t_{g,\rightarrow}D^t_{ax,j,\rightarrow}\frac{\partial w^t_{j,g,\rightarrow}}{\partial z}\right) + r^t_{j,g,\rightarrow} - \varepsilon^t_g\frac{\partial \rho^t_{g,\rightarrow}w^t_{j,g,\rightarrow}}{\partial t}$$

$$\rho^s_{g,\rightarrow}v^s_{g,\rightarrow}\frac{\partial w^s_{j,g,\rightarrow}}{\partial z} = \frac{\partial}{\partial z}\left(\rho^s_{g,\rightarrow}D^s_{ax,j,\rightarrow}\frac{\partial w^s_{j,g,\rightarrow}}{\partial z}\right) + \frac{6\left(1-\varepsilon^s_g\right)}{d^s_p} j^s_{j,\rightarrow} + \left(1-w^s_{j,g,\rightarrow}\right)\left\langle M^s_{\rightarrow}\right\rangle \frac{2\pi r_{i,s}}{\pi r^2_{i,s}-\pi r^2_{o,t}} J_{\rightarrow} - \varepsilon^s_g\frac{\partial \rho^s_{g,\rightarrow}w^s_{j,g,\rightarrow}}{\partial t}$$

$$0 = -\frac{6\left(1-\varepsilon^s_g\right)}{d^s_p} j^s_{j,\rightarrow} + r^s_{j,s,\rightarrow}$$

For the backward direction similar equations apply, indicated with ($\leftarrow$).

7.2. The high frequency switching model (HFSM)

For the limiting case of very short switching times in a reverse flow reactor, the HFSM can be implemented. In this limiting case, the reverse flow reactor approximates a countercurrent reactor, as was described by Nieken et al. [NKE95]. This allows quick calculation of the cyclic steady state, as was described by Smit [Smi06]. The method of implementation as given by Smit has been followed and is not repeated here. A further improvement could be the application of symmetrical boundary conditions, so that the number of required grid cells can be cut in half, but it is thought that elaborating this part of the scheme would require more time than it saves in calculation time, so that this step is not taken. Some other measures to accelerate convergenge however were taken and are described in appendix H.

The core difference between a countercurrent reactor and the HFSM approximation, is that both flows share the same energy balance for the HFSM, whereas in a countercurrent reactor each tube has it’s own energy balance.

The governing equations for the HFSM model are shown in tables 7.1 and 7.2; these were directly taken from the work of Smit [Smi06]. For the present work these were modified to take into account two concentric cylinders instead of a cylinder in a square beam. Also, as for the dynamic model, an accumulation term for mass is present. The reaction is supposed to take place in the shell tube. The equations for the dynamic model can be easily derived from these by eliminating the averaging procedure from the equations for the energy balance. It can then simulate reverse flow by periodically changing the boundary conditions.

A graphical representation of the HFSM discretisation, in this case for a uniform grid with uniform heat production consisting of 8 grid cells, is shown in figure 7.2.

Table 7.2.: Energy conservation equations of the High Switching Frequency Model (HSFM).

Energy conservation equations:

$$\left(\frac{1}{2}\varepsilon_g^s\left(\rho_{g,\rightarrow}^s C_{p,g,\rightarrow}^s+\rho_{g,\leftarrow}^s C_{p,g,\leftarrow}^s\right)+\rho_{bulk}^s C_{p,s}^s\right)\frac{\partial T^s}{\partial t}=$$
$$-\frac{1}{2}\left(\rho_{g,\rightarrow}^s v_{g,\rightarrow}^s C_{p,g,\rightarrow}^s+\rho_{g,\leftarrow}^s v_{g,\leftarrow}^s C_{p,g,\leftarrow}^s\right)\frac{\partial T^s}{\partial z}+\frac{1}{2}\frac{\partial}{\partial z}\left(\left(\lambda_{eff,\rightarrow}^s+\lambda_{eff,\leftarrow}^s\right)\frac{\partial T^s}{\partial z}\right)$$
$$-\frac{1}{2}\sum_j\left(\frac{r_{j,g,\rightarrow}^s}{M_j}H_{j,g,\rightarrow}^s+\frac{r_{j,g,\leftarrow}^s}{M_j}H_{j,g,\leftarrow}^s\right)+\frac{\pi r_{i,s}\left(\alpha_{\rightarrow}^{s-tw}+\alpha_{\leftarrow}^{s-tw}\right)}{\pi r_{i,s}^2-\pi r_{o,t}^2}\left(T^{tw}-T^s\right)$$
$$+\frac{\pi r_{o,s}\left(\alpha_{\rightarrow}^{s-ow}+\alpha_{\leftarrow}^{s-ow}\right)}{\pi r_{i,s}^2-\pi r_{o,s}^2}\left(T^{ow}-T^s\right)$$

$$\left(\frac{1}{2}\varepsilon_g^t\left(\rho_{g,\rightarrow}^t C_{p,g,\rightarrow}^t+\rho_{g,\leftarrow}^t C_{p,g,\leftarrow}^t\right)+\rho_{bulk}^t C_{p,s}^t\right)\frac{\partial T^t}{\partial t}=$$
$$-\frac{1}{2}\left(\rho_{g,\rightarrow}^t v_{g,\rightarrow}^t C_{p,g,\rightarrow}^t+\rho_{g,\leftarrow}^t v_{g,\leftarrow}^t C_{p,g,\leftarrow}^t\right)\frac{\partial T^t}{\partial z}+\frac{1}{2}\frac{\partial}{\partial z}\left(\left(\lambda_{eff,\rightarrow}^t+\lambda_{eff,\leftarrow}^t\right)\frac{\partial T^t}{\partial z}\right)$$
$$-\frac{1}{2}\sum_j\left(\frac{r_{j,g,\rightarrow}^t}{M_j}H_{j,g,\rightarrow}^t+\frac{r_{j,g,\leftarrow}^t}{M_j}H_{j,g,\leftarrow}^t\right)+\frac{\left(\alpha_{\rightarrow}^{t-tw}+\alpha_{\leftarrow}^{t-tw}\right)}{r_{i,t}}\left(T^{tw}-T^t\right)$$

$$\rho_s^{tw}C_{p,s}^{tw}\frac{\partial T^{tw}}{\partial t}=\frac{\partial}{\partial z}\left(\lambda^{tw}\frac{\partial T^{tw}}{\partial z}\right)+\frac{r_{o,t}\left(\alpha_{\rightarrow}^{s-tw}+\alpha_{\leftarrow}^{s-tw}\right)}{r_{o,t}^2-r_{i,t}^2}\left(T^s-T^{tw}\right)$$
$$+\frac{r_{i,t}\left(\alpha_{\rightarrow}^{t-tw}+\alpha_{\leftarrow}^{t-tw}\right)}{r_{o,t}^2-r_{i,t}^2}\left(T^t-T^{tw}\right)$$

$$\rho_s^{sw}C_{p,s}^{sw}\frac{\partial T^{sw}}{\partial t}=\frac{\partial}{\partial z}\left(\lambda^{sw}\frac{\partial T^{sw}}{\partial z}\right)+\frac{r_{o,s}\left(\alpha_{\rightarrow}^{fb-sw}+\alpha_{\leftarrow}^{fb-sw}\right)}{r_{o,s}^2-r_{i,s}^2}\left(T^{fb}-T^{sw}\right)$$
$$+\frac{r_{i,s}\left(\alpha_{\rightarrow}^{s-sw}+\alpha_{\leftarrow}^{s-sw}\right)}{r_{o,s}^2-r_{i,s}^2}\left(T^s-T^{sw}\right)$$

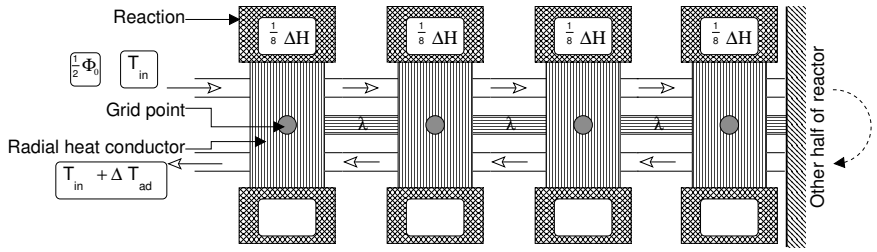

Figure 7.2.: Grapical representation of the discretisation scheme used for the HFSM

8. Design Calculations on reverse flow membrane reactor

This chapter presents a structured approach towards obtaining an acceptable performance configuration for the design chosen. Cofeed calculations from literature studies already indicate the bad selectivity and high temperature excursions. These were also found from initial calculations for cofeed (not shown) and thus cofeed operation was not further considered. First of all steady-state solutions for conventional single direction flow membrane reactors operated at assumed isothermal conditions are shown. Different reactor lengths will be evaluated for a fixed feed ratio of oxygen and methane, initially with fixed mass flux of oxygen (and methane). In order to shown only the influence of the oxygen flux on the reaction kinetics, the pressure was set constant for these simulations (only). At the same time, however, in reality the pressure drop over the reactor increases as the length increases. A trade-off has to be chosen here.

The result will be a tube of a length for which no significant benefit from further increasing the tube length, at the cost of a higher and possibly severe pressure drop, will be expected. For the configuration chosen the ratio CH_4:O_2 will be set to 4, which is the stoichiometric ratio of the main desired reaction, reaction 2.2. It may be desirable to change this ratio because part of the oxygen is lost to for example the consecutive oxidative dehydrogenation or for other reasons than the desire for high yield. Hence results for a ratio CH_4:O_2 of 3 are given as well. The cooling requirement along the tube can be calculated by evaluating the change in enthalpy over the length. Given an overall heat transfer coefficient from the tube internals to the bed, the required temperature difference between the tube internals and the bed can be estimated.

8.1. Yield vs. tube length

As initial parameters, the parameters as shown in table 8.1 were used. In the current study, in order to phase out any mixed effects, isothermal and isobaric conditions are implied. The overall mass feed of both oxygen and methane is also constant. However, their ratio is varied as described in appendix N, in which also the tube radii can be found. For consecutive calculations however the ratio of CH_4:O_2=4 will be maintained.

In order to keep the overall mass flow of oxygen into the catalyst section constant, the membrane flux was adjusted according to equation 8.1. The mass flux of methane is constant by default because the flux is set and the inlet surface is constant.

$$\phi_m = \frac{\Phi_{n,O_2,memb}}{\pi \cdot (d_m + 2 \cdot d_{w,m}) \cdot F_p \cdot L_{cat}} \tag{8.1}$$

From figures 8.1, 8.2 and 8.3 it can be seen that the mole fraction in the outlet flow reaches an optimum at another length than the yield with respect to methane. The value of considering the outlet mole fraction, however, is not as big as considering the yield. As far as the separations are concerned, a more realistic indication of the ease of operation is considering the mole fraction of C_2 *after* H_2O and CO_2 have been removed, since the separation of these two components is generally considered to be relatively easy and must be done before the (more severe) separation of C_2 product.

It can be seen that the yield, after increasing with increasing tube length (which can be explained by a decreasing average oxygen mole fraction), comes to an optimum and next drops

Table 8.1.: First guesses for parameters for demonstration of the effect of lengthening the tube on yield

Variable	Value	Comment
T	810 and 780 $^{\circ}\mathrm{C}$	Isothermal conditions implied. Evaluated for both ends of region of operation to evaluate sensitivity.
P	1.2 bar	
$\frac{\Phi_{n,\mathrm{CH_4}}}{\Phi_{n,\mathrm{O_2}}}$	4 or 3	See also appendix N.
$\Phi_{n,\mathrm{CH_4},tube}$	3.8 or 3.4 $\mathrm{mmol/s}$	
d_m, $d_{w,m}$, d_c	0.011 or 0.0129, 0.001,0.025 m	Retain high L/d ratio for 1D approximation. Radial transport not yet considered.
$F_p = \frac{L_m}{L_{cat}}$	Primarily $\frac{2}{3}$	< 1 to prevent O_2 breakthrough.
Dil	0.1	Catalyst diluted 10 times

(which can be ascribed to consecutive reactions). To obtain a reasonable yield without over stretching the length of the catalytic section a length of $1\mathrm{m}$ is chosen, anticipating an additional pressure drop from inert sections. Please not that the yield predicted for this case is higher than the best obtained experimental yield. More on this in chapter 10.

Figure 8.4 shows the mole fraction of C_2 product in a hypothetical product stream from which all H_2O and CO_2 have been removed. It is clear that also in this respect a length of $1\ \mathrm{m}$ is not a bad choice. The ratio of mole fractions for this length, for a uniform temperature of 810 $^{\circ}\mathrm{C}$and CH_4: O_2=4, is given by $O_2 : CO_2 : H_2O : CH_4 : CO : H_2 : C_2H_4 : C_2H_6 = 0.000 : 0.025 : 0.342 : 0.397 : 0.003 : 0.052 : 0.157 : 0.024$.

Without showing the exact results, it is given here that the calculated pressure drop for a catalyst section with a length of $5\mathrm{m}$ is in the order of $0.2\mathrm{bar}$, which is the maximum considered acceptable. Hence, the preference for a high yield prevails over the constraint for pressure drop in this case. If the total flow through the tube would be increased, this situation could turn around.

From figures 8.1 until 8.4 it is also seen that changing the CH_4:O_2 ratio from 4 to 3 could have some advantages, too. The yield remains about the same and the mole fractions of C_2 product after removal of CO_2 and H_2O are more advantageous than for the case of a ratio of 4:1. Additionally, the increase of oxygen flux and the decreased selectivity collaborate in increasing the heat production per tube, which in certain cases could come in handy. However, the selectivity dramatically drops. When using conventional separation technologies, the CO_2 and H_2O separated from the C_2-rich stream can be considered waste. For the current work a ratio of 4:1 is set, mainly based on the requirement that unconverted methane is needed after OCM completion in order to be able to operate the fluidized bed. Increasing the ratio CH_4:O_2, as far as it is allowable as far as safety is concerned (since at present the lower explosion limit is unknown), remains an option to be kept in mind.

8.2. Cooling

Up to now isothermal and isobaric conditions have been implied. In reality, the temperature difference between the fluidized bed and the tube is the driving force for the cooling. The

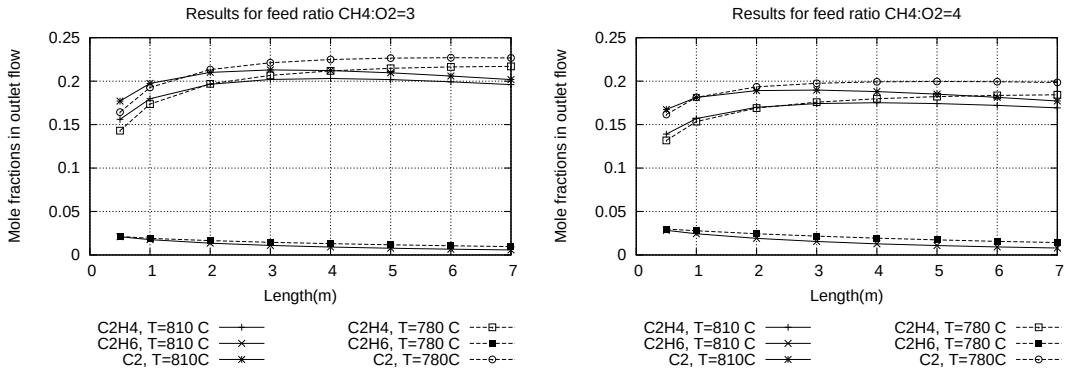

Figure 8.1.: Outlet product mole fraction as a function of reactor length for isothermal reaction conditions as indicated in table 8.1. Left for molar feed ratio CH_4:O_2=3, right for CH_4:O_2=4.

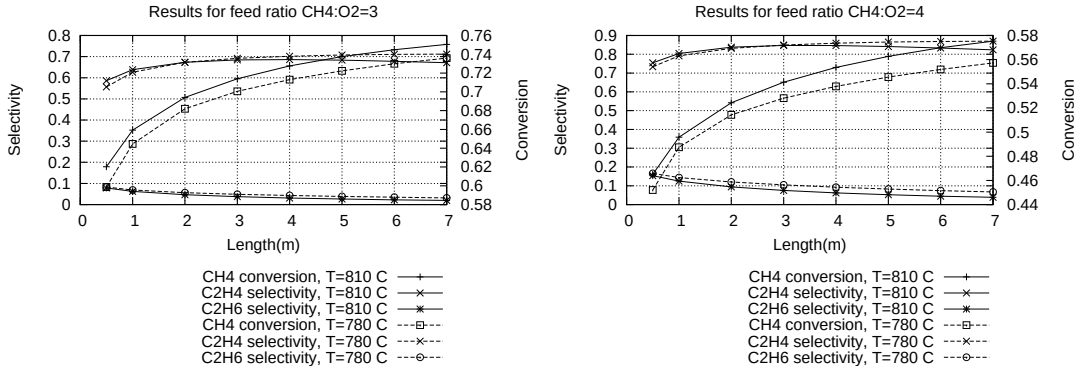

Figure 8.2.: Product selectivity and CH_4conversion as a function of reactor length for isothermal reaction conditions as indicated in table 8.1. Left for molar feed ratio CH_4:O_2=3, right for CH_4:O_2=4.

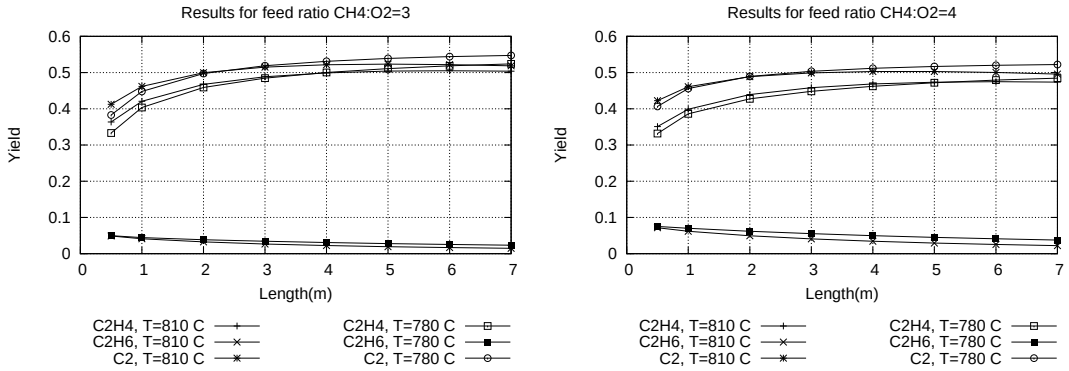

Figure 8.3.: Outlet product yield as a function of reactor length for isothermal reaction conditions as indicated in table 8.1. Also because of intention for lab application. Left for molar feed ratio CH_4:O_2=3, right for CH_4:O_2=4.

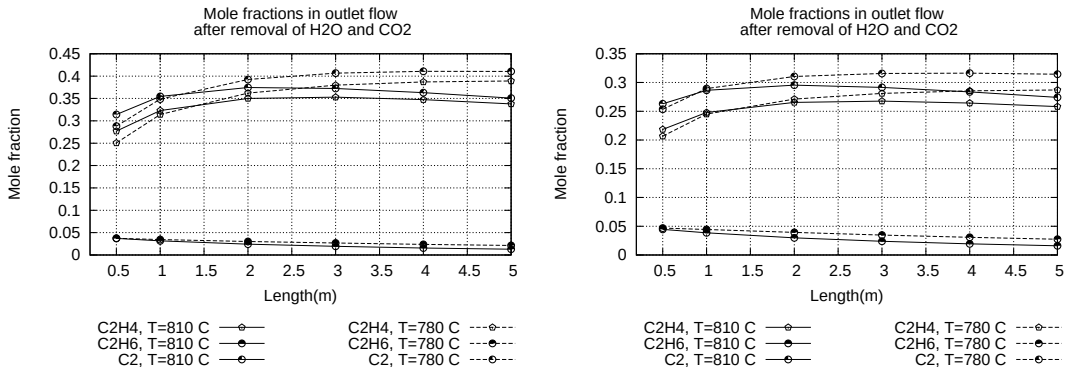

Figure 8.4.: Mole fraction of C_2 in a hypothetical product stream after removal of all H_2O and CO_2 product. Left for molar feed ratio CH_4:O_2=3, right for CH_4:O_2=4

absolute value of the amount of cooling required is given by the total reaction enthalpy released, which can be adjusted by changing the absolute and/or relative mass flows. At the same time, extinguishing the desired reaction must be prohibited, thus the temperature in the reaction zone must stay in the range of 800°C. Full extinguishing of the OCM reactions is prohibited if the temperature of the fluidized bed is controlled to be at most 30°C lower than that of the OCM catalyst section. The latter maximum allowable temperature difference was also chosen for mechanical reasons.

The cooling requirement for each section of the tube can be evaluated by evaluating the change in enthalpy over the length of tubing, given an imposed constant temperature. The heat production (evaluated with imposed absence of heat transfer between the catalyst and the walls to avoid cluttering of the results by accumulation in the wall) is then compared with the temperature difference required to obtain the proposed state of operation per location. For these calculations the isobaric constraint has been relieved.

For calculating the cooling capacity, the choice is made to use only a very rough flat plate approximation; the overall heat transfer resistance is then given by equation (8.2). (Heat transfer resistance inside the tube wall is neglected.)

$$\frac{1}{\alpha_{cb,fb}} = \frac{1}{\alpha_{cb,w}} + \frac{1}{\alpha_{w,fb}} \tag{8.2}$$

The heat transfer coefficient from the wall to the fluidized bed, $\alpha_{w,fb}$ is estimated to be 350 $\mathrm{W/m^2/K}$, based on the work of Kunii and Levenspiel [KL91]. The heat transfer from the fixed bed to the tube wall is expected to be the limiting step. However, when calculating the heat transfer from the fixed bed to the tube wall using the Dixon-Cresswell [DC79] approach as was proposed by Smit [Smi06], trouble occurs, since a heat transfer coefficient in the order of 500 $\mathrm{W/m^2/K}$ is predicted. Looking at the order of magnitude of the different contributions it was found that for small tube diameters the heat transfer coefficient as calculated is strongly dependent on the tube radius. Indeed, when setting the tube diameter to the order of 5 cm a more realistic (but still high) value of about 300 $\mathrm{W/m^2/K}$ is obtained. In fact, Dixon and Cresswell [DC79] comment on the absence of thorough knowledge in the case of low d_t/d_p ratio, although in their case they specifically point to axial instead of radial dispersion. In order to be able to proceed with the demonstration of the principle, the overall heat transfer coefficient from bed to wall is set constant at 300 $\mathrm{W/m^2/K}$. However of course before actually building a reactor the real properties of this parameter will have to be elucidated.

So given these chosen parameters, it can now be calculated that the overall heat transfer coefficient for the given approximation is:

$$\frac{1}{\alpha_{cb,fb}} = \frac{1}{300} + \frac{1}{350} \approx \frac{1}{161}\mathrm{m^2K/W} \tag{8.3}$$

Reflecting the actual method of calculation used in the model, quantities are now evaluated per $\mathrm{m^3}$ of a particular reactor section. To calculate the cooling capacity per $\mathrm{m^3}$ catalyst section, first the cooling surface per $\mathrm{m^3}$ is needed. Neglecting the thickness of the outer tube wall, this is given by the outer circumference of the catalyst section divided by it's cross surface.

$$Av_{fb} = \frac{d_{c,o}}{\frac{1}{4}\left(d_{c,o}^2 - d_{c,i}^2\right)} = \frac{0.025}{\frac{1}{4}\left(0.025^2 - 0.013^2\right)} = 219\mathrm{m^2/m^3} \tag{8.4}$$

Now the cooling capacity can be estimated from:

$$Q_c = Av_{fb} \cdot \alpha_{cb,fb} \cdot \Delta T = 219 \cdot 161 \cdot 30 = 1.354\mathrm{MW/m^3} \tag{8.5}$$

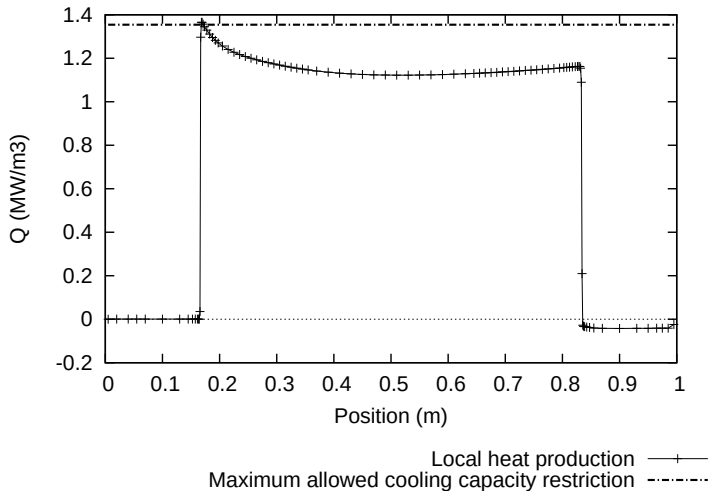

Figure 8.5.: Local heat production by reaction with parameters as given in table 8.1, a molar feed ratio of CH_4: O_2= 4 and a reactor length of $1\mathrm{m}$

The results for the hypothetical case described before is shown in figure 8.5. It can be seen that (due to the use of the distributive feed) *the heat production is relatively uniform*; this fits well with the assumed approach of a uniform temperature of the outer wall since this will result in a relatively *uniform temperature difference* between the wall and catalyst.

8.3. Demonstration of the membrane reactor

The next step is to include heat transfer into the model. At this point the model is operated with flow in only one direction with the gas entering at the temperature of the fluidized bed. An example of the resulting temperature- and composition profile is shown in figures 8.6 and 8.7.

It can be seen that the estimation of the temperature difference obtained with the given mass fluxes has been quite good, since the temperature difference is indeed about 30 $^{\circ}\mathrm{C}$. The resulting temperature profile is, as expected from the quite evenly distributed heat production and constant external temperature, quite homogeneous. It is also seen that the thermal contact of the *entire* catalytic section, including the part where there is no oxygen flux, results in an outgoing temperature about equal to that of the fluidized bed. The same was observed (not shown) for the case of a somewhat lower inlet temperature; the fluidized bed then heats up this feed before the reaction sets in. It is therefore thought that for initial calculations it is safe to proceed with a single direction flow model. Due to the very fast reaction, the oxygen mole fraction is practically zero. Reverse flow calculations will be done in a later stage, in order to evaluate:

- The case where the part of the catalytic bed without oxygen feed is not in thermal contact with the fluidized bed. Thus the temperature of the gas entering the fluidized bed can in principle very easily differ from that of the fluidized bed.
- The effect of switching flow direction on product composition and the temperature profile.

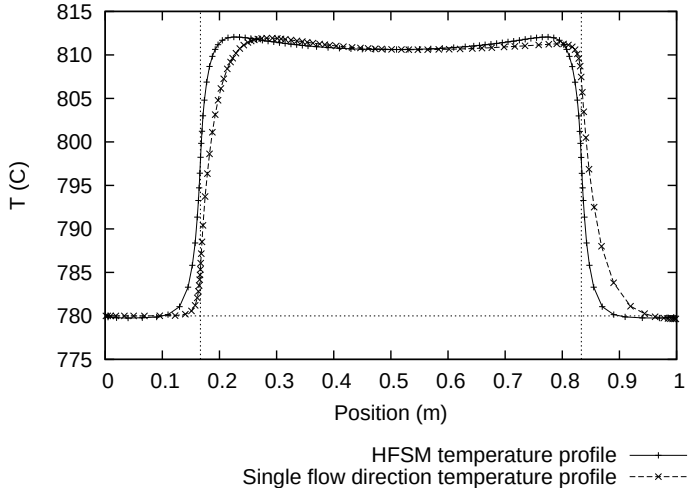

Figure 8.6.: Example of calculated temperature profile for membrane oxygen flux. Parameters shown in table 8.1 and for feed ratio CH_4: O_2=4. For both HFSM and single direction flow.

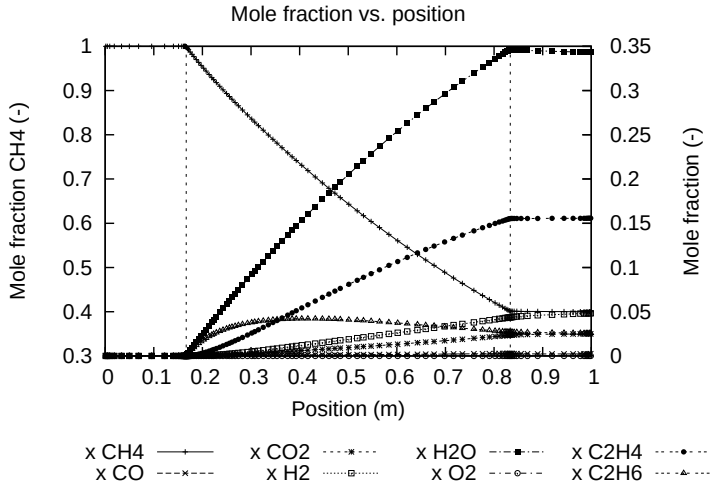

Figure 8.7.: Example of calculated gas phase composition for membrane oxygen flux as originally proposed

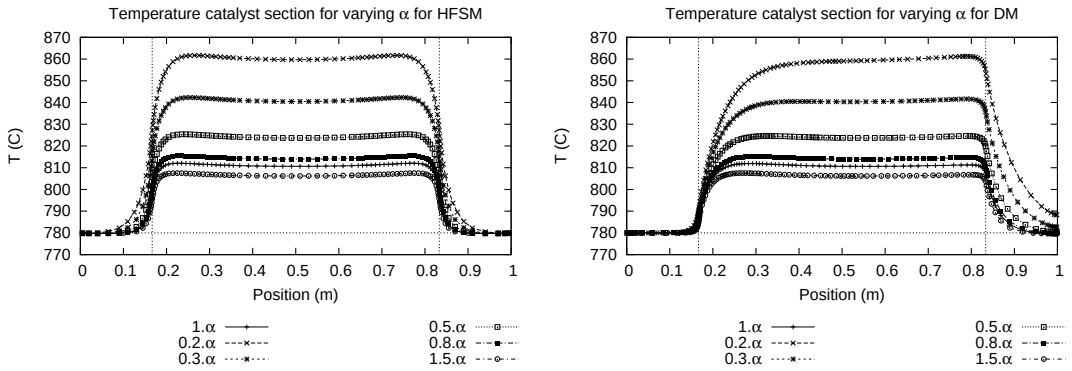

Figure 8.8.: Effect of varying α_{bw} on temperature profiles for HFSM (left) and single flow direction (right).

Of special interest is the duration of this effect, as well as any influence of increasing the length of the reactor.

It has also been tested what are the effects and duration of a switch in flow direction. Such a test was typically started after a steady state for single flow direction was reached. It was found that the mass balances adjust to the flow direction on a time scale of a few seconds, whereas for the temperature profile to become steady again it takes a few hundred seconds. The results are not shown. Because of the relatively low influence on simulation results, this finding has been used to increase the speed of the numerical code. This is described in appendix H.

8.3.1. Changing $\alpha_{w,fb}$

Previously, for the heat transfer coefficient from fluidized bed to tube wall a value of $\alpha_{w,fb} = 350\mathrm{W/m^2/K}$ was chosen. It's exact value, however, is unknown. The goal of this section is to evaluate how important this is by varying *only* this variable for the base case as given in table 8.1 with CH_4: O_2=4.

First, the primarily affected variable, temperature, is considered. The effect is shown in figure 8.8, for both the HFSM calculation as the DM calculation that directly followed it. (Steady state was reached.) It is seen that only a very significant reduction of the heat transfer coefficient (a factor a half) results in a significant effect on temperature.

Next, the effect on product composition at the end of a cycle of the DM is compared. The mole fractions for C_2H_4 and C_2H_6 are plotted in figure 8.9. The factor x given in $x.\alpha$ is the factor with which the coefficient has been multiplied. The product distribution is not very severely affected. Also, CH_4 conversion does not differ more than 1% over the range evaluated (not shown). Therefore it is considered valid to set α_{bw} to a fixed value for the range considered.

The other heat transfer coefficient ($\alpha_{cb,w}$) in equation (8.2) is of a similar, if not even more inexact, nature. Since the chosen value is in the same range as that of $\alpha_{w,fb}$ and the inner surface of the tube is of similar magnitude as it's outer surface, similar effects on the results of the 1D-model can be expected from modifying this variable.

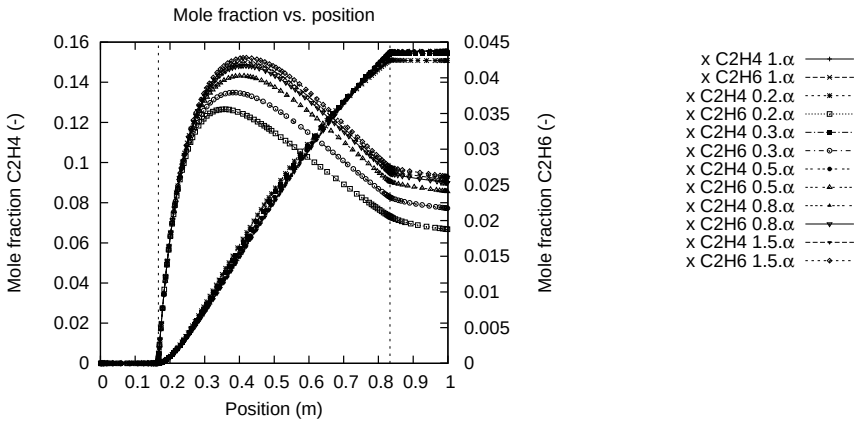

Figure 8.9.: Mole fractions of C_2H_4 and C_2H_6 as a fucntion of the heat transfer coefficient α_{bw}. Note the two individual axis for the y-scale.

8.3.2. Length of inert sections

The minimum length of the inert sections, required for letting the temperature of the entering gas streams be within reasonable approximation of that of the fluidized bed when entering the catalytic section, is determined using the HFSM.

The main disadvantage of using inert sections is that the pressure drop increases. But in order to be able to enter the catalyst section with a reasonable temperature for a reasonably long switching time, a sufficiently long inert section is required; of course a trade-of has to be found here. In order to reduce the pressure drop in the inert sections, the particle diameter in these sections is set to 3 mm. For the acceptable outlet temperature (when the DM is invoked) a value of 200 $^{\circ}\mathrm{C}$ is chosen.

For the calculations, the choice was made to invoke the reactions too, to see if any possible side-effects occur. It can be seen from figure 8.10 that, as far as the HFSM is concerned, there is no significant effect on the temperature profile in the reaction of changing the length of the inert section. Figure 8.11 gives the results for the temperature profiles for the inert sections. In order to be on the safe side, a length of the inert section (per side) of $1\mathrm{m}$ is chosen, so that the switching frequency can be reduced and a margin of safety is built in for the case of non-pseudohomogeneous situations. For this case the overall pressure drop is in the order of $0.05\mathrm{bar}$. A desired outlet temperature below $200^{\circ}\mathrm{C}$ is desired and is achieved for this choice, as can be seen from the following paragraphs.

For the inert sections the diameter of the particles was set to $3\mathrm{mm}$ instead of the $2\mathrm{mm}$ for the catalyst section, in order to reduce the pressure drop. The material for the inert particles was alumina, that of the catalytic bed was the carrier material of the catalyst, CaO.

8.4. Effect of switching time on results

Given a length of inert section, changing the switching time for the concept studied primarily results in a different inlet temperature. Hence, a good estimate can be obtained from two separate, quickly-calculated simulations:

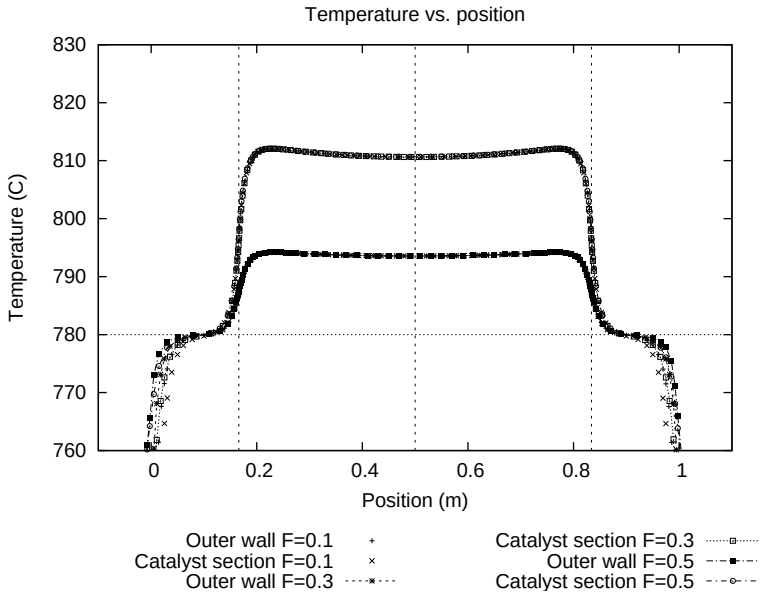

Figure 8.10.: Detail of the calculated temperature profiles for the HFSM solution for the base case with different length of inert sections. F is the fraction of the total reactor length that is inert section

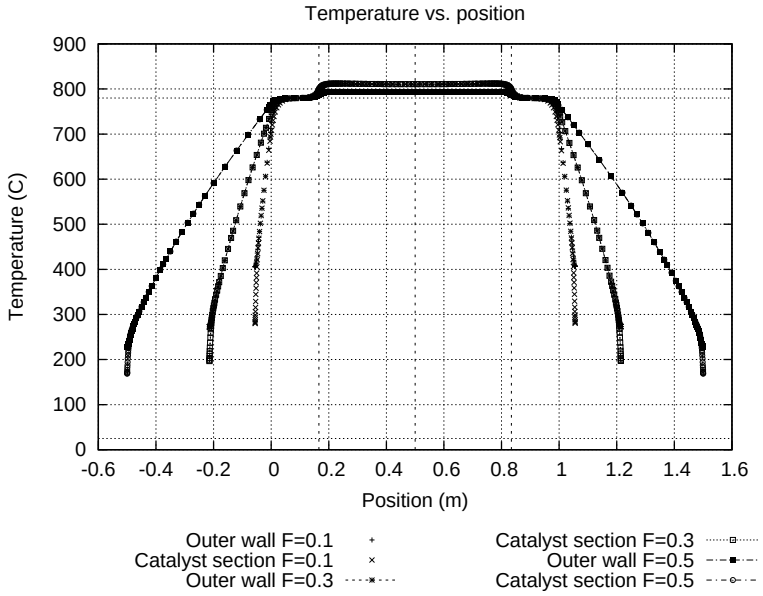

Figure 8.11.: Calculated temperature profiles for the HFSM solution for the base case with different length of inert sections. F is the fraction of the total reactor length that is inert section

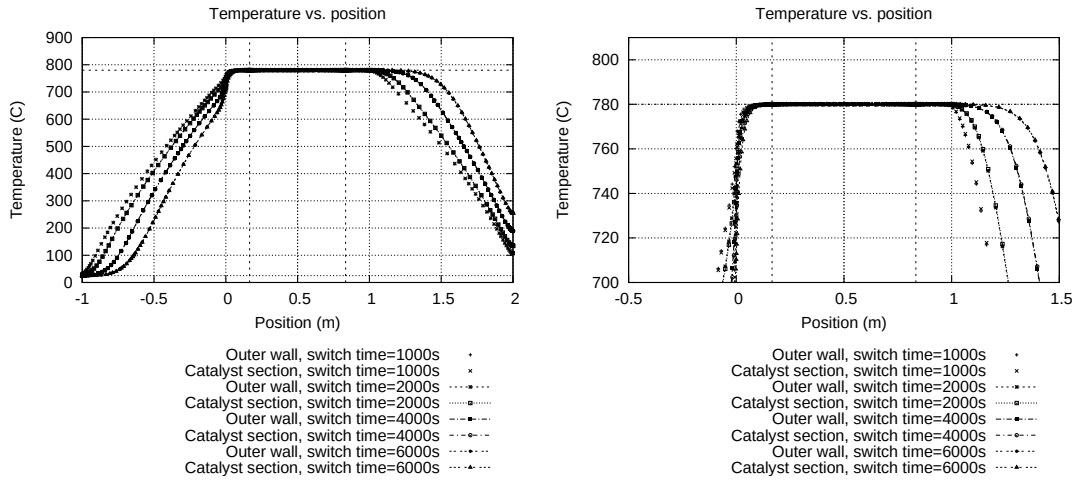

Figure 8.12.: Temperature profiles at the end of a cycle towards the right, after 59 switches from HFSM startup, as a function of switching time. Heating allowed for entire catalytic section. Simulation for simplified case without reactions and only two chemical components.

- DM simulations without any reactions. The number of components concerning the mass balances can be reduced to one or two. Used to study the temperature at the inlet of the catalytic section as a function of time.
- HFSM simulations for the catalytic section with different inlet gas temperatures.

8.4.1. Allowed switching time

In order to get a quick estimate of the allowed switching time taking into account the desires for fast quenching and an acceptable outlet temperature (and, if the fluidized bed would not sufficiently heat the reaction section, a sufficient inlet temperature) the model is run for just two chemical components (oxygen and methane) without reactions, greatly reducing the number of equations to be solved and greatly increasing the calculation speed. This can give a quick estimation of the movement of the velocity profiles, given a switching time, although of course the exact shape can slightly differ from the solution now obtained; at present only the order of magnitude is of interest. The result is shown in figure 8.12. This gives the indication that a switching time in the order of 4000s is acceptable (mainly based on the outlet temperature).

This figure already gives a hint at the result of the following subsection: the heating by the fluidized bed before the onset of reaction is so good that the reaction is not really affected by the inlet temperature into the reaction section.

8.4.2. Influence of inlet temperature on reaction

As can be seen from figure 8.13 for the current process setup the reaction is not severely affected by the temperature at which the gas enters the catalytic section. This is ascribed to the intense heating by the fluidized bed in the section prior to the onset of the reaction. Because the

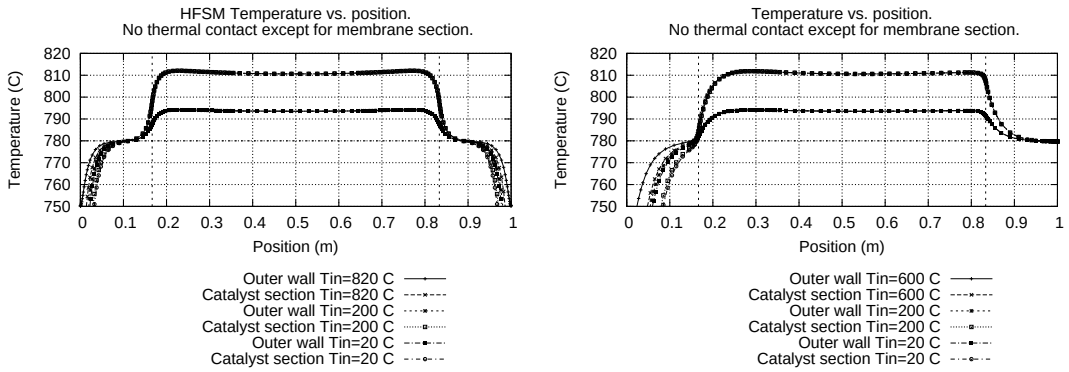

Figure 8.13.: Resulting temperature profiles for different inlet temperatures into the catalyst section. Entire catalytic section in contact with the fluidized bed. Left for HFSM and right for single flow direction (towards the right).

temperature for the reaction is not (seriously) affected, no special attention is given to the product distribution here; the results are hardly affected.

8.5. Application of cooling of only the reaction section

Although the usefulness in reality, considering the increase in complexity versus the relatively small temperature difference between the reaction section and the fluidized bed, can be rather limited, from an academic point of view it is very interesting to look at the situation in which there is no cooling except for the part in which the oxygen fluxes through the membrane.

Results of varying the ingoing temperature are shown in figure 8.14. This shows considerable penetration of a low temperature profile into the reaction zone. This especially unfeasible because it results in lower temperature in the region with high partial pressure of methane, resulting in a relatively high occurrence of the combustion reaction because of it's significantly lower activation energy. The adverse effects, however, are somewhat counteracted by the relatively long length of the reactor compared to the length of the zone with low temperature in this case.

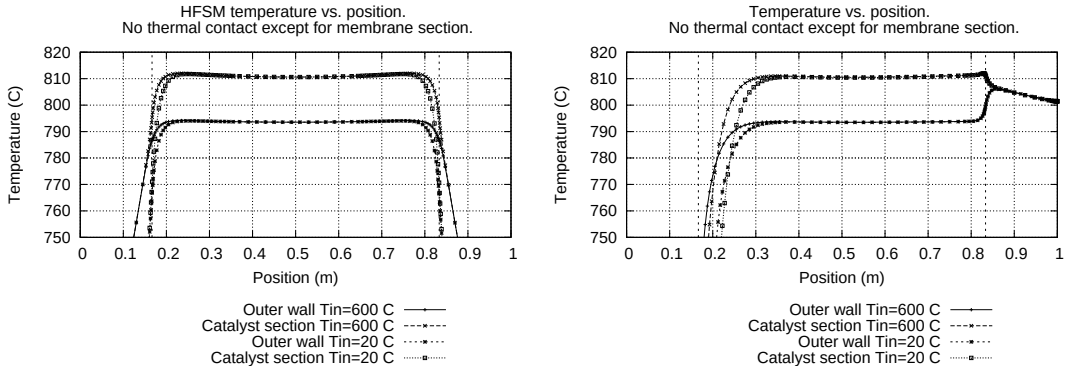

Figure 8.14.: Resulting temperature profiles for different inlet temperatures into the catalyst section. Only catalytic section fed by O_2 membrane in thermal contact with the fluidized bed. Left for HFSM and right for single flow direction (towards the right).

9. Full process considerations

9.1. Overall thermal efficiency

One of the major goals of the concept of the combination of steam reforming with oxidative coupling of methane is to arrive at an overall more or less autothermal process. This chapter focusses on if this can already be achieved with the base case chosen, and if not, in what direction a change is desired.

The heat production for OCM was calculated for a given inlet ratio of CH_4: O_2= 4 and a given outlet composition given in table 9.1.

From this stream both C_2H_4 and C_2H_6 are removed and steam is added until the ratio H_2O:CH_4 is 4. Then the ingoing stream with composition as shown in table 9.2 is obtained with an ingoing temperature of 100°C. For this stream, the equilibrium composition after steam reforming was calculated for different temperatures at 1bar; this is also given in table 9.2. The required data was taken from thermodynamic data tables [DD85] and the program used applied minimisation of the Gibbs free energy. Now for the given temperature and stream composition the enthalpies of the different ingoing- and outgoing streams can be calculated, and from this the heat requirement to perform steam reforming up to equilibrium for the given outlet temperature. The mass flow was based on the product flow of a single tube. From this, it was calculated that for steam reforming of the undesired product stream of OCM up to 500°C the heat requirement is 337W per tube and for the case of steam reforming up to 780°C the heat requirement is 688W per tube, respectively. For the calculations again the data provided by Daubert and Danner [DD85] were used.

It is obvious that when the fluidized bed for steam reforming is operated at 780°C the heat requirement of the fluidized bed for reforming the undesired product stream of the OCM tube exceeds the generation of heat by the tube. This shortage can be overcome by partially operating the fluidized bed as an autothermal reformer, by adding oxygen for partial combustion of the product stream. Addition of even more fuel and reforming gas may be needed to keep the reforming bed in operation; this is the topic of chapter 9.2. Another option would be to decrease the ratio CH_4:O_2, but this would at the same time result in a lower flow of methane, requiring the methane outflow of more tubes to keep the bed fluidized. On the other hand it could help separations and selectivity, so this is certainly a topic to look into and this is done in appendix I.

Yet another option is to use a prereformer, which is common practice in industry. Prereforming the steam reforming mixture up to somewhat more than 500°C would bring the required

Table 9.1.: Composition for OCM outlet for thermodynamic calculations

Mole fractions at outlet of OCM reactor							
O_2	CO_2	H_2O	CH_4	CO	H_2	C_2H_6	C_2H_4
0.0000	0.0250	0.3440	0.3999	0.0023	0.0477	0.0258	0.1554
Mole fractions after removal of $C_2H_4$and C_2H_6							
O_2	CO_2	H_2O	CH_4	CO	H_2	C_2H_6	C_2H_4
0.0000	0.0305	0.4201	0.4884	0.0028	0.0583		

Table 9.2.: Stream compositions for the example for steam reforming (mole fractions).

	O_2	CO_2	H_2O	CH_4	CO	H_2
Feed stream, 100°C	0.000	0.012	0.771	0.193	0.001	0.023
Steam reformed, 500°C	0.000	0.081	0.494	0.081	0.011	0.333
Steam reformed, 780°C	0.000	0.068	0.358	0.000	0.080	0.493

enthalpy change into the desired amount per tube and would also avoid excessive temperature differences within the same piece of equipment.

For further calculations it is assumed that a prereformer is used and that a uniform temperature can be obtained within the fluidized bed. Also, the only methane fed to the steam reforming is assumed to unconverted methane coming from the OCM tubes. With this choice, the process loses it's autothermal operation. The use of a conventional prereformer enables the use of conventional technology. Besides it enholds a physical separation of combustion and reforming streams, reducing the load on subsequent separation equipment.

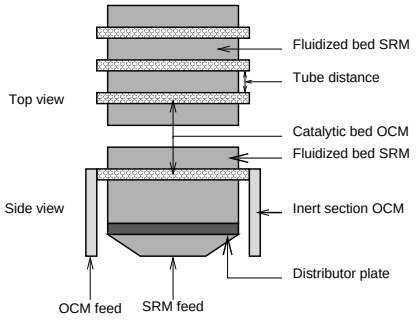

Figure 9.1.: Configuration of the fluidized bed with horizontal tubing

Table 9.3.: Conditions for approximation of volume flow SRM

Variable	Value
Pressure	$1.2\ \mathrm{bar}$
Temperature	$780\ ^\circ\mathrm{C}$
Conversion	40%

9.2. On the geometry of the fluidized bed

Now that simulations on the OCM tube have been run, the question remains how exactly the fluidized bed should be constructed, and if it can be operated at all. The main concern with the author is, on this part, if the bed can be fluidized at all with the amount of gas available. Although the detailed design of a fluidized bed due to time restrictions falls outside of the current project, and although it is always risky to do any predictions on such a vast topic using limited considerations, it is thought worth the trouble to give some comments on this part. Consider figure 9.1. The goal of the following exercise is to determine the superficial gas velocity. For the base case, it was calculated that the methane flow entering a single OCM tube is $3.8\mathrm{mmol/s}$ with a conversion of 49%. Using the variables shown in table 9.3, it can then be calculated that the volume flow induced in the fluidized bed by a single tube is (at least, neglecting the net production of moles by the steam reforming and any addition of e.g. fuel for autothermal reforming) $0.7\mathrm{L/s}$. Now considering a spacing between the tubes of $10\mathrm{cm}$, per tube (with a length of $1\mathrm{m}$) there is a surface of $0.1\mathrm{m}^2$ for the gas to flow through; this gives a superficial velocity for the gas of $0.7\mathrm{cm/s}$ *per tube vertically aligned*. The nice thing about the horizontal configuration is that the tubes can be aligned in the vertical without too much trouble, increasing the gas flow per inlet area for the fluidized bed. With about 5 tube layers the desired superficial velocity is reached. Assuming a required increase in length of $10\mathrm{cm}$ per tube layer, this would give a height for the tube bundle of $0.5\mathrm{m}$, which in itself is not an exception, which is actually rather low.

The low requirement for number of tubes aligned in the vertical opens the option for vertical placement of the tubes, shown in figure 9.2. The vertical placement has the advantage that the brittle membrane tubes do not have to deal with gravity. In order to obtain a superficial velocity of $3.3\mathrm{cm/s}$, when assuming the tubes are placed in a u-tube arrangement (so that the tube sticks twice through the cross-surface), it can be calculated that each tube should occupy a

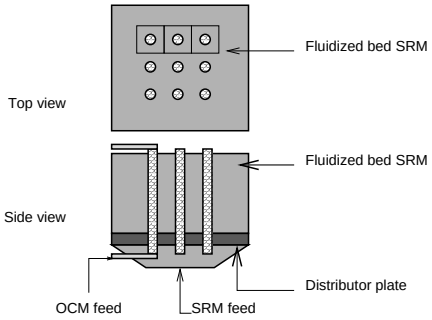

Figure 9.2.: Fluidized bed configuration with vertical tubing

square with a length of 15cm. (Instead of square arrangements also for example a honeycomb arrangement can be thought of.) This measure seems practical and also leaves flexibility to find a solution for mounting the outlets for the steam reforming gas.

Losses of mixing properties of the fluidized bed can supposedly made up for by decreasing the distance between the vertical (u-)tubes even further, increasing the superficial velocity even further, of course avoiding the situation of creating a riser.

It should be mentioned here that implicitly the choice has already been made to control the energy balance in OCM the bed with the SRM reaction and not vice versa because the product quality for the steam reforming reaction is not severely affected by temperature excursions.

9.3. Benchmarking

However well the concept may seem to work, of course there are other processes around that may be built instead. An example is conventional steam reforming followed by Fischer Tropsch followed by cracking. Making a full economic evaluation, including all required separation equipment, would go too far. However a first *very* rough indication can be gotten by looking at the throughput in standard cubic metres gas per second per cubic metre reactor. Without calculating and by just looking at pictures of ethane crackers or industrial steam reformers in Ullmann's Encyclopedia of Industrial Chemistry or Kirk-Othmer's it can be said that compared to industrial reactors it is low. On the part of steam reforming alone it will certainly not be able to be competetive with conventional technology. A benefit compared to other routes must thus be that ethene (and ethane) is directly produced instead of indirect, possibly avoiding the purchase and operation of significant pieces of process equipment.

Part IV.

Discussion and Conclusions

10. Discussion and recommendations

10.1. On the concept of reverse flow with membrane feed

When the concept was first thought of, the idea was to operate the fluidized bed at a temperature around 500°C. [1] This temperature is outside the region of approximately 800°C that would be favourable for performing OCM. At lower temperatures, outside of the region of validity of the kinetics of Stansch [SMB97], which are used for the current model, unselective reactions could prevent the reaction from being extinguished (although the model, in this region in which its kinetics are not valid, predicts otherwise) but the loss of selectivity by itself makes operation of OCM at lower temperatures highly undesirable. In order to obtain a relatively fast reduction of temperature for (the start of) quenching of the reaction after the formation of ethane and ethene, it would be desirable to allow thermal contact between the colder fluidized bed and the oxygen-lean section of catalyst. However, at the same time it was suspected that due to convection of cold gas into the oxygen-rich section a significant penetration of a low-temperature profile into the reaction section could occur. (The gas could be either cold from cooling by the fluidized bed or, if the design of the gas treatment before entering the oxygen-rich section is considered not yet determined, by insufficient preheating.) Hence, the reverse flow concept was introduced in order to center the temperature profile and in this way limit the reaction region with low temperature. In order to investigate the effects of this mode of operation, it was considered that a detailed model was needed, which was built.

The introduction of reverse flow in a natural way led to the addition of inert sections at the inlet and outlet of the reactor. The reverse flow could now simultaneously be used to allow for fully cold feed and (especially) cold outlet streams. Formation of coke would be reduced as a result of the already severe reduction of temperature achieved by cooling by the fluidized bed.

The high temperature difference between the catalyst and the fluidized bed would also allow for a relatively high throughput as long as the rate of heat removal (and not the pressure drop) is the bottleneck.

When the desired temperature of the fluidized bed was changed into a significantly higher temperature of 780°C for mechanical reasons, on the part of the reactor concept some advantages were lost, and one was gained, namely that the OCM reaction can run feasibly at the temperature of the fluidized bed. For the current concept using the model as built it has been shown that conceptually steady states are reached for both single direction flow and for reverse flow. From the study of the influence of α_w it was seen that the C_2 yield is not very severely dependent on the exact temperature profile; the question rises if the increased complexity of the reverse flow operation is worth the expected benefit from the use of the inert sections. This would have to compete with conventional technology for fast quenching outside of the reaction section, delivering possibly useful high temperature steam, that is available in the form of transfer line heat exchangers [SSO01], possibly having a longer residence time before quenching is achieved than the inert sections. For this equipment coking is reported for the case of ethane cracking. Coking, causing blocking of the channels, would be disastrous for a packed bed, for which the cleaning is not as straightforward as for the conventional technology. The advantages

[1] Implicitly it was also assumed that heat transfer whitin the catalytic bed would be far better than heat transfer from the catalytic bed (through the tube wall) into the fluidized bed, avoiding a strong radial temperature profile in the catalytic section. In retrospect this assumption is suspect to doubt.

of the use of a membrane reactor however stand and have been extended with the integration of cooling by fluid bed. Despite the loss of some initially promising advantages, in the new concept, the three distinctive features of the fluidized bed reactor combined with the membrane reactor stand:

1. A low oxygen partial pressure for the OCM reaction, combined with
2. A relatively uniform evolution of heat combined with a relatively uniform removal of heat.
3. Low temperature feed and product with fast quenching due to the use of inert sections.

If the use of inert sections without a negative contribution by coking is feasible must be found experimentally; the prediction of the formation of coking seems to be considerably difficult, looking at industrial experience [SSO01]. The steam formed as a by-product of the OCM reaction may be helpfull in preventing coke formation and/or accumulation.

10.2. On the catalyst activity and other catalysts

The kinetics implemented are those provided by Stansch et al. [SMB97]. Adjustment of their extensive reaction scheme should allow for easy implementation of kinetics as derived by other authors. In the current work, opposed to the kinetic measurements performed by Stansch et al. using particles with a diameter in the order of $0.3\mathrm{mm}$, the catalyst is assumed to be present as particles with a diameter of $2\mathrm{mm}$. The adoption of an effectiveness factor based on the concentration of oxygen seems not to be very feasible because oxygen is nothing but a vehicle in a complex reaction system; a more practical and most likely as effective approach is to multiply the reaction rates all with the same reducing factor, possibly derived from detailed numerical calculations for a limited number of different reactor sections. These detailed calculations could also take into account intra-particle temperature effects. In order to account for possible loss of catalyst activity due to the use of larger particles, the catalyst was diluted with a factor 10. If this would not be done, as far as the catalyst is concerned local conversion could be increased and thus in principle a higher local heat production at low pressure drop (due to reduced length of tubing) could be obtained. However, apart from the undesired high temperature difference required to sufficiently cool such a tube, for such a relatively short tube penetration of a low temperature profile into the reaction section is very likely. Last, and most of all, it is considered a good choice to retain a margin for correction.

The increase of particle diameter also affects the ratio of the thin gas volume over the catalyst surface, in which the reaction supposedly takes place, compared with the total open gas volume. On the catalyst studied by Stansch et al. [SMB97] it must be remarked that it is *very* fast, for example compared with the catalyst studied by Tuinier [Tui07]. From the discussion on this in the appendix it can be estimated (taking the correction of $\delta = V/A$ for spherical particles into account) that for the catalyst particles as studied by Stansch et al. in order to achieve a particle effectiveness of one, the particle diameter in the order of at most a few times 10 micrometers would be needed, whereas for the case of Tuinier this would be in the range of hundreds of micrometers, which was the actual size used. More on this is given in the following paragraph.

The effect of diffusion limitation in the radial direction (although because of the small sized particles in the order of $300\mu\mathrm{m}$ not for the catalyst particles) should already be observable for the results of studies performed by Spek [Spe07], provided the calculation of the Thiele modulus given in the appendix is valid for this situation of the catalyst included between concentrial cyllinders with diameters of 3.0 and 2.5 cm, with oxygen feed from the outer cylinder. A literature reference to calculations of Thiele moduli for these cases is also provided by Spek [Spe07].

Given the small particle size these experiments could very well be approximated by a pseudo-2D approximation. It would be interesting to see if the outer ring of the catalytic bed acts as a sort of “Hinterland”, into which C_2 product can diffuse and be relatively safe from reaction.

10.3. On increasing tube diameters and radial profiles

When increasing just the tube diameter of the catalyst section (and thus retaining that of the membrane), this very likely increases the gradient of oxygen concentration. The effect of this gradient is much more severe as for the case studied by Kürten [Kur03], who studied a membrane tube for which the flux of oxygen was inward and for which depletion of oxygen in the middle of the tube was found. Therefore, it is not advisable to increase the tube diameter much.

An additional reason is that in this case the oxygen flow through the tube would have to increase, possibly causing an inhomogeneous distribution of the oxygen flux. Besides increasing this flux could result in a dangerously high mole fraction of oxygen (in the sense of promotion of unselective reactions and possible formation of explosive mixtures) at the wall. On the other hand the flux also may not become so low that counter-diffusion could occur, possibly forming explosive mixtures in the oxygen tube. [Kur03] Last but not least increasing the diameter can also give rise to a very significant temperature profile over the tube diameter.

All this calls for a method of determining an upper bound for which the pseudo-1D model is valid. Iordanidis [Ior02] shows that for strongly exothermic reactions 1-D models can deviate significantly from 2-D models for the same case. Iordanidis also shows the concept of the cell model, dividing a catalyst section into multiple concentric rings, which would be the simplest and yet very likely effective method to be implemented in the current model. Additionally, this author provides relations for amonst others heat transport in packed beds. Kürten gives an overview of modelling studies of packed bed membrane reactors in literature, some of which concerning 2-D modelling. However, most studies have been pseudo-homogeneous, one-dimensional reactor models.

Tubes of $2.5\mathrm{cm}$ diameter are not an exception in process industry, and ceramic tubes with a diameter in the order of $1\mathrm{cm}$ are commercially available. Hence choosing these dimensions, provided that the pseudo-1D assumption holds, is a rather practical choice.

Some very early calculations were done in the appendix on radial transport of heat and of mass (oxygen). For transport of heat it was found that this is (just) sufficient for the current case. For the transport of oxygen throughout the catalyst section, however, a strong indication was found that the reaction is diffusion limited and that thus in close proximity to the tube wall severe bypassing may occur due to a lack of oxygen. This is in part caused by the swift reaction over the catalyst as studied by Stansch et al. [SMB97]. On the other hand, it is also inherent to the design chosen, with the oxygen feed tube in the middle, instead of (as commonly found in literature) having a membrane tube wall for the catalyst section. The reaction rate can be decreased by choosing a less active catalyst; this however does not eliminate the concentration gradient needed for the transport of oxygen, causing local high partial pressures of this gas. The radial dispersion could to a limited extent be increased by increasing the flow rate. Swapping the oxygen feed and the catalyst section however is thought highly impractical because of heat transport limitations. The possibility of diffusion limitation, therefore, can be considered the Achilles heel of the reactor concept.

10.4. Process safety

In the current process, volume containing oxygen-rich gas has been kept as small as possible. However, a thorough HAZOP study was not performed. This should be performed before proceeding towards experimental validation. First steps to be taken are evaluation of the lower explosion limit and the possible hazards of special operations such as reactor shutdown.

10.5. On the model

Using the reverse flow model developed and successfully applied by Smit [Smi06] to catch the key concepts of reverse flow seemed natural at first hand and has been a valuable tool in showing the concept intended. From this work also the order of magnitude of the allowable diameter of catalyst particles was inherited. However, it turns out that the actual exothermicity and the scavenging of reactant by the OCM reaction seems to have been underestimated somewhat. More detailed calculations on radial transport than the preliminary indications provided in the appendices are needed before building an actual reactor.

The possible error in the radial concentration profile of oxygen was increased by leaving the feeding of oxygen through the outer wall of the catalyst compartment for feeding at the inner radius, so that on average (over volume) the distance of catalyst particles to the feed point of oxygen becomes larger.

An obvious flaw in the current model is imposing a heat transfer coefficient between the catalytic bed and the tube all, which was for possible unapplicability of in radial heat transport relations as found in literature, which were derived for deeper packed beds. However it was shown in the appendix that if uniform heat production would occur (which was the assumption) the catalytic bed sufficiently conducts heat, although the acceptable limit is almost reached. In reality, production would take place preferentially near the oxygen feed wall, thus increasing the temperature difference. The use of an overall heat transfer coefficient loses it's validity here. For the case no significant temperature gradient occurs it has been shown overall results are not very strongly dependent on a change in the overall heat transfer coefficient.

Finally it should be mentioned here that in the model calculations the heat conducting and accumulating properties of both tubes were set equal to that of steel, although especially for the inner tube it is expected that it will be made of ceramic material. Because of the relatively uniform production of heat in the catalytic section and the resulting uniform temperature profile in the tube walls this is thought to have had no significant impact on the results obtained.

10.6. On the results

The results serve to reach the goal of demonstrating the concept as originally thought of and promote to continue investigating this promising concept. On the accuracy, however, there are some doubts. First of all a yield far higher than reported in literature is obtained. When looking at the reaction scheme provided by Stansch et al. [SMB97] for low partial pressures two reactions become dominant: the oxidative coupling of methane (2.2) and the oxidative dehydrogenation of ethane (2.7), which results in very high methane conversions and production of exactly the desired product. It is thought that an actual experimental reactor will have a lower yield, partly due to side-reactions and partly due to bypassing. With respect to the thermal efficiency it may be necessary to operate at a somewhat lower CH_4:O_2 molar feed ratio, as can be seen from the initial thermodynamic calculations included in the appendix.

If a relatively uniform temperature profile exists in the radial direction of the OCM tube, however, operation of the reactor in reverse flow would provide similar results as found here, since as far as heat is concerned the reactor does behave as if it is pseudohomogeneous and 1D. In this way the temperature profile in the reactor can be controlled as it was proposed in this work. The radial and axial concentration profiles then respond to this well controlled temperature profile, although the mixing cup composition, and along with it the actual local heat production, at the end of the reactor may deviate significantly from that obtained from the pseudohomogeneous 1D calculations used in this work.

10.7. Other processes

The current concept might be very suitable for similar processes such as partial oxidations. No work was performed on this part in the current project.

10.8. Concepts in literature

The literature search performed for this project has been very limited. Therefore a literature search should be performed to see if a similar concept has been used before, possibly providing new insights. The most similar concept known to the author is that of Alonso et al. [ALPP01] These authors brought a porous membrane tube into contact with a bed fluidized by an oxygen-rich gas, so that oxygen could penetrate into the tube and react within the tube with a hydrocarbon. The fluidized bed would then ensure cooling. This particular configuration is, however, considered unsuitable for application in this case. An overview of packed bed membrane reactor studies is given by Kürten [Kur03].

Also it is recommended to have a further look at similar processes, in particular ethene cracking. The latter has a very similar separation requirement (including removal of carbon dioxide and steam) and the same problem of potential undesired gas-phase reactions.

10.9. Materials to be used

One of the remaining tasks after this work, apart from the absence of information on safety of operation, is that the materials to be used are not explicitly elucidated. Currently, the idea is that the oxygen-carrying tube will be a ceramic tube. The outer tube is thought to be a metal tube with on the inner side a coating preventing coking.

From the work of Smit [Smi06] it was inherited that alumina was used in the inert sections. In retrospect, a better choice would be the use of CaO, which is also the carrier material of the catalyst, because of it's higher heat capacity.

10.10. On the viability of the process

In literature, often the need for a recycle is pointed at as the reason why OCM could probably never become commercially attractive. The current process does not have a recycle. The underlying problem of the recycle, however, has not been eliminated. This concerns the cost of separation and recompression. Unless a revolution in separation technology occurs it is expected that the method of recovery of C_2H_6 and C_2H_4 will remain cryogenic techniques. However, as recent as 2001 OCM was mentioned in Kirk-Othmer's encyclopedia of industrial chemistry [SSO01] as

an economically potentially attractive route to ethene, independent of crude oil, if methane is available in abundance at low cost.

The constraint that the fluidized bed needs to be operated with the undesired product stream from the OCM section puts severe constraints onto the process layout and operation. For example for the case of a relatively low production per OCM tube, in order to obtain sufficient gas to operate the fluidized bed, these should be stacked in the vertical, which would in the practical sense eliminate the option of suspending the OCM tubes in the vertical. Also even in the current project discussion appeared on if for the calculations for overall thermal efficiency only methane or also other waste products should be steam reformed. It is recommended to leave this restriction and to regard steam reforming as a particularly suitable way of cooling.

Because of the possibly dynamic nature, and because it is typically kinetically instead of thermodynamically controlled, the OCM reaction has been the main point of focus in this work. However, of course before building an actual reactor significant work on the use of a fluidized bed steam reforming reactor is needed, although experimental studies can already be found in literuture. This study should include evaluation of the option of increasing the pressure for steam reforming. However, from chapter 9.2 it might be concluded that reduction of the size of the steam reforming section by increasing the pressure very well may be undesirable.

10.11. Catalyst stability

For the Li/MgO catalyst for OCM, several studies report that significant lithium loss and sintering occurs under oxidative coupling conditions. [CMS94b] Use of reverse flow operation could prevent excessive loss of lithium and could hence elongate catalyst lifetime.

Tuinier [Tui07] experimentally found that the state of oxidation of the $Mn/Na_2WO_4SiO_2$ catalyst is of major importance for the selectivity of the catalyst: an oxidized catalyst has a higher selectivity. In order to maintain this oxidized state only a low O_2 partial pressure is needed.

The La_2O_3 catalyst as used by Stansch seems to be stable.

10.12. Suggested experimental procedure

Before experiments are conducted, diffusion limitation should be extensively considered. First off this can be done by more detailed “old-fashioned” calculations of the Thiele moduli. If this looks promising then further calculations can be conducted with 2D, or perhaps even 3D models (with the dimensions being the axial position, the radial position, and in the case of 3D also the catalyst radial position). In order to avoid embarking into experiments that measure what is not desired, also considerable attention should be given to catalyst design, which was already pointed at by Krishna et al. [KS94] but was, for the benefit of conceptual demonstration of the concept already conceived, left for future work in this work. Both will also help in the interpretation of experimental results.

Before performing experiments on this possibly explosive system a thorough HAZOP study should be performed. Modifications, such as using air instead of oxygen, as described by Smit [Smi06], might be required but should still allow for demonstration of the concept.

The actual use of steam reforming reactions in the fluidized bed, which would require the use of a relatively large volume of methane gas in an experimental setup, can possibly be avoided by using a fluidized bed with an alternative method of cooling.

11. Conclusion

In order to achieve an understanding for the possibilities for autothermal combination of endothermic steam reforming (SRM) and exothermic oxidative coupling of methane (OCM), a project to come to a possible (conceptual) design for such a process was performed by means of numerical simulations.

The reaction concept conceived is to use distributive feed of oxygen for the OCM reaction, performed in a tube. Not only does this allow for a low partial pressure of oxygen, increasing product selectivity, this also allows for a relatively uniform production of heat along the tube. Matching this with a uniform temperature at the outside of the tube results in a (similarly) uniform temperature profile within the tube for OCM reaction. The uniform production and consumption of heat avoids delicate process operation such as found for other variants of processes for combination of exothermic and endothermic processes as found in literature. Additionally, the concept allows for reverse flow operation for the OCM reaction, the prime advantage of which is allowance for very fast quenching using inert sections. The cost-intensive separations after the OCM reaction section, however, cannot be avoided.

An advanced pseudo-1D model, based on the work of Smit [Smi06], has been built to study the effect of reverse flow on process operation. The model mainly focusses on the OCM reaction section and regards the fluidized bed as a heat sink. Amongst others reaction kinetics as provided by Stansch et al. [SMB97] and thermodynamics are included.

The expected relatively uniform temperature profile is reflected by modelling results. Initial calculations led to an OCM reaction tube with a length of $1\mathrm{m}$ of which the middle $\frac{2}{3}\mathrm{m}$ was distributively fed with oxygen. The temperature of the fluidized bed was set to $780^{\circ}\mathrm{C}$ and the desired temperature of the OCM catalyst section was chosen to be $810^{\circ}\mathrm{C}$.

It has been shown that yield in the temperature region of operation is relatively insensitive to the exact local temperatures (varying by about $15^{\circ}\mathrm{C}$) in the OCM section, so that it is safe to state that if the temperature profiles look alike the product distributions also look alike (although in principle the temperature profile also depends on the mass balance; they are inter-related). Since the temperature profiles for the OCM reaction section look alike both for reverse flow and OCM, it is expected that operating in reverse flow or not does not significantly affect product distribution. However, fast quenching by use of inert sections directly attached to the catalytic section (thus without a valve and/or associated piping and the like in between) becomes available by using reverse flow.

A crucial assumption when conceiving the reactor concept has been that a sufficient radial distribution of mass and heat can be achieved, which in fact is the Achilles heel of this concept, since opposed to conventional membrane reactors the distributed reactant is not fed through the outer wall of a tube inwards, but from a tube suspended in another tube outwards.

Considering autothermal operation it was found that on the part of OCM sacrifices must be made on the part of selectivity in order to be able to reform its waste stream by steam reforming autothermally. For the non-autothermal case an indication that on the part of fluidization, the fluidized bed for SRM can be fluidized for a feasible reactor configuration, was obtained. However imposing autothermal opertion does severely limit possible reactor configurations.

All of the advantages described before are true provided that the assumption of the homogeneous profiles for temperature and oxygen concentration is true. The validity of this assumption should be checked before conducting further work.

Part V.

Background information

Bibliography

[AL02] F.T. Akin and Y.S. Lin. Oxidative coupling of methane in dense ceramic membrane reactor with high yields. *Aiche Journal*, 48(10):2298–2306, 2002.

[ALPP01] M. Alonso, M.J. Lorences, M.P. Pina, and G.S. Patience. Butane partial oxidation in an externally fluidized bed-membrane reactor. *Catalysis Today*, 67(1-3):151–157, 2001.

[ALRCK01] P. Aguiar, N. Lapena-Rey, D. Chadwick, and L. Kershenbaum. Improving catalyst structures and reactor configurations for autothermal reaction systems: application to solid oxide fuel cells. *Chemical Engineering Science*, 56:651–658, 2001.

[Ann00] Martin van Sint Annaland. *A novel reversible flow reactor coupling endothermic and exothermic reactions*. PhD thesis, University of Twente, 2000.

[AP06] Nor Aishah Saidina Amin and Soon Ee Pheng. Influence of process variables and optimization of ethylene yield in oxidative coupling of methane over Li/MgO catalyst. *Chemical Engineering Journal*, 116:187–195, 2006.

[BB98a] M. Baerns and O. Buyevskaya. Simple chemical processes based on low molecular-mass alkanes as chemical feedstocks. *Catalysis Today*, 45:13–22, 1998.

[BB98b] M. Baerns and O. Buyevskaya. Simple chemical processes based on low molecular-mass alkanes as chemical feedstocks. *Catalysis Today*, 45:13–22, 1998.

[BWDB96] N.A. Baronskaya, L.S. Woldman, A.A. Davydov, and O.V. Buyevskaya. Ethylene recovery from the gas product of methane oxidative coupling by temperature swing adsorption. *Gas Sep. Purif.*, 10(1):85–88, 1996.

[Chr96] Thomas S. Christensen. Adiabatic prereforming of hydrocarbons - an important step in syngas production. *Applied Catalysis A: General*, 138:285–309, 1996.

[CMS94a] J. Coronas, M. Menendez, and J. Santamaria. Development of ceramic membrane reactors with a non-uniform permeation pattern. application to methane oxidative coupling. *Chemical Engineering Science*, 49(24A):4749–4757, 1994.

[CMS94b] J. Coronas, M. Menéndez, and J. Santamaría. Methane oxidative coupling using porous ceramic membrane reactors - ii. reaction studies. *Chemical Engineering Science*, 49(12):2015–2025, 1994.

[CPRL97] Eric M. Cordi, Sergei Pak, Michael P. Rosynek, and Jack H. Lunsford. Steady-state production of olefins in high yields during the oxidative coupling of methane: Uitilization of a membrane contactor. *Applied Catalysis A: General*, 155:L1–L7, 1997.

[CYE03] Zhongxian Chen, Yibin Yan, and Said S.E.H. Elnashaie. Novel circulating fast fluidized-bed membrane reformer for efficient production of hydrogen from steam reforming of methane. *Chemical Engineering Science*, 2003. Article in press.

[DC79] A.G. Dixon and D.L. Cresswell. Theoretical preidcition of effective heat-transfer parameters in packed-beds. *Aiche Journal*, 25(4):663, 1979.

[DC04] D.L.Hoang and S.H. Chan. Modeling of a catalytic autothermal methane reformer for fuel cell applications. *Applied Catalysis A: General*, 268:207–216, 2004.

[DD85] T.E. Daubert and R.P. Danner. *Data Compilation tables of properties of pure compounds*. American Institute of Chemical Engineers, New York, 1985.

[DSF+92] F. M. Dautzenberg, J. C. Schlatter, J. M. Fox, J. R. Rostrup-Nielsen, and L. J. Christiansen. Catalyst and reactor requirements for the oxidative coupling of methane. *Catalysis Today*, 13:503–509, 1992.

[ELF] M.O. McLinden E.W. Lemmon and D.G. Friend. "thermophysical properties of fluid systems" in nist chemistry webbook, nist standard reference database number 69. http://webbook.nist.gov/ [December 19, 2007].

[FEHA99] J. Frauhammer, G. Eigenberger, L.v. Hippel, and D. Arntz. A new reactor concept for endothemric high-temperature reactions. *Chemical Engineering Science*, 54:3661–3670, 1999.

[GGM+04] B. Glöckler, A. Gritsch, A. Morillo, G. Kolios, and G. Eigenberger. Autothermal reactor concepts for endothermic fixed-bed reactions. *Chemical engineering Research and Design*, 82(A2):148–159, 2004.

[GPB04] Fausto Gallucci, Luca Paturzo, and Angelo Basile. A simulation study of the steam reforming of methane in a dense tubular membrane reactor. *International Journal of Hydrogen Energy*, 29:611–617, 2004.

[HH01] Kaihu Hou and Ronald Hughes. The kinetics of methane steam reforming over a ni/α-al$_2$o catalyst. *Chemical Engineering Journal*, 82:311–328, 2001.

[HLW00] Peter Haussinger, Reiner Lohmller, and Allan M. Watson. Hydrogen. *Ullmann's Encyclopedia of Industrial Chemistry*, 2000.

[HRM+06] Heinz Hiller, Rainer Reimert, Friedemann Marschner, Hans-Joachim Renner, Walter Boll, Emil Supp, Miron Brejc, Waldemar Liebner, Georg Schaub, Gerhard Hochgesand, Christopher Higman, Peter Kalteier, Wolf-Dieter Mller, Manfred Kriebel, Holger Schlichting, Heiner Tanz, Hans-Martin Stnner, Helmut Klein, Wolfgang Hilsebein, Veronika Gronemann, Uwe Zwiefelhofer, Johannes Albrecht, Christopher J. Cowper, and Hans Erhard Driesen. Gas production. *Ullmann's encyclopedia of industrial chemistry*, 2006.

[Ior02] A.A. Iordanidis. *Mathematical Modeling of Catalytic Fixed Bed Reactors*. PhD thesis, University of Twente, 2002.

[JJ00] Ralph Jacobs and Wouter Jansweijer. A knowledge-based system for reactor selection. *Computers and Chemical Engineering*, 24:1781–1801, 2000.

[KFE00] G. Kolios, J. Frauhammer, and G. Eigenberger. Autothermal fixed-bed reactor concepts. *Chemical Engineering Science*, 55:5945–5967, 2000.

[KFE02] Grigorios Kolios, Jörg Frauhammer, and Gerhard Eigenberger. Efficient reactor concepts for coupling of endothermic and exothermic reactions. *Chemical Engineering Science*, 57:1505–1510, 2002.

[KL91] Daizo Kunii and Octave Levenspiel. *Fluidization engineering*. Butterworth-Heinemann, second edition, 1991.

[KLL97] Y.K. Kao, L. Lei, and Y.S. Lin. A comparative simulation study on oxidative coupling of methane in fixed-bed and membrane reactors. *Ind. Eng. Chem. Res.*, 36:3583–3593, 1997.

[KS94] R. Krishna and S.T. Sie. Strategies for multiphase reactor selection. *Chemical Engineering Science*, 49(24A):4029–4065, 1994.

[KTG+05] Worapon Kiatkittipong, Tomohiko Tagawa, Shigeo Goto, Suttichai Assabumrungrat, Kampol Silpasup, and Piyasan Praserthdam. Comparative study of oxidative coupling of methane modeling in various types of reactor. *Chemical Engineering Journal*, 115:63–71, 2005.

[Kur03] Ulrich Kurten. *Modeling of packed bed membrane reactors: Impact of oxygen distribution on conversion and selectivity in partial oxidation systems*. PhD thesis, University of Twente, 2003.

[Lam94] L. Lamport. *LaTeX A Document Preparation System — User's Guide and Reference Manual*. Addison-Wesley, Reading, MA, 1994.

[LDMM97] Yaping Lu, Anthony G. Dixon, William R. Moser, and Yi Hua Ma. Analysis and optimization of cross-flow reactors for oxidative coupling of methane. *Ind. Eng. Chem. Res.*, 36:559–567, 1997.

[LSM94] D. Lafarga, J. Santamaria, and M. Menendez. Methane oxidative coupling using porous ceramic membrane reactors - i. reactor development. *Chemical Engineering Science*, 49(12):2005–2013, 1994.

[Lun00] Jack H. Lunsford. Catalytic conversion of methane to more useful chemicals and fuels: a challenge for the 21st century. *Catalysis Today*, 63:165–174, 2000.

[MB95] L. Mleczko and M. Baerns. Catalytic oxidative coupling of methane - reaction engineering aspects and process schemes. *Fuel Processing Technology*, 42:217–248, 1995.

[MPNH96] L. Mleczko, U. Pannek, V.M. Niemi, and J. Hiltunen. Oxidative coupling of methane in a fluidized-bed reactor over a highly active and selective catalyst. *Ind. Eng. Chem. Res.*, 35:54–61, 1996.

[MV03] Maria Makri and Costas G. Vayenas. Successful scale up of gas recycle reactor-separators for the production of C_2H_4 from CH_4. *Applied Catalysis A: General*, 244:301–310, 2003.

[NKE95] U. Nieken, G. Kolios, and G. Eigenberger. Limiting cases and approximate solutions for fixed-bed reactors with periodic flow reversal. *Aiche Journal*, 41(8):1915–1925, 1995.

[Pat05] C.S. Patil. *Membrane reactor technology for ultrapure hydrogen production*. PhD thesis, University of Twente, 2005.

[PM98] Ulrich Pannek and Leslaw Mleczko. Reaction engineering simulations of oxidative coupling of methane in a circulating fluidized-bed reactor. *Chem. Eng. Technol.*, 21(10):811–821, 1998.

[PQL98] Sergei Pak, Ping Qiu, and Jack H. Lunsford. Elementary reactions in the oxidative coupling of methane over $Mn/Na_2WO_4/SiO_2$ and $Mn/Na_2WO_4/MgO$ catalysts. *Journal of Catalysis*, 179:222–230, 1998.

[QZWT96] X.-Q. Qiu, Q.-M. Zhu, N.B. Wong, and K.-C. Tin. Catalytic contribution of reactor wall materials on oxidative coupling of methane. *Journal of Chemical Technology and Biotechnology*, 65(4):380–384, 1996.

[SCB+01] C.R.H. de Smet, M.H.J.M. de Croon, R.J. Berger, G.B. Marin, and J.C. Schouten. Design of adiabatic fixed-bed reactors for the partial oxidation of methane to synthesis gas. application to production of methanol and hydrogen-for-fuel-cells. *Chemical Engineering Science*, 56:4849–4861, 2001.

[SHK02] W.P.M. van Swaaij, A.G.J. van der Ham, and A.E. Kronberg. Evolution patterns and family relations in gs reactors. *Chemical Engineering Journal*, 90:25–45, 2002.

[Sin62] J.R. Singham. Tables of emissivities of surfaces. *Int. J. Heat Mass Transfer*, 5:67–76, 1962.

[Sin03] R.K. Sinnott. *Coulson and Richardson's Chemical Engineering, Volume 6*. Butterworth-Heinemann, third edition, 2003.

[SKSM05] K. Sundmacher, A. Kienle, and A. Seidel-Morgenstern. *Integrated Chemical Processes.* WILEY, 2005.

[SMB94] D. Schweer, L. Mleczko, and M. Baerns. Ocm in a fixed-bed reactor: limits and perspectives. *Catalysis Today*, 21:357–369, 1994.

[SMB97] Z. Stansch, L. Mleczko, and M. Baerns. Compehensive kinetics of oxidative coupling of methane over the La_2O_3/CaO catalyst. *Ind. Eng. Chem. Res.*, 36:2568–2579, 1997.

[Smi06] Joris Smit. *Reverse flow catalytic membrane reactors for energy efficient syngas production*. PhD thesis, University of Twente, 2006.

[SNVS99] G. Sarocco, H.W.J.P. Neomagus, G.F. Versteeg, and W.P.M. van Swaaij. High-temperature membrane reactors: potential and problems. *Chemical Engineering Science*, 54:1997–2017, 1999.

[Spe07] P.W. Spek. Packed bed (membrane) reactors for oxidative coupling of methane, 2007.

[SSO01] K. M. Sundaram, M. M. Shreehan, and E. F. Olszewski. Ethylene. *Kirk-Othmer Encyclopedia of Chemical Technology*, 10:593–632, 2001.

[Ste03] James Stewart. *Calculus, Early Transcendantals*. Thomson Brooks/Cole, fifth edition, 2003.

[Sti04] E.H. Stitt. Multifunctional reactors? 'up to a point lord copper'. *Trans IChemE, part A, Chemical Engineering Research and Design*, 82(A2):129–139, 2004.

[TCA93] Anna Lee Tonkovich, Robert W. Carr, and Rutherford Aris. Enhanced c2 yields from methane oxidative coupling by means of a separative chemical reactor. *Science*, 262(5131):221–223, 1993.

[Tec05] Aspen Technology. Aspen plus version 12.1, 2005.

[TMB02] Ching Thian Tye, Abdul Rahman Mohamed, and Subhash Bhatia. Modeling of catlaytic reactor for oxidative coupling of methane using La_2O_3/CaO catalyst. *Chemical Engineering Journal*, 87:49–59, 2002.

[Tri97] D.L. Trimm. Coke formation and minimisation during steam reforming reactions. *Catalysis Today*, 37:233–238, 1997.

[Tri99] D.L. Trimm. Catalysts for the control of coking during steam reforming. *Catalysis Today*, 49:3–10, 1999.

[Tui07] M.J. Tuinier. Kinetic aspects of oxidative coupling of methane on a $Mn/Na_2WO_4/SiO_4$ catalyst, 2007.

[VDI93] *VDI Heat atlas*. VDI Verlag, 1993.

[VGA+98] S.N. Vereshchagin, V.K. Gupalov, L.N. Ansimov, N.A. Terekhin, L.A. Kovrigin, N.P. Kirik, E.V. Kondratenko, and A.G. Anshits. Evaluation of the process of oxidative coupling of methane using liquefied natural gas from deposits of krasnoyarsk region. *Catalysis Today*, 42:361–365, 1998.

[WK] Thomas Williams and Colin Kelley. gnuplot: data and function plotting utility. http://www.gnuplot.info/ [December 3, 2007].

[WVSB01] K.R. Westerterp, W.P.M. Van Swaaij, and A.A.C.M. Beenackers. Chemical reactor design and operation, 2001.

[xfi] Xfig, drawing program for the x windows system. http://www.xfig.org/ [December 7, 2007].

[XXL+02] Longya Xu, Sujuan Xie, Shenglin Liu, Liwu Lin, Zhijian Tian, and Aiming Zhu. Combination of CH_4 oxidative coupling with C_2H_6 oxidative dehydrogenation by CO_2 to C_2H2. *Fuel*, 81:1593–1597, 2002.

[ZB91] Zhaolong Zhang and Manfred Baerns. Hydrogen formation by steam-refomring and water-gas shift reaction in the oxidative methane coupling over calcium oxide-cerium dioxide catalysts. *Applied Catalysis*, 75:299–310, 1991.

[ZW07] Heinz Zimmermann and Roland Walzl. Ethylene. *Ullmann's Encyclopedia of Industrial Chemistry*, 2007.

A. Model validation

One of the major tasks has been the building of the model and the associated debugging. Of course, checking for errors is necessary. This appendix gives an impression of the findings.

A.1. Validation of kinetics

The kinetics provided by Stansch et al. [SMB97] have been implemented. The validation of the kinetics was done by simulating the experiment as performed by Stansch et al. [SMB97], which also consisted of a tube submerged in a fluidized bed, in the case of Stansch et al. [SMB97] using cofeed for their kinetic measurements. For experiments as performed by Stansch et al. experimental data was gathered from the paper of Stansch et al. [SMB97] as well as from the paper of Tye et al. [TMB02]. The results never deviated more than 20%, which is the margin of error by scatter indicated by Stansch et al. [SMB97]. It must also be noted here that Stansch et al. [SMB97] do not clearly indicate if the rate constant given for thermal dehydrogenation of ethane to ethene should be related to only the gas volume fraction or to the entire volume. It was found that this does not seriously affect the results (it affects the yield of ethene for cofeed in the order of promille) and hence the choice was made to relate it to the gas volume fraction only (to be on the prudent side when predicting the rate of C_2H_4 formation). Because of the lengthy elaboration and relatively small added value not all results are reproduced here; only the case for the comparison with the work of Tye et al. [TMB02] is shown for demonstation.

A.1.1. Comparison with Tye et al.

Tye et al. [TMB02] implicitly check their kinetic model with a uniform temperature assumption. To duplicate this, in the model the heat transfer coefficients from the wall to the gas and from the wall to the fluidized bed were set to very high values, resulting in negligible heat transfer resistance. Moreover, from the equations used it seems that Tye et al. assume that the thermal dehydrogenation of ethane to ethene only takes place in the gas phase. Therefore, the rate constant of this reaction was multiplied with a factor 0.4, the void fraction of the bed. The results of the calculations are shown in table A.1. The following can be observed:

1. Correspondence with experimental results is reasonable, especially for the less exothermic case for full oxygen conversion by combustion. (Cases 1, 2 and 3.)
2. For the reaction mixture for which more heat is released in case of full conversion of oxygen (the reaction mixtures with a high fraction of oxygen), the correspondence is less; the assumption of isothermicity thus might not be valid. Therefore, nonisothermal simulations have been conducted, which are also represented in table A.1.
3. The results for the nonisothermal case are almost the same as those calculated for the isothermal case, although in the nonisothermal case the temperature reported was the maximum temperature obtained and the average temperature in the reactor is significantly lower. This speaks in favour of the method applied by Stansch for reporting the temperature of the reaction.

Another thing that should be mentioned is that there is no full correspondence of the calculated results with the results calculated by Tye et al. A possible explanation for this could be that Tye et al. considered the superficial velocity, dependent on both net production of moles of gas and on thermal effects due to the reaction, to be a constant. The current model is too sophisticated to adapt it quickly to see if when making this assumption the same results are obtained; it would be faster to rebuild the model of Tye et al. in for example MathCad.

However, for now the most important thing is that the simulations done in this work correspond reasonably with the *experimental* values reported, which is the best that can be expected for these low values

Table A.1.: Comparison of simulated results with results as given by Tye et al. [TMB02]. Conditions: $\frac{m_{cat}}{\dot{V}_{STP}} = 3.70\mathrm{kgs/m^3}$, thermal dehydrogenation of ethane only taking place in the bulk gas fraction.

	Runs 1 (750°C)	2 (800°C)	3 (830°C)	4 (750°C)	5 (800°C)	6 (830°C)
Feed mole ratio						
x CH_4	0.612	0.612	0.612	0.699	0.699	0.699
x O_2	0.051	0.051	0.051	0.095	0.095	0.095
x N_2	0.337	0.337	0.337	0.206	0.206	0.206
CH_4conversion (%)						
Experimental	4.9	7.9	9.9	4.1	7.1	14.4
Simulation, Tye	4.9	8.5	10.9	3	5.8	13.7
Simulation, this work	4.2	7.0	8.6	6.3	11.0	15.1
Simulation, this work, nonisothermal				6.9	9.9	12.3
C_2 selectivity (%)						
Experimental	55.6	69.2	72.5	35.6	53.7	69.6
Simulation, Tye	54.6	64.5	66.4	31.7	46.4	58.9
Simulation, this work	55.8	64.3	64.4	33.2	43.3	44.4
Simulation, this work, nonisothermal				34.5	43.0	43.4
C_2 yield (%)						
Experimental	2.7	5.5	7.2	1.5	3.8	10
Simulation, Tye	2.7	5.5	7.3	1	2.7	8.1
Simulation, this work	2.3	4.5	5.5	2.1	4.8	6.7
Simulation, this work, nonisothermal				2.4	4.3	5.3

of the space velocity, having a large potential experimental error. This is because of the high sensitivity of the conversion to space velocity in this region.

A.2. Validation of the model by comparison with the analytical approximation for maximum temperature in reverse flow

A.2.1. Analytical approximation

Nieken et al. [NKE95] present limiting cases to predict key parameters in the operation of reverse flow reactors for the simple case of a first order reaction. In the current discussion, the treatment as given by Nieken et al. is even further simplified by eliminating the dependence on temperature of the reaction rate. Assuming full conversion before the middle of the reverse flow reactor is reached, the maximum temperature for the case of infinitely short switching times is then given by:

$$\frac{(-\Delta H_r)\cdot \dot{m}^2 \cdot g^0}{2\cdot M_j \cdot A^2 \cdot \lambda_{eff}} = \int_{T^0+\Delta T_{ad}}^{T_{max}} M_j \cdot a_v \cdot B\left(T_{av}\right) dT^* \tag{A.1}$$

Note that there is an important difference with the work of Nieken et al: the lower boundary for the integral is given by $T_0 + \Delta T_{ad}$ instead of $T_0 + \Delta T_{ad}/2$. The cause of this is the assumption of infinitely fast exchange of heat between the solid and gaseous phase, caused by adopting the pseudohomogeneous model. The concept of λ_{eff} might also be different between the current approach and that of Nieken et al. [NKE95], but no further attention needs to be paid to this because it was derived from the equations as given by Smit [Smi06] for the case of the HFSM (pseudohomogeneous model) that indeed equation A.1 can be used for the current case, given the value of λ_{eff}. For the latter equations as given by Smit [Smi06] will be used for full model, although for the validation given in this section it is fixed.

When assuming independence of the reaction rate on the temperature equation A.1 can be further simplified and be rewritten into:

$$T_{max} = \left(T^0 + \Delta T_{ad}\right) + \frac{(-\Delta H_r)\cdot \dot{m}^2 \cdot g^0}{2\cdot M_j^2 \cdot A^2 \cdot \lambda_{eff}\left(a_v \cdot B\left(T_{av}\right)\right)} \cdot \frac{1}{Dil} \tag{A.2}$$

Equation A.2 introduces the dilution factor, giving the fraction of carrier material that acts as catalyst; e.g. a dilution factor of 0.1 means that the catalyst is 10 times less active than the catalyst as was used by Stansch et al. [SMB97].

A.2.2. Elaboration

Table A.2 gives the coefficients for the parameters used in equation A.1 along with comments on their source. The reaction used is basically the combustion of methane in a strongly diluted stream of oxygen in methane.

$$CH_4 + 2O_2 \rightarrow CO_2 + 2H_2O \tag{A.3}$$

The kinetics used for this reaction were loosely based on the kinetics as given by Stansch, although the reaction order of oxygen was set to one and the dependence on the exact partial pressure of methane was eliminated.

From the numbers given in table A.2 it is straightforward to calculate that when plotting T_{max} against $\frac{1}{Dil}$, the intercept is given by 522 K and the slope is given by 17.8 K. Plotting the results in this way allows for separate study of possible defects in ΔT_{ad} and the combination of the other variables.

A.2.3. Results

Some numerical results of comparing the calculated results are shown in figure A.2.3. The same results are shown in table A.2.3. It can be seen that the results agree fairly well.

Table A.2.: Coefficients for use in equation A.1

Variable	Value	Comments
ΔH_r	-400 $\mathrm{kJ/mol}$	Reaction enthalpy per mole oxygen reacting.
$\frac{\dot{m}}{A}$	0.85 $\mathrm{kg/m^2/s}$	When pressure drop is allowed, this gives a reasonable pressure drop of 0.2barfor $L = 1.2\mathrm{m}$.
L	1.2 m	Length of the reactor. Value inspired by Smit [Smi06].
P	1.2 bar	Imposed constant pressure within reactor, similar to experimental conditions of kinetics.
g^0	0.0101	Low enough to avoid excessive temperatues.
M_j	0.015 $\mathrm{kg/mol}$	The molar mass of all components was set constant and equal to this value to ensure that the partial pressure is proportional to the mass fraction.
λ_{eff}	8 $\mathrm{W/m^2/K}$	Follows from a lengthy calculation using actual model equations, is now set fixed.
a_v	3333 $\mathrm{m^2/m^3}$	The specific surface; it is easily derived that for a packed bed this is calculated from $\frac{6}{d_p \cdot (1-\varepsilon)}$. Calculated for particles with $d = 3\mathrm{mm}$
$B(T_{av})$	$1.366 \cdot 10^5$ mol $O_2/\mathrm{m^3/s}$	Calculated from $A_0 \exp\left(\frac{E_a}{RT}\right) \cdot \frac{\rho_{bulk,cat}}{a_v} \cdot P_{CH_4}^{0.24}$, with $A_0 = 2.00E-6$ $\mathrm{mol/g/s/Pa^{0.24}}$, $E_a = 48$ $\mathrm{kJ/mol}$, $R = 8.31$ $\mathrm{J/molK}$, $T = 973$ Kand $\rho_{bulk,cat} = 2160$ $\mathrm{kg/m^3}$.
C_p	1200 $\mathrm{J/K/kg}$	Chosen value.
ΔT_{ad}	224 K	For estimation simply divide reaction enthalpy per gram mixture by the heat capacity

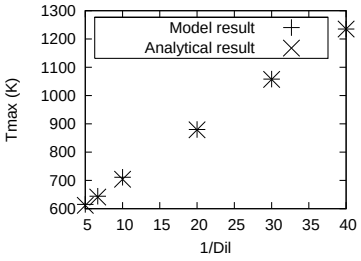

Dil	$\frac{1}{Dil}$	T_{max}, Analytical	T_{max}, model
0.025	40	1235	1235
0.033	30.0	1058	1057
0.05	20	880	879
0.1	10	711	704
0.15	6.67	644	641
0.2	5	615	612

Figure A.1.: Comparison of calculated results for both the analytical solution and solution using the numerical model of equation A.2, using the parameters of table A.2

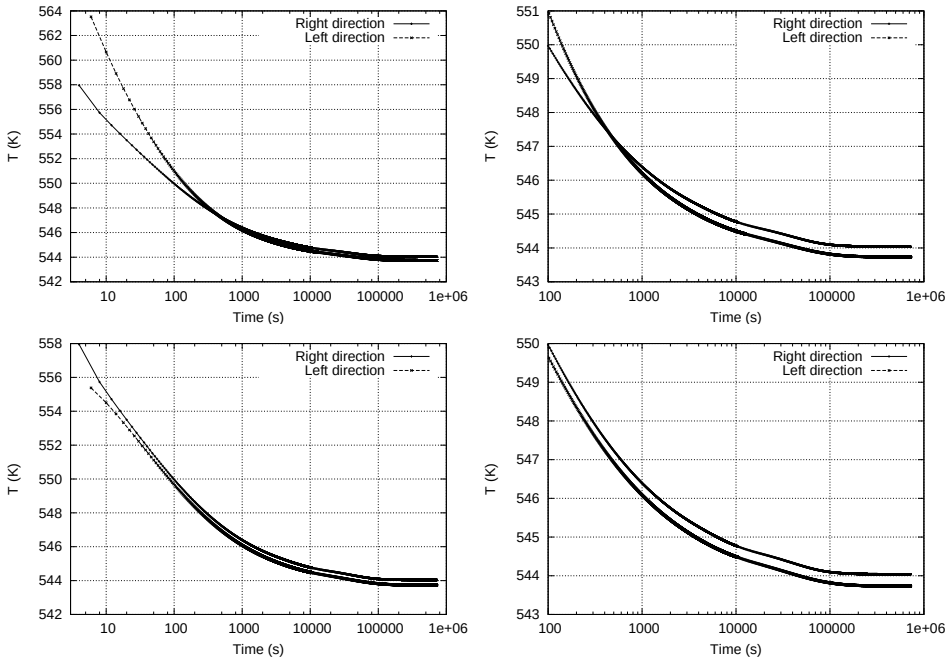

Figure A.2.: Demonstration of the divergence of the simplified dynamic model. Startup conditions: top: converged HFSM followed by first a full switching time to the right; bottom: converged HFSM followed by first a half switching time to the right

A.3. An inconsistency in the model

An inconsistency in the model that should be reported here is that results are not exactly the same if flow goes from the end of the reactor towards the beginning instead of the other way around. This was demonstrated using the simplified case as was used for validation of the calculated maximum temperature in a reverse flow reactor, as described in this appendix. When running the dynamic model, the result is convergence to a difference, as is demonstrated by figure A.2. This figure shows the outlet temperature at the end of a cycle; apparently the model converges to a minimum. One might suspect that this could have something to do with the grid refinement. Indeed, when setting the grid fixed (using an arctangentional grid refinement to allow for sufficient grid cells in the region of chemical reaction) the result as shown in figure A.3 is obtained, which does seem to converge to a shared value. However, when looking carefully at the raw data, it is seen that even with a fixed grid the results are not exactly the same for forward and backward blow directions, which from a computational point of view should be impossible. At present is is suspected that there is a small mistake in the WENO schemes applied, an effect which can be amplified by the grid refinement. (Generally, the grid of even the HFSM is not completely symmetrical when applying grid adaptation.) However, checking the numerical scheme is, from a practical point of view, a task too ambitious for the current project. It was therefore chosen to proceed with the current model, including the automatic grid adaptation, which will provide valuable information, despite the possibility of a small deviation of the results.

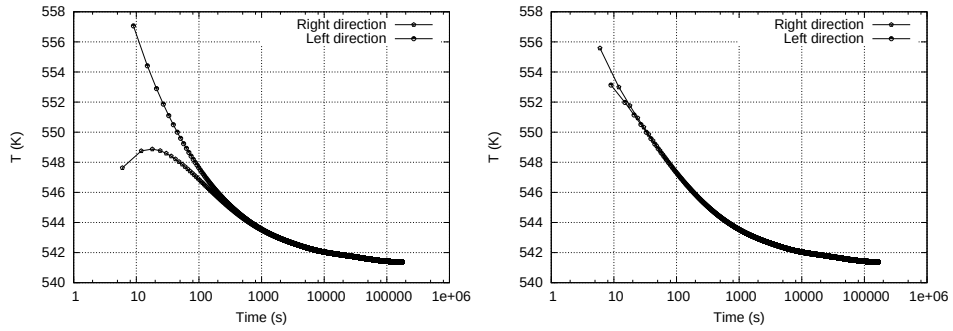

Figure A.3.: Demonstration of outlet temperatures for the simplified dynamic model with fixed grid. Left: after HFSM convergence first a full blow to the right. Right: after HFSM convergence first a half blow to the right.

B. Double packed bed: dead end reactor

Packed beds for both steam reforming and oxidative coupling have been discarded as an option. However, still it is the author's opinion that is is good to have and idea of what such a reactor would look like, thus of what has been discarded. The following is the original description of one of the first designs made.

B.0.1. Considerations

A first suggestion for the configuration of a combined reactor is given in figure B.1. The advantages of this type of reactor are expected to be the following:

- Possibly turbulent flow in the methane(/oxygen) feed tube. This has been designed to assure good oxygen/methane premixing before entering the catalytic zone, to avoid reaction at the wall as described by Coronas et al. [CMS94b]. Residence time in the premixing tube must be low in order to avoid gas-phase reaction.
- The dead-end reactor configuration has been chosen mainly to avoid problems due to thermal expansion.
- Cocurrent flow of the SRM has been chosen in order to remove the initial heat front at the start of the OCM reaction. In industrial, large scale tubular top-heated steam reformers it is also common to inject the SRM gas at the hot part of the reactor, allowing a large reaction rate over a large portion of the tube. [HLW00]
- The dead-end design will allow to adapt relative residence times by changing relative diameters.

A probable disadvantage of this type of reactor is difficulties in measurements of temperatures *in situ,* since it is difficult to place a thermocouple without piercing the walls. The dead-end principle, in fact is already applied in high-pressure SRM. An industrial design is given by Häussinger et al. [HLW00]. The elevated pressure of 0.3-0.5MPa provides higher heat transfer coefficients.

As described in section 6.3, the option of using a fixed bed for both the steam reforming and the oxidative coupling has been discarded because of the possibly delicate operation.

Concept dead end reactor

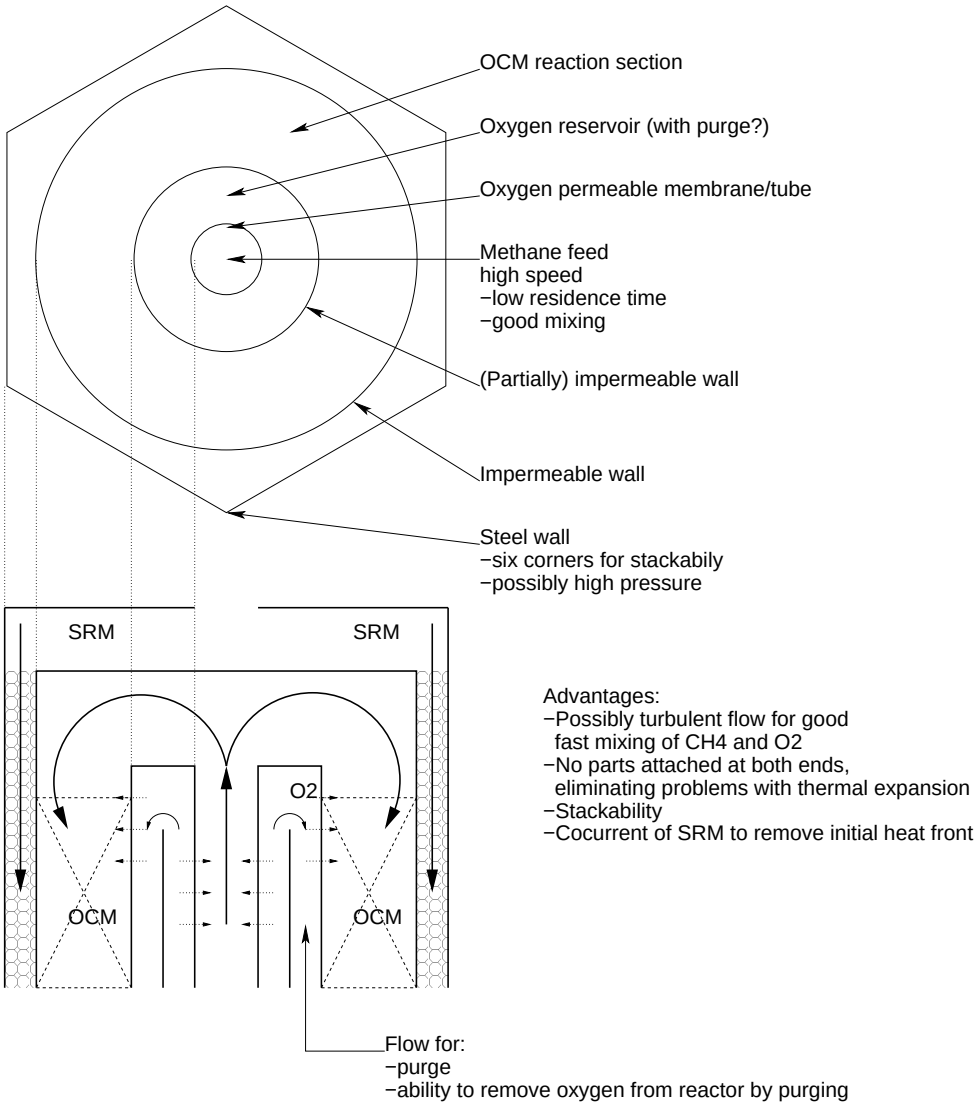

Figure B.1.: Dead-end reactor concept for combination of SRM and OCM.

C. Adiabatic temperature change for OCM reactions

In order to check the thermodynamics as programmed into the model as well as the stoichiometry for the individual OCM reactions as given by Stansch et al. [SMB97], the adiabatic temperature change of the individual reactions was calculated twice.

The first calculation was done using Aspen, using the stoichiometric reactor (with a heat duty of zero, basically setting it to adiabatic behaviour). Because of the very high heat effects it was necessary to dilute the reaction mixture, which was always chosen to be in stoichiometric ratio, with nitrogen. Otherwise the steep temperature change would cause the model further developed in this work to crash (by working out of the bounds of applicability of the relations used), and in case of an endothermic reaction the temperature would drop to very low temperatures causing even the Aspen simulation not to converge.

The second calculation was done using the model, for which the heat transfer coefficient for the gas phase to the wall was set to zero. Secondly, because the temperature at the inlet is fixed, it was necessary to apply an inert zone at the inlet of the reactor, which acted as a thermal barrier, inhibiting heating or cooling of the reaction front by conduction. (Another option would have been to set the thermal conduction of the pseudo-homogeneous gas phase to zero.) Visual inspection was used to see if the temperature profile at the inlet was flat. For the calculation of course only one reaction was allowed at a time. In order to ensure full conversion of the reactants the reaction rates were increased temporarily artificially.

The inlet conditions are given in table C.1, together with the calculated results. Inlet temperature was always 700°C, inlet pressure was 1bar for the Aspen simulation. For the model the pressure varies in the range 1-1.2bar along the tube. However, because of the high dilution the molar gas flux is relatively independent on the conversion, making the enthalpy and thus the adiabatic temperature change independent of pressure for (ideal) gases at low pressure.

It can be seen that the results correspond very well; it can therefore be concluded that for the individual reactions both the stoichiometry and the thermodynamic properties of the elements involved have been implemented correctly.

In order to see if the calculations would also work for multiple reactions, the adiabatic temperature change was also calculated for all 10 reactions as given by Stansch et al. [SMB97] occurring simultaneously. (Inlet composition: $x_{O_2} = 0.1$, $x_{N_2} = 0.2$ and $x_{CH_4} = 0.7$.) A first indication is an adiabatic temperature rise of 450-510°C. The overall reaction as simulated thus is strongly exothermic, as it is reported to be in literature [SMB97, DSF+92].

As a final check, right before producing the results represented in this work, the same calculations performed here for a single tube were repeated for the membrane reactor, using either the combustion of methane or the coupling of methane to ethane (reactions (2.1), eqrefeq:stansch2 and (2.2) on page 2.1, respectively). The results agree with those previously calculated.

Table C.1.: Comparison of adiabatic temperature change as calculated with the model and with Aspen [Tec05] for the OCM reactions as given by Stansch et al. [SMB97]. Inlet temperature 700°C.

Reaction	Inlet components	Mole fractions	Ad. Outlet temperature, model (°C)	Ad. Outlet temperature, Aspen (°C)
1	CH_4 O_2 N_2	0.0159 0.0317 0.9524	1072.0	1072.0
2	CH_4 O_2 N_2	0.0163 0.0041 0.9796	742.7	742.6
3	CH_4 O_2 N_2	0.0161 0.0161 0.9677	829.8	829.9
4	CO O_2 N_2	0.0163 0.0081 0.9756	839.3	839.1
5	C_2H_6 O_2 N_2	0.0082 0.0041 0.9877	725.7	725.6
6	C_2H_4 O_2 N_2	0.0081 0.0163 0.9756	884.1	883.9
7	C_2H_6 N_2	0.0083 0.9917	664.2	664.1
8	C_2H_4 H_2O N_2	0.0081 0.0163 0.9756	643.0	642.6
9	CO H_2O N_2	0.0161 0.0161 0.9677	717.2	717.1
10	CO_2 H_2 N_2	0.0161 0.0161 0.9677	682.7	682.5

D. Calculation of u_{mf}

The minimum superficial velocity required to fluidize the bed, is calculated with the help of the work of Kunii and Levenspiel [KL91]. First of all the type of particles needs to be characterized.

Patil [Pat05], uses a catalyst with an u_{mf} as small as $0.271\mathrm{cm/s}$ at $600^{\circ}\mathrm{C}$ and atmospheric pressure for a mixture of catalyst- and (mainly) inert particles (alumina) with a mean particle size of $92\mu\mathrm{m}$. Chen et al. [CYE03] use for their modeling of a fast fluidized bed a particle diameter of $186\mu\mathrm{m}$ with a particle density of $2270\mathrm{kg/m^3}$ for a (more conventional) Nickel-based (Ni/Al_2O_3) catalyst. In the current work the intention is to use a bubbling fluidized bed, not a fast fluidized bed. Hence, u_{mf} will be calculated for these catalyst particles. For very small particles ($Re_{p,mf} < 20$), a relation for u_{mf} is given by [KL91]:

$$u_{mf} = \frac{d_p^2 \left(\rho_s - \rho_g\right) g}{150\mu} \frac{\varepsilon_{mf}^3 \phi_s^2}{1 - \varepsilon_{mf}} \tag{D.1}$$

For the calculation, a temperature of $780^{\circ}\mathrm{C}$ is assumed. First of all, the viscosity of the steam reforming gas is estimated by using only the viscosity of steam at $780^{\circ}\mathrm{C}$ and $1\mathrm{bar}$ pressure. This was found from the data of NIST [ELF] to be 39.6 $\mu\mathrm{Pas}$. (And 28.6 $\mu\mathrm{Pas}$ for $500^{\circ}\mathrm{C}$.) The density of the gas was calculated from the gas composition for the outgoing stream of steam reforming gas at $780^{\circ}\mathrm{C}$ at $1\mathrm{bar}$ as given in table 9.2 to be 1.1 $\mathrm{kg/m^3}$. Because the shape factor is unknown, an approximation will have to be used which is also given by Kunii and Levenspiel [KL91] (for fine particles):

$$u_{mf} = \left(\frac{\mu}{\rho_g d_p}\right) \cdot \left[(33.7)^2 + 0.0408 \cdot Ar\right]^{\frac{1}{2}} - 33.7 \tag{D.2}$$

In this, A_r is the Archimedes number, which is calculated from:

$$\begin{aligned} Ar &= \frac{d_p^3 \rho_g \left(\rho_s - \rho_g\right) g}{\mu^2} \\ &= \frac{\left(182 \cdot 10^{-6}\right)^3 \cdot 1.1 \cdot \left(2270 - 1.1\right) \cdot 9.81}{\left(39.6 \cdot 10^{-6}\right)^2} = 94.1 \end{aligned} \tag{D.3}$$

Thus, now u_{mf} follows from:

$$u_{mf} = u_{mf} = \left(\frac{39.6 \cdot 10^{-6}}{1.1 \cdot 182 \cdot 10^{-6}}\right) \cdot \left[(33.7)^2 + 0.0408 \cdot 94.1\right]^{\frac{1}{2}} - 33.7 = 1.12\mathrm{cm/s} \tag{D.4}$$

Taking a superficial velocity of three times u_{mf}, the superficial gas velocity is now found to be $3.3\mathrm{cm/s}$.

E. Porous tube oxygen flux

For the majority of calculations in this work, the oxygen flux has been imposed. Following the example of Smit [Smi06], the dusty gas model is used to give an estimate of what fluxes would be realistic for a porous tube. Since the pressure drop as calculated is relatively low, for the current estimation the pressure will be considered constant on both sides of the tube wall.

As Smit already describes, the distributor tube does not necessarily need to be a ceramic tube; it could also be sintered metal filters or tubes with discrete holes. However, in order to suppress side-reactions a ceramic tube is chosen in this case. Smit indicates that the tube should be resistant to high temperatures. Moreover, a good distribution of the gas must be ensured by a proper flow resistance of the membrane or filter.

As an example, the same ceramic membrane as used by Smit was used. The permeation rate is calculated according to the Dusty Gas Model, as introduced by Mason and Malinauskas. The relation to be used is taken directly from the work of Smit [Smi06]:

$$J = \frac{1}{R_g \cdot T^{tw}} \left(K_0 \frac{4}{3} \sqrt{\frac{8 R_g T^{tw}}{\pi \langle M^s \rangle}} + B_0 \frac{p_g^s + p_g^t}{2\eta_g^s} \right) \frac{\left(p_g^s - p_g^t\right)}{(r_i + \delta_m) \ln\left(\frac{r_i + \delta_m}{r_i}\right)} \tag{E.1}$$

The values of the relevant coefficients are given in table E.1. The viscosity $\eta_{g,s}$ was estimated to be 39.6 $\mu\mathrm{Pa}\cdot\mathrm{s}$. The molar flux found is then $7.73 \cdot 10^{-3}$ $\mathrm{mol/m^2/s}$. The molar flow through the membrane wall found is then found from multiplication with the membrane surface to be $1.8 \cdot 10^{-4}$ $\mathrm{mol/s}$. The total required flow of oxygen for operation of the base case used in this work, however, is $9.5 \cdot 10^{-4}\mathrm{mol/s}$. Thus a modification of the membrane as used by Smit [Smi06] is needed. The similar order of magnitude, however, is promising. When using the parameters as used by Spek [Spe07] ($B_0 - 2.02 \cdot 10^{-15}$, $K_0 = 2.47 \cdot 10^{-8}$ and $\eta = 1.77 \cdot 10^{-5}\mathrm{Pa}\cdot\mathrm{s}$, the latter actually derived for nitrogen), an O_2 flow of $15.5 \cdot 10^{-4}$ $\mathrm{mol/s}$ is found. The finding of a suitable ceramic membrane for the operation of the operation studied thus is very plausible.

Table E.1.: Variables for use in the dusty gas model, equation (E.1)

B_0	$6.9 \cdot 10^{-16}\mathrm{m^2}$	K_0	$2.24 \cdot 10^{-9}\mathrm{m}$
δ_m	$65 \cdot 10^{-6}\mathrm{m}$		

F. Physical properties

Physical properties not mentioned here were generally taken from the work of Smit [Smi06]. The particle density of the catalyst ($3600 \mathrm{kg/m^3}$) was taken from the work of Stansch [SMB97] and multiplied with 0.6 to correct for porosity.

F.1. Thermal properties of CaO

For simulating the catalytic bed, three thermal properties of solid CaO, the carrier of the catalyst, are required. These are the thermal heat capacity, the thermal heat conductivity and the emissivity. The thermal heat capacity and conductivity are given by Daubert and Danner [DD85]. They can both be calculated using the power law as given in equation (F.1), in which Y is the desired property and T is the temperature in K. The coefficients to this equation are given in table F.1.

$$Y = A + B \cdot T + C \cdot T^2 + D \cdot T^3 + E \cdot T^4 \tag{F.1}$$

The molar mass of CaO (burnt lime) is 56.0774 $\mathrm{kg/kmol}$ [DD85].

Table F.1.: Coefficients for heat capacity and thermal conductivity of CaO [DD85]

Property	Units	A	B	C	D	E	T-range (°C)
C_p	$\mathrm{J/kmol/K}$	4.7250E+04	6.8000E+00	-5.6700E-04	0	0	327-2900
λ	$\mathrm{W/m/K}$	1.0242E+01	-4.3696E-03	1.5000E-06	0	0	800-1000
λ	$\mathrm{W/m/K}$	2.0330E+01	-3.3523E-02	2.9296E-05	-8.7500E-09	0	200-800

The emissivity of CaO (pigment) can be found from table F.2. Surprisingly, a decrease in emissivity with increasing temperature is shown for multiple pigments including Al_2O_3, although in the current model the emissivity of the latter compound is set a constant. It has to be checked if this assumption has a significant influence on the model. It must also be kept in mind that values for emissivity can deviate significantly between different sources [VDI93].

Table F.2.: Emissivity of CaO (pigment) [Sin62]

Temperature (°C)	-156.7	51.7	399	816	1093	1371
Emissivity (%)	94	96	78	27	27	27

G. Modelling for increased troughput

For reasons of curiosity, a first attempt was made to model the reactor for the case the fluidized bed would be operated at 500°C. Given the increase of the temperature difference from 30°C to about 300°C, the local generation of heat would also have to increase with a factor of about 10 for constant heat transfer properties. An option for this would be to increase both the local flux of oxygen and the inflow of methane with a factor 10. For the given tube dimensions this gives an inacceptable pressure drop and at the same time it affects the residence time in the tube. The latter, however, could also be beneficial (if the thermal dehydrogenation of ethane is neglected) for increasing the production per tube per hour. Hence below a variant of this concept, increasing the flow through the tube with a factor 2.5, is shown. Avoiding the pressure drop (and restoring the residence time) for an increase could be done by increasing the tube diameters. However, it is feared that for this case the 1-D assumption will fail and that a distinct radial temperature- and concentrationprofile will develop.

When increasing the flow with a factor 2.5, the local heat production is expected to increase with the about same factor, and hence the temperature difference between the desired operating temperature of 810°C and the fluidized bed was set to $3 \cdot 30 = 90$°C, resulting in a temperature for the fluidized bed of 720°C. Please note that for this temperature the kinetics as measured by Stansch [SMB97] (measured for 700-830°C) is still valid.

The results for this case with increased convective transport can be seen from figure G.1. For the case shown the entire catalytic bed was in contact with the fluidized bed. It can be seen that for the case of single direction flow there is a significant portion (approximately 24 cm) of the catalyst section with temperatures significantly below 800°C, whereas for the HFSM result this fraction is smaller (approximately 10 cm). Another feature of the HFSM profile is that high temperature is reached after about 5 cm instead of 24, so that the unselective combustion reaction in this CH_4-rich environment is prohibited. Moreover, since all consecutive reactions of desired products have activation energies in the order of a few hundred kJ/mol, the temperature should be decreased as fast as possible after completion of the desired reactions, a feature which is accomplished better by the reverse flow operation than by the single direction flow. Hence this special case serves as a demonstration of the benefits originally expected from the use of reverse flow in this type of reactor, apart from the possibility of cooling in an inert packed bed.

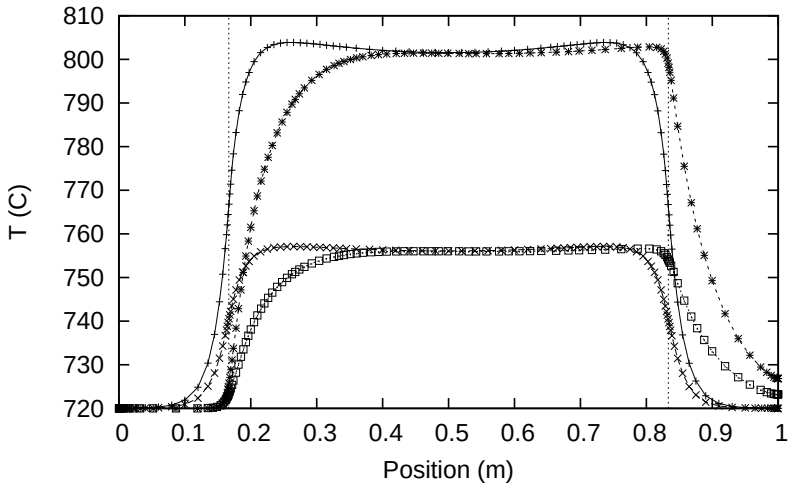

Figure G.1.: Demonstration for flow rates increased with a factor 2.5 and reduced fluidized bed temperature of 720°C

H. Some modifications to increase the speed of convergence of the model

This appendix describes some tricks implemented into the model. They are simple in nature, but resulted in significant time savings in reaching convergence. This has been especially useful in debugging sessions.

H.1. Larger minimum timestep

When observing the model at work, it was observed that, after changing the flow direction, very roughly half the time spent on calculating until the next change of direction, was used for solving the mass balances with a typical time step in the order of $0.001\mathrm{s}$ which was the set minimum. After the mass profiles would become relatively constant, the temperature profile would be solved at a typical timestep of at least $0.1\mathrm{s}$. A typical switching time, however, would be in the order of a few hundred seconds. Hence far too much time was spent on calculating a relatively insignificant phenomenon. The practical approach was then taken to increase the minimum timestep to $0.1\mathrm{s}$ for most simulations.

H.2. Initial high tolerance

For converging to a steady state solution, the HFSM uses the same time-stepping algoritm the DM does. The point is that no accurate solution is needed untill the steady state solution is found. Therefore, a small extension of the model was made that would initially set the tolerance for the energy and mass balances relatively high, which effectively reduced the number of iterations taken per timestep. After convergence was reached (zero iterations and maximum time step for four consecutive timesteps), the tolerance was reset to default and calculations were continued with this much better initial guess. Implementation of this extension has saved roughly 30% of the time required for HFSM convergence. This method however is not suitable if multiple steady states exist and the one resulting from a given starting condition needs to be found; the iteration might overshoot this solution.

H.3. Initial high timestep for HFSM

Since only the steady state is of interest for the HFSM, accurate solution of time steps is not required. The algorithm used for solving the HFSM is the same as that for the DM and is based on time stepping. The time step increases by 10% if increasing the timestep does not severely affect accuracy. But when starting at $0.001\mathrm{s}$ for the HFSM, many timesteps are required before a reasonably big timestep, even if clearance to increase the timestep is given at every timestep. Therefore the minimum timestep for the HFSM was set to $5\ \mathrm{s}$. After HFSM convergence was reached, before switching to the DM the minimum timestep was reset to (usually) $0.1\mathrm{s}$.

H.4. Initial high tolerance for DM

A possible procedure to obtain the cyclic steady state for reverse flow is to start from a converged HFSM solution and then start cycling, as was also described in another appendix. First of all it is noted here that it would be wise to use only half a switching time for the first blow, since the HFSM solution has similarities with the temperature profile obtained for the DM when the cycle is half-way through. Now the point is that it typically it takes very many cycles to simulate the transfer from a HFSM solution to a cyclic steady state for the DM. Nieken et al. [NKE95] mention 200 cycles as an indication, but do not give

a definition for convergence. For these cycles between the HFSM solution and the DM cyclic steady state the exact results are not of interest to the current project. Therefore, similar to the case for the HFSM, after HFSM convergence first a predefined number of cycles is calculated with a high tolerance, reducing the number of iterations per timestep (and also reducing accuracy). This should result in a better initial guess for the temperature profile in the DM. After the predefined number of cycles with high tolerance has been run, a predefined number of cycles with default tolerance was run. There has been no extensive testing with this method, which in itself looks promising. Neither was a convergence criterium included into the model itself, or was too much time spent on finding the "holy grail" of reverse flow calculations, which would be an instantaneous solution of the DM cyclic steady state profile. Thus, on the part of DM convergence, some work still can be done, although the added value of this, partly due to the advent of faster computers, should be carefully considered.

I. Overall heat balance for CH_4: O_2= 3

As an addition to chapter 9.1, the situation for CH_4: O_2= 3 is calculated here. The composition of the outgoing stream of the OCM reactor was based on the isothermal calculations with T=810°C and a reactor length of 1m. Further dimensions are given in appendix N, from which it can be concluded that the inflow of methane into the OCM tube also was somewhat lower. The corresponding compositions are given in table I.1. For this tube 330W heat is produced. The heat required is 231W per tube for steam reforming up to 500°C and 485Wfor steam reforming up to 780°C. Thus in this case the heat requirements more or less match at the expense of a loss of selectivity in the OCM reaction tube.

Table I.1.: Upper table: Composition for OCM outlet for thermodynamic calculations. Lower: Stream compositions for the example for steam reforming (mole fractions).

Mole fractions at outlet of OCM reactor							
O_2	CO_2	H_2O	CH_4	CO	H_2	C_2H_6	C_2H_4
0.00	0.04	0.40	0.29	0.00	0.06	0.02	0.18
Mole fractions after removal of $C_2H_4$and C_2H_6: inlet stream SRM							
O_2	CO_2	H_2O	CH_4	CO	H_2	C_2H_6	C_2H_4
0.00	0.05	0.50	0.36	0.01	0.08		

	O_2	CO_2	H_2O	CH_4	CO	H_2
Feed stream, 100°C	0.0	0.026	0.745	0.186	0.003	0.040
Steam reformed, 500°C	0.0	0.088	0.490	0.085	0.011	0.326
Steam reformed, 780°C	0.0	0.072	0.355	0	0.084	0.489

J. Reactor design: conceptual approach

A conceptual approach using unit operations has been used to come up with a basic reactor design. The main conclusions are given here.

J.1. Both catalysts in the same space: SRM followed by OCM

J.1.1. Concept

The first concept that was considered was the case shown in figure J.1. It represents a porous support layer. On the right, this support layer has been impregnated with SRM catalyst. On the left, it has been impregnated with OCM catalyst. In between there is an inert porous support layer, which ensures a thermal connection between the SRM and OCM catalyst.

The idea is that the ethane and ethene formed by the OCM catalyst should not contact the SRM catalyst since typically a nickel catalyst is also used in prereforming of hydrocarbons for syngas production [Chr96]. Therefore, on the right hand side there is a slight overpressure. This should induce a flow from right to left which prevents oxygen from reaching the SRM catalyst by diffusion. Oxygen, flowing in from the left[1], can however reach the OCM catalyst by diffusion. Oxygen partial pressure should be low to ensure good selectivity towards ethane and ethene.

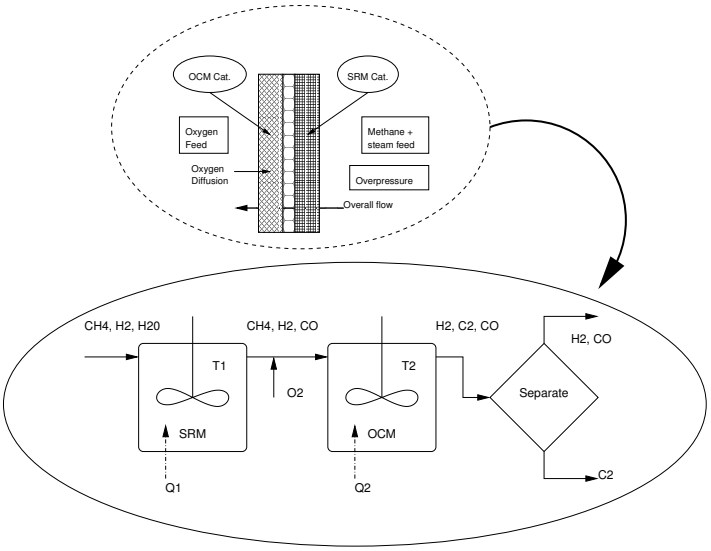

Figure J.1.: Schematical representation of first base case, including translation to Aspen

J.1.2. Results

Multiple configurations were tested by solving basic mass balances with Aspen. For the sake of brevity these calculated results and the (more or less trivial) approximations used are not given here. The main

[1] Since at this point only unit operations are considered, it is not given how this would exactly be done.

conclusions are as follows:

- The extent of the SRM reaction needs to be limited, since if equilibrium is reached at typical temperatures for OCM no CH_4 is left for the OCM reaction. SRM, however can according to Gallucci, Paturzo and Basile [GPB04] also be operated in a temperature range of 300-500°C, possibly limited by kinetics.
- (Obviously) steam will reach the OCM catalyst. It is not known if this would destroy the catalyst.
- (Obviously) hydrogen is present in the OCM catalyst section and subsequent streams. This presents a major safety issue and might also lead to significant consumption of O_2 intended for the OCM reaction.
- Variants to this base case, considering a separation section in between the SRM and OCM section, do not very significantly affect the results. The *basic problem* is that even when assuming no negative effects on the reactions a very diluted product stream is obtained. Before C_2 products can be recovered in a cryogenic separation, CO_2 and water need to be removed from the product stream. The product stream has a high volume and moreover hydrogen is present in a stream that would have to be separated typically in a distillation column, making this a very costly way of operation.

Because of the undesirable composition of the product stream and unknowns about the way the reactions are affected by added components, this way of operation is discarded.

J.2. Separation of catalysts in space: OCM followed by SRM

It is trivial that if the catalysts are separated in space, allowing for a separation of chemical components in between, OCM is followed by SRM and not the other way around; typically it would be desirable to convert all methane and whatever other alkanes in the feed stream to synthesis gas in the SRM section. Hence the process schemes elaborated in section 5 prevail.

From the results it is confirmed that this mode of operation gives a much less diluted product stream going to the cryogenic distillation. Also the volumetric flow rate going to the cyrogenic section is significantly lower.

J.3. Conclusions

Based on the following two main arguments:

1. Cryogenic distillation is generally considered the method of choice to remove the C_2 products from the OCM product stream. This favours the desire for a high vapour pressure of C_2 product and for low volumetric flow going to a separation section.
2. Side reactions may be detrimental to product yield when combining the SRM and OCM catalysts in the same space; avoiding this may require very delicate operation.

The configuration of choice is the OCM followed by SRM, with separation in between, as elaborated in section 5. By doing Aspen simulations it has been found that for a typical reaction mixture coming from an OCM reactor, sending all methane coming from this step to a steam reformer gives a steam reforming process that typically requires more heat than is released by the OCM reaction. This requires special attention in further work.

K. Materials of construction

In general, it is reported that temperatures should not exceed $1000^{\circ}\mathrm{C}$ if conventional reactor materials are to be used.

K.1. Reactor wall

Stainless steel catalyses the burning of hydrocarbon products [LSM94]. Different materials of construction for oxygen permeating membranes in oxidative coupling of methane are discussed by Saracco et al. [SNVS99]. Moreover, references for both catalytic and noncatalytic membrane materials are given by Akin and Lin [AL02]. Inspiration can also be gotten from the existing cracking of hydrocarbons to ethene process, which also operates at elevated temperatures and has to deal with coking, causing not only problems with heat transfer but also with the stability of the metals of construction [ZW07].

K.2. Gaskets

Lafarga et al. have evaluated different materials for use for gaskets in an oxygen rich environment and finally selected graphite for this purpose. Also by design the surface exposed to hot oxygen has been minimized.

The problem finding the right sealing materials in itself is a good reason to look for a reactor concept in which the outlet and inlet temperature of the reactor are low. This would allow to use for example silicon rubber as gaskets. [FEHA99]

K.3. Catalyst carrier

Catalysts carriers made of monolithic material can suffer from thermal cracking [SHK02]. This is also why Frauhammer et al. [FEHA99] limited the temperature in their experiments using a honeycomb monolith.

L. Required radial diffusion of mass

The goal of this chapter is to determine if exhaustion of oxygen at could occur along the radial direction. A worst case approach is taken for the rate of oxygen consumption. The reactor is considered to be pseudohomogeneous. The goal is to determine the minimum value of the radial dispersion coefficient required to obtain an acceptable oxygen concentration along the radius of the catalytic bed.

L.1. Mass balance

The steady state mass balance for oxygen for a cylindrical slab is given by (taking a pseudohomogeneous approach with simplified kinetics):

$$\frac{d}{dr}\left(r \cdot \frac{dc_{\mathrm{O}_2}}{dr}\right) = -r \cdot \frac{Dil \cdot \rho_{bulk,cat} \cdot k_r \cdot c_{\mathrm{O}_2}^n}{D_{\mathrm{O}_2}} = -r \cdot \frac{K_r \cdot c_{\mathrm{O}_2}^n}{D_{\mathrm{O}_2}} \tag{L.1}$$

L.2. Reaction kinetics

The reaction kinetics are composed as follows:

- The reaction order n is the highest order in oxygen found in the kinetics of Stansch et al. [SMB97]. This is 0.96, for reaction (2.6) on page 6. In order to allow for a clear analytical solution that approximates this situation very well (actually it provides an even worse case), the reaction order n is set to one.
- $k_r \cdot \gamma$ is determined as the sum of $k_{0,j} e^{E_{a,j}/RT} p_c^{m,j}$ for reactions (2.1) until (2.6), multiplied with the appropriate stoichiometric coefficient for oxygen. The temperature is set constant at $810^{\circ}\mathrm{C}$. The inhibiting effect of carbon dioxide as given by Stansch, thus, is neglected. Furthermore p_C is set constant at $1.2\mathrm{bar}$, the maximum pressure obtainable for any component in the reactor. The factor γ is there between the kinetics by Stansch et al. [SMB97] and that in the current work in order to be able to use concentrations instead of partial pressures, as Stansch et al. do. It's value is found from the equation for reaction velocity r_c (using the ideal gas law):

  $$\begin{aligned} r_c &= (k_r \cdot \gamma) \cdot p_i = k_r \cdot p_i \cdot \frac{c_i}{p_i} \\ \gamma &= \frac{c_i}{p_i} \\ c_i &= \frac{n_i}{V} = \frac{\varepsilon \cdot p_i}{RT} \\ \frac{1}{\gamma} &= \frac{RT}{\varepsilon} \end{aligned}$$

  Working in this way it turns out that reaction (2.2) is dominant by far and $k_r \cdot \gamma$ has a value of $2.66\mathrm{mol/kg/s \cdot Pa^{-1}}$. Multiplication with $\frac{1}{\gamma}$ then gives that k_r has a value of 59.8 $\mathrm{kmol/m^3/s/kg/mol/m^3}$.
- The bulk density of the catalyst is given by $0.6 \cdot 3600 = 2160\mathrm{kg/m^3}$.
- The catalyst dilution Dil is 0.1.

L.3. Solution of the differential equation

Integrating the differential equation once gives:

$$r \cdot \frac{dc}{dr} = -\frac{1}{2} r^2 \left(\frac{K_r}{D_{O_2}} \right) \cdot c_{O_2} + C_1 \tag{L.2}$$

Since the solution of this equation is rather elaborate and only an estimate of an order of magnitude is required, a simplification is imposed. A flat plate approach is imposed, which allows for the use of analytical solutions provided in literature [WVSB01] for the derivation of effectiveness factors of catalyst particles. Since there can be no diffusion through the outer wall, this wall acts as a symmetry boundary condition. The approach now is to use the actual thickness of the catalyst section as the distance to the middle of the flat plate. This poses less severe requirements on the part of diffusion than would actually be the case for diffusion through the cylindrical slab; if problems occur here, they are certainly to be expected for the situation in the actual catalyst section.

Having taken the approach taken here, the next step is to calculate the Thiele modulus Φ. For this as a first approximation the typical value of $D_A = 0.1\mathrm{cm}^2/\mathrm{s}$ [WVSB01], which is the diffusion coefficient in the gas phase (neglecting possible enhancement by convection) is used.

$$\Phi = \delta \sqrt{\frac{K_r}{D_A}} \approx 0.006 \cdot \sqrt{\frac{1.3 \cdot 10^7}{10^{-5}}} = 6.8 \cdot 10^3 >> 1 \tag{L.3}$$

This means that, for this worst case considered, all oxygen reacts in a very thin slab next to the membrane wall and no oxygen reached the tube wall. Not in this flat plate approximation and not in the actual cylindrical catalyst section. On the other hand it should not be forgotten that the power n_j for reaction (2.2), the most dominant contribution to K_r, is not 1 but 0.4; this also has a major effect on the conversion factor $\frac{1}{\gamma}$ since $\left(c_{O_2} \cdot \frac{1}{\gamma} \right)^n = p_{O_2}^n$. However, elaboration of the full mass transport is left for future work, and a strong indication is obtained here that this should be one of the first things to be considered.

In order to get a first indication if this would be worth the trouble, instead of a reaction order of one, a reaction order of 0.5 in O_2 (again for all reactions) is considered here. Relations for the Thiele modulus for non-first order reaction kinetics are given by Westerterp et al. [WVSB01]. A catalyst slab with an effectiveness factor of one is obtained for Thiele moduli Φ up to 0.2, for which the Thiele modulus is given by:

$$\Phi = \delta \sqrt{\left(\frac{2}{n+1} \frac{k_n}{D_A} c_{A,i}^{n-1} \right)} \tag{L.4}$$

Assuming the oxygen is present in it's stoichiometric ratio CH_4: O_2= 4 throughout the entire reaction section, it's concentration is calculated from

$$c_{O_2} = \frac{1}{4+1} \frac{\varepsilon \cdot p}{RT} = \frac{1}{5} \cdot \frac{0.4 \cdot 1.2 \cdot 10^5}{8.31 \cdot 1083.15} \approx 1\mathrm{mol/m}^3 \tag{L.5}$$

Actually, it is lower due to the distributive feed (and reaction), but the Thiele ratio is relatively insensitive to the induced error; far more relevant is the ratio $\frac{k_r}{D}$. The reaction rate constant as determined from the kinetics by Stansch is now basically equal to $k_r \cdot \gamma^{0.5}$, so that K_r is now obtained by multiplication of $2.66\mathrm{mol/kg/s/Pa}$ with $\left(\frac{1}{\gamma} \right)^{0.5}$. Thus

$$\Phi \approx 0.006 \sqrt{\left(\frac{2}{1.5} \frac{8.6 \cdot 10^4}{10^{-5}} 1^{-0.5} \right)} = 642 >> 0.2 \tag{L.6}$$

This indicates that the reaction is severely mass transport limited. On the other hand it can be calculated that for the case of CH_4: O_2=4 the flow of oxygen out of the membrane has a radial velocity of about $2.6\mathrm{mm/s}$ at the outer membrane wall. However, of course this radial velocity might have only a limited

enhancement of transport into the bed. Moreover, most of the bed exists of particles of significant size which are assumed to be macroporous, so that the gas-phase diffusivity gives a more reasonable estimate than relations given for the effective radial diffusivity (without convection from the side wall taken into account) as given by Iordanidis [Ior02] (which predict it to be a factor of about 10 higher for the given case). It is also well known that in packed beds bypassing occurs at the walls [Ior02]. A future study of transport limitation should thus also have a strong focus on less active catalysts, such as that studied by Tuinier [Tui07]. However already from the above calculation it can be seen that if the reaction rate is decreased with a factor 1000 opposed to the diluted catalyst, which would approximately be the case by changing the catalyst used by Stansch et al. by that studied by Tuinier, and if at the same time the effective radial diffusion by contribution of convection could be increased by a factor 10 (requiring additionally decrease of particle diameters, in turn affecting the effective radial diffusivity), still severe reduction of the radial dimension δ of the catalyst section would be required, although a combination of this and the allowance of a radial gradient in oxygen concentration could also be feasible. Oxygen, it must not be forgotten, is only a vehicle, with an order of dependence lower than 1, in the reaction scheme. Significant reduction of the reaction velocity should be avoided because this simply reduces the conversion per kg catalyst, but also increases the significance of side-reactions, which were shown to have a significant contribution for measurements as performed by Tuinier [Tui07] for mole fractions of O_2 over approximately 4% already. Last, in future evaluation it should not be forgotten that the curvature (opposed to the flat plate approach taken here) should be taken into account and for the case of diffusion from the middle of a cylinder to the outside makes the situation worse.

L.4. Some more considerations

The model assumes the oxygen concentration to be homogeneous along the radial position. Additionally, Fick's law, applied here, is basically only valid for strongly diluted systems. Moreover, the diffusion coefficient was not corrected for the porosity of the bed or for any influence for transport through the bed. However, for an order of magnitude estimation, the current approach will do. It does not give an answer to the question *how fast* (considering a frame of reference moving with the flow) an acceptable steady state concentration of oxygen at the wall is reached. The latter should also be checked in future projects.

Also note that the current discussion relates to the gas phase outside of the catalyst particles. Within the particles diffusion limitation can still occur and should be evaluated in further work. By ensuring a relatively homogeneous composition of a gas phase at a given axial position, however, apart from temperature effects the conditions are now the same for all particles at the same axial position.

M. Minimum required radial heat conduction

The goal of this chapter is to indicate which should be the minimum heat conduction of the catalytic bed in the radial direction in order to keep the radial temperature difference for a given axial position within it within an acceptable range of (say) $10^{\circ}\mathrm{C}$. Again a pseudo homogeneous approach is taken.

M.1. Energy balance and solution

In order to obtain a quick estimate, a uniform production of heat q throughout the catalyst section fed with oxygen is assumed. Given an overall heat production of $275\mathrm{W}$ per tube (including the endothermic reaction in the post-membrane zone, which is neglected here), q is calculated from:

$$\begin{aligned} q &= \frac{Q}{L_m \cdot \frac{1}{4}\pi\left(d_t^2 - (d_m + 2\cdot d_w)^2\right)} \\ &= \frac{275}{\frac{2}{3}\cdot\frac{1}{4}\pi\left(0.025^2 - 0.013^2\right)} = 1\mathrm{MW/m^3} \end{aligned} \tag{M.1}$$

The steady state energy balance is given by:

$$-\lambda_r \frac{d}{dr}\left(r\cdot\frac{dT}{dr}\right) = q\cdot r \tag{M.2}$$

Given the boundary conditions that at the membrane wall ($r_m = 0.5\cdot d_m + d_{w,m}$), $\left(\frac{dT}{dr} = 0\right)$, and that at this same outer membrane wall, $T = T_m$, the solution is given by:

$$T = \frac{1}{4}\left(\frac{-q}{\lambda_r}\right)\cdot r^2 - \left(\frac{1}{2}\left(\frac{-q}{\lambda_r}\right)\right)\cdot r_m^2\cdot\ln(r) + C_2 \tag{M.3}$$

With C_2 given by:

$$C_2 = T_m - \frac{1}{4}\left(\frac{-q}{\lambda}\right)r_m^2 + \left(\frac{1}{2}\left(\frac{-q}{\lambda}\right)\right)\cdot r_m^2\ln(r_m) \tag{M.4}$$

Thus the temperature difference between the catalyst at the tube wall and that at the membrane is given by:

$$\Delta T = T_m - T_w = \left(\frac{1}{4}\cdot\left(\frac{-q}{\lambda}\right)\right)\cdot\left(r_m^2 - r_w^2\right) + \left(-\frac{1}{2}\cdot\left(\frac{-q}{\lambda}\right)\cdot r_m^2\right)\cdot\ln\left(\frac{r_m}{r_w}\right) \tag{M.5}$$

It is seen that for large and approaching r_i the solution approaches that for a flat plate, which is as expected. Also the case for r_m approaching zero behaves as expected.

M.2. Results

Using equation M.5, the minimum required radial conduction coefficient $\lambda_{r,req}$ for maintaining a maximum temperature difference of $10^{\circ}\mathrm{C}$ is found from:

$$\begin{aligned} \lambda_{r,req} &= \frac{1}{4}\cdot\left(\frac{-q}{\Delta T}\right)\cdot\left(r_m^2 - r_w^2\right) + \left(-\frac{1}{2}\left(\frac{-q}{\Delta T}\right)\cdot r_m^2\right)\ln\left(\frac{r_m}{r_w}\right) \\ &= \frac{1}{4}\cdot\left(\frac{-10^6}{10}\right)\cdot\left(0.0065^2 - 0.0125^2\right) + \left(-\frac{1}{2}\left(\frac{-10^6}{10}\right)\cdot 0.0065^2\right)\ln\left(\frac{0.0065}{0.0125}\right) \\ &= 1.47\mathrm{W/m^{\circ}C} \end{aligned} \tag{M.6}$$

The heat conductivity of the stagnant bed (including radiation) as given by the model is in the order of 2 $\mathrm{W/m/^{\circ}C}$, calculated based on the Zehner and Schlünder approach described by (among others) Smit [Smi06], although that of the solid itself is $7.3\mathrm{W/m/^{\circ}C}$, as can be calculated from the physical properties of CaO. This approach does not yet take into account the contribution of convective transport, although the contribution of this transport is expected to be only limited due to the low heat capacity of the gas. Please note that only a temperature difference within the bed is considered and that in this way the heat transfer between bed and wall is not directly relevant here.

The question rises what λ_r would relate to the chosen $\alpha_{bw} = 300\mathrm{W/m^2/^{\circ}C}$. The overall heat transfer coefficient for heat transport through a tube wall is given by [Sin03]:

$$\frac{1}{\alpha} = \frac{d_o \ln\left(\frac{d_o}{d_i}\right)}{2 \cdot \lambda_r} \tag{M.7}$$

The model assumes that the temperature in the catalyst section is homogeneous (for a given axial position); it is as if the volume-averaged temperature is the actual temperature over the entire radius of the catalyst section. In the actual case, however, this temperature is only reached at a given radial position. Finding this from volume-averaging is an elaborate procedure, and therefore another approach is taken here. Given the chosen α and given the minimum required λ_r, a value for the maximum allowed d_i, relating to the allowed position for the position with the volume averaged temperature, can be obtained. Some rewriting gives:

$$d_i = \frac{d_o}{\exp\left(\frac{2 \cdot k_w}{\alpha d_o}\right)} \tag{M.8}$$

Filling out this equation, it is found that $d_i = 0.0169\mathrm{m}$, which means that $r_i < r_m$. This means that the chosen value of α (assuming negligible heat transfer resistance from bed to wall) relates to a λ_r far greater than $\lambda_{r,req}$, which means that the choice for this high value of α reflects the assumption of a radially homogeneous temperature profile.

N. Changing the ratio CH_4:O_2

For the demonstation of the effects of changing the ratio CH_4:O_2 from the default value of 4 to the value of 3, which are the same ratios as were used by Coronas et al. [CMS94b] for their membrane reactor, it is desirable that at the same time the residence time of the system remains the same or of similar magnitude. Because of the stoichiometry of the reaction the calculation of residence time is not straightforward. Although in principle the average residence time of for example a C-atom could be calculated, a shortcut approach is taken here. The method of changing the ratio CH_4:O_2 chosen is to change the diameter of the inner (membrane) tube. Looking at figure N.1 this means keeping all sizes but d_m the same. In this way the flux through the membrane can remain the same.

The old and new values of the diameters along with the characteristic fluxes are given in table N.1. The calculation itself, using an increase the inner diameter of the inner tube untill the ratio in overall molefluxes to obtain an overall mole feed ratio as desired, is relatively straightforward and is not given here. It is important to note that in practice the membrane of a tube with a porous membrane is found on the inside of the tubing and hence the flux on the inside of the tube was set fixed; hence the flux in the model, which relates flux to the outside of a tube, has to be adjusted. Due to the quadratic increase of the inlet surface of the O_2 tube combined with the linear increase of the outer surface with the increase of the tube diameter, in principle the inlet flux of the O_2 tube could have been lowered a bit to $0.27\mathrm{kg/m^2}$, but because of the relatively small influence of the remaining small stream on the termal properties of the reactor this stream was left as it is. In the situation of the ratio CH_4:O_2=4 the flux of O_2 is such that there is an inflow into this tube that is 10% larger than that needed for flux through the membrane. This was done to avoid numerical problems and can be left out in reality.

For the estimation of residence time, the flux through the catalytic section is considered. Thus, for the inlet section, it is simply the inlet flux of methane. After reaction, in the outlet section, a good estimate is considered to be the sum of the overall inlet mole flow of methane and oxygen. For the catalytic section then, since the flux of O_2 through the membrane is considered constant, it is then the average of the fluxes of the inlet section of the inlet and outlet section. The total residence time then is the sum of the residence times for these three sections. This was calculated at a constant temperature of $800^\circ\mathrm{C}$ and a pressure of 1 bar to be 0.94sfor the case of a molar ratio of CH_4:O_2=4 and to be 0.91sfor the case of a molar ratio of CH_4:O_2=3. This was considered to be sufficiently close to legitimately avoid modification of the inlet flux of methane for the case of CH_4:O_2=3.

Table N.1.: Size of tubing for different overall molar feed ratios

Variable	Value for CH_4:O_2=4	Value for CH_4:O_2=3
d_m	$0.0110\mathrm{m}$	$0.0129\mathrm{m}$
$d_{w,m}$	$0.001\mathrm{m}$	$0.001\mathrm{m}$
d_c	$0.025\mathrm{m}$	$0.025\mathrm{m}$
$d_{w,t}$	$0.001\mathrm{m}$	$0.001\mathrm{m}$
$\Phi_{O_2,m,inner}$	$0.00132\mathrm{kg/m^2/s}$	$0.00132\ \mathrm{kg/m^2/s}$
$\Phi_{O_2,m,outer}$	$0.00112\ \mathrm{kg/m^2/s}$	$0.00114\mathrm{kg/m^2/s}$
Φ_{m,in,CH_4}	$0.17\mathrm{kg/m^2/s}$	$0.17\mathrm{kg/m^2/s}$
Φ_{m,in,O_2}	$0.352\mathrm{kg/m^2/s}$	$0.352\mathrm{kg/m^2/s}$
L_m	$\frac{2}{3}\mathrm{m}$	$\frac{2}{3}\mathrm{m}$

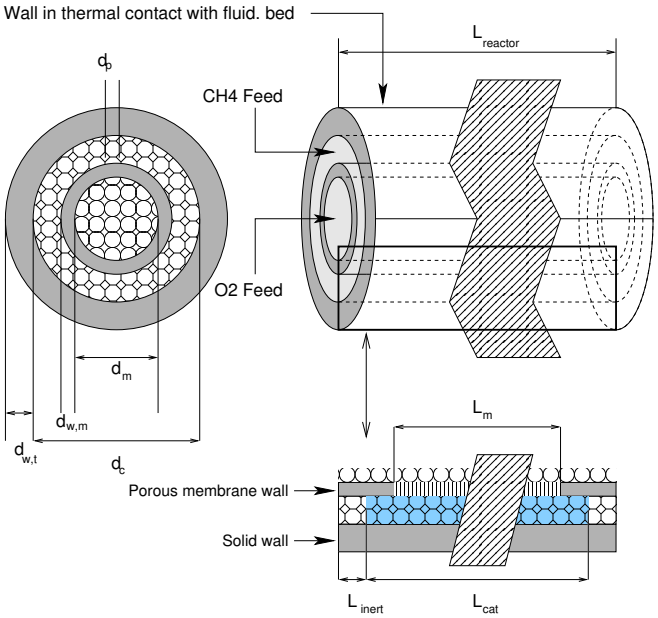

Figure N.1.: Configuration with concentric tubes showing the measures used in the description of this paragraph